**AWARD NUMBER:** W81XWH-10-2-0054

**TITLE:** "Stem Cell Therapy for Healing Wounded Skin and Soft Tissues."

**PRINCIPAL INVESTIGATOR:** Dr. Kai P. Leung

**RECIPIENT:** The Geneva Foundation

Tacoma, WA 98402

**REPORT DATE:** March 2014

**TYPE OF REPORT:** Final

**PREPARED FOR:** U.S. Army Medical Research and Materiel Command
Fort Detrick, Maryland 21702-5012

**DISTRIBUTION STATEMENT:**

Approved for public release; distribution unlimited

The views, opinions and/or findings contained in this report are those of the author(s) and should not be construed as an official Department of the Army position, policy or decision unless so designated by other documentation.

# REPORT DOCUMENTATION PAGE

*Form Approved*
*OMB No. 0704-0188*



| 1. REPORT DATE *(DD-MM-YYYY)* | 2. REPORT TYPE | 3. DATES COVERED *(From - To)* |
|---|---|---|
| March 2014 | **Final** | 15June2010-14December2013 |

**4. TITLE AND SUBTITLE**
"Stem Cell Therapy for Healing Wounded Skin and Soft Tissues."

**5a. CONTRACT NUMBER**

**5b. GRANT NUMBER**
W81XWH-10-2-0054

**5c. PROGRAM ELEMENT NUMBER**

**6. AUTHOR(S)**
Kai P. Leung WC, SK Hong, TA Mustoe. RG Hale, Leung KP

email: kai.p.leung.civ@mail mil

**5d. PROJECT NUMBER**

**5e. TASK NUMBER**

**5f. WORK UNIT NUMBER**

**7. PERFORMING ORGANIZATION NAME(S) AND ADDRESS(ES)**

The Geneva Foundation

Tacoma, WA 98402

**8. PERFORMING ORGANIZATION REPORT**

**9. SPONSORING / MONITORING AGENCY NAME(S) AND ADDRESS(ES)**
US Army MRMC
Ft Detrick, MD 21702-5012

**10. SPONSOR/MONITOR'S ACRONYM(S)**

**11. SPONSOR/MONITOR'S REPORT NUMBER(S)**

**12. DISTRIBUTION / AVAILABILITY STATEMENT**

Approved for public release; distribution unlimited

**13. SUPPLEMENTARY NOTES**

**14. ABSTRACT**

Profiling of Paracrine Factors Secreted by Leporine-deprived Mesenchymal Stem Cells

**15. SUBJECT TERMS**

Adipose-derived mesenchymal stem cells: cytokines; paracrine factors

| 16. SECURITY CLASSIFICATION OF: | | | 17. LIMITATION OF ABSTRACT | 18. NUMBER OF PAGES | 19a. NAME OF RESPONSIBLE PERSON |
|---|---|---|---|---|---|
| a. REPORT | b. ABSTRACT | c. THIS PAGE | | | USAMRMC |
| U | U | U | UU | 57 | 19b. TELEPHONE NUMBER *(include area code)* |

## Table of Contents

**INTRODUCTION:**
Exogenously applied stem cells can integrate into wounds, and if properly directed to regenerate tissue rather than to rapidly restore the barrier function, should be able to regenerate tissue for improved wound healing. We hypothesize that when applied topically to wounds, adult, adipose-derived mesenchymal stem cells that are directed toward tissue regeneration can reduce inflammation, increase angiogenesis, reduce scarring, and improve the restoration of skin functions. The goal of the proposed research is to define the function of stem cells alone or in atrix to promote healing by regeneration to improve wound repair outcomes.

**BODY:**
Year 1

**I. Isolation and culture of rabbit primary cell lines.**

**1. Adipose derived stem cell (ASC)**

ASCs were isolated from young female New Zealand White rabbits (3-4 months old, ~2.5-3.5 kg). Briefly, a ventral midline incision was made through the rabbit's dermis, and additional incisions were made from flank to flank at the rostral and caudal aspects of the midline incision. The skin was separated from the underlying adipose tissue. The inguinal fat pads were dissected out and placed in sterile, pre-warmed phosphate-buffered saline (PBS). Each fat pad yielded approximately 5-10 grams of tissue after removing evident blood vessels. Fat pads were then washed several times in PBS, minced manually, and digested in 0.075% Type II collagenase type in Hank's Buffered Salt Solution (HBSS) for 1 hour at 37°C in a shaking water bath. After digestion and inactivation of collagenase, the stromal vascular fraction (SVF) containing ASCs was isolated by centrifugation at 500 × g for 5 minutes. The SVF was resuspended in HBSS and filtered through a 100 μm sterile nylon mesh filter and then spun again at 500 × g for 5 minutes. The resultant pellet was resuspended in 10 ml of red blood cell (RBC) lysis buffer, and allowed to sit at room temperature for 10 minutes. The supernatant was removed by centrifugation following RBC lysis and the pellet was resuspened in Dulbecco's Modified Eagle Medium: Nutrient Mixture F-12 (DMEM/F12) containing 10% fetal bovine serum (FBS) and plated in 10 cm plates. After overnight culture, the media was then removed and replaced. Cells were typically confluent within 3-4 days (Figure 1A). Four primary rabbit ASC cell lines and passaged 0 to 5 (P0-P5) per each ASCs were made. The lines were stored in liquid nitrogen.

**2. Dermal fibroblast (DF)**

DFs were isolated from the ears of young female New Zealand White rabbits. The rabbit ear tissue was cut into squared pieces (~ 1 × 1 $cm^2$) and the skin tissue from the dorsal side removed. After washing with PBS, the tissue was placed with the epidermis face down in a tissue culture-grade petri dish. PBS containing Dispase at 5 mg/ml was added and incubated overnight at 4°C. Epidermal tissue was carefully excised, and dermal tissue was minced manually and digested in 0.25% Type II collagenase in HBSS at 37°C overnight. After digestion, the solution was filtered through a 100 μm sterile nylon mesh filter and spun at 500 × g for 10 minutes. The pellet was resuspended in DMEM medium containing 10% FBS and plated in 10 cm dishes (Figure 1B). Three primary rabbit DF cell lines were made and stored in liquid nitrogen.

**3. Bone marrow derived mesenchymal stem cell (BM-MSC)**

BM-MSCs were isolated from the femoral medullary cavities of young female New Zealand White rabbits. Briefly, bone marrow was collected in PBS containing 2 units/ml heparin and left at room temperature for 10 minutes. After removing the floating fat layer, the solution was added to 5 ml of Ficoll-Paque Plus (1.077 g/ml, GE Healthcare, Piscataway, NJ) in a 15 ml tube and centrifuged at 2,000 × g for 30 minutes. The interface layer containing BM-MSCs was recovered and washed in HBSS. BM-MSCs were then cultured in Minimum Essential Medium (MEM) containing 10% FBS (Figure 1C). Seven primary rabbit BM-MSCs lines were made and stored in liquid nitrogen.

## II. Characterization of rabbit mesenchymal stem cells

Unlike embryonic stem cells, which have specific makers such as Oct-4 and SSEA, MSCs cannot be characterized by specific markers because definitive cellular markers have not yet been identified. Thus, a series of positive and negative surface markers are needed for the characterization of MSCs [1-4]. We selected CD29, CD44, CD90, and CD105 as positive markers. CD34 (endothelial cell marker) and CD45 (hematopoietic cell marker) were used as negative markers.

### 1. Analysis of MSC surface markers by Western blot analysis

All the antibodies that we tested were made to detect human antigens. Specificity of CD29, CD44, CD90, CD105, and CD34 were confirmed by Western blot analysis (data not shown). However, rabbit CD45 specific antibodies were not found by Western blot analysis using anti-CD45 antibodies from four different vendors (Abcam, BD Biosciences (San Jose, CA), Santa Cruz Biotechnology (Santa Cruz, CA), Thermo Scientific (Rockford, IL)). Rabbit ASCs and BM-MSCs cells [passage 1 to 9 (P1-P9)] were washed with PBS, harvested, and lysed with RIPA buffer (150 mM NaCl, 1% NP- 40, 0.5% deoxycholic acid, 0.1% SDS, 50 mM Tris-Cl, pH 7.5). Equal amounts of protein were added to a 10% SDS polyacrylamide gel and transblotted on polyvinylidene difluoride-nitrocellulose filters. Membranes were incubated with anti-CD29 (1:5,000 dilution; Abcam, Cambridge, MA), anti-CD44 (1:5,000 dilution; Abcam), anti-CD90 (1:5,000 dilution; Abcam), or anti-CD105 (1:2,500 dilution, Abcam) and then incubated with horseradish peroxide-conjugated secondary antibody (1:5,000 dilution; Vector Laboratories, Burlingame, CA). Specific bands were visualized using an Enhanced Chemiluminescence (ECL) detection kit (GE Healthcare). The blots were probed with anti- -actin antibody (1:5,000 dilution; Sigma–Aldrich, St. Louis, MO) to serve as a control for gel loading. Expression of CD29, CD44, CD90, and CD105 were detected without significant changes from passage 1 through passage 9 in both ASCs and BM-MSCs (Figure 2).

### 2. Analysis of MSC surface markers by immunofluorescence microscopy

To characterized native surface antigens without denaturing, we performed immunofluorescence microscopy on test cells. ASCs and BM-MSCs were cultured on glass cover slides, fixed in 4% paraformaldehyde, and immunostaining was performed. Fixed cells were incubated with anti-CD29 (1:200 dilution; Abcam), anti-CD44 (1:200 dilution; Abcam), anti-CD90 (1:200 dilution; Abcam), anti-CD105 (1:100 dilution, Abcam), or anti-CD34 (1:100 dilution; Abcam) as primary antibodies. Alexa Fluor 488 (Molecular Probes, Eugene, OR) conjugated secondary antibodies were used to detect specific primary antibodies. Expression of CD44 was prominent both in ASCs and BM- MSCs (Figure 3). Expression of CD29 and CD105 were detected although the signal was weak in ASCs. However, those antibodies could not detect native antigen of CD29 and CD105 in BM-MSCs. The anti-CD90 antibody did not detect rabbit CD90 antigen in either ASCs or BM-MSCs. In summary, among four antibodies used for Western blot analysis only anti-CD44 works for the detection of native form of rabbit CD44 antigen in ASCs and BM-MSCs.

### 3. Analysis of MSC surface markers by Flow cytometry

We attempted to characterize the population of MSCs, which have CD29, CD44, CD90, and CD105 by flow cytometry. A total of $1 \times 10^6$ ASCs (or BM-MSCs) was incubated with mousse anti-CD29 and CD90 antibodies. Flow cytometry was performed with R-Phycoerythrin (PE)-conjugated anti-mouse IgG antibody (Molecular probes) using the Flow Cytometry Core Facility at the Northwestern University. Zenon Rabbit IgG Labeling Kit (Molecular Probes) was used for anti-CD44 and CD105 antibodies, which were made in rabbit, to reduce non-specific signals for the flow cytometry. However, none of the antibodies were able to detect the presence of specific rabbit surface antigen using flow cytometry (data not shown).

### 4. Differentiation of rabbit MSCs

MSCs have the ability to differentiate into mesodermal cells such as adipocytes, chondrocytes, osteocytes, and myocytes in response to appropriate intrinsic or extrinsic signaling [1, 5, 6]. We wanted to address the multipotency of our rabbit ASCs and BM- MSCs and used DFs as controls as a means to determine the functionality of these isolated rabbit mesenchymal cell. This was due to the fact that while the characterization of these rabbit MSCs using surface antigens worked well using Western blot analysis, there are issues with regard to the characterization of these cells using immunofluorescence microscopy and flow cytometry.

**4a. Adipogenic differentiation.**

ASCs, BM-MSCs, or DFs were seeded in 24 well plate at a concentration of $2 \times 10^4$ and cultured in the Adipogenesis Differentiation Medium (Life Technologies, Carlsbad, CA). After 8 days culturing, cells were fixed in 4% paraformaldehyde and stained with Oil Red O staining. There were significant amounts of lipid droplets accumulated in the cytoplasm of both ASCs and BM-MSCs (Figures 4A & C). In contrast lipid droplets were found in the cytoplasm of DFs (Figure 4B). fewer lipid droplets were found in the cytoplasm of DFs (Figure 4B).

**4b. Osteogenic differentiation.**

ASCs, BM-MSCs, or DFs were seeded in a collagen-coated (50 g/ml) 24 well plate at a concentration of $1 \times 10^4$. The cells were cultured in the Osteogenesis Differentiation Medium (Life Technologies). Cells were fixed in 4% paraformaldehyde and Alizarin Red S staining was performed to detect the presence of accumulated calcium. Positive staining for the presence of calcium was found in ASCs and BM-MSCs but not in DFs in day 28 culture (data not shown). Both ASCs and BM-MSCs showed high accumulation of calcium at day 35 culture (Figures 5A & C). DFs also showed accumulation of calcium, but with a lesser amount as compared to that of ASCs and BM-MSC at day 35 culture (Figure 5B).

**4c. Chondrogenic differentiation.**

A total of $8 \times 10^4$ ASCs, BM-MSCs, or DFs in 20 l of culture medium were plated in the middle of each well in a 24 well plate. Chondrogenesis Differentiation Medium (Life Technologies) was added to cells following 3 hour of incubation. Cells were continued to be cultured to 14 or 21 days, fixed in 4% paraformaldehyde, and stained with Alician Blue, which detect sulfated proteoglycan-rich matrix. Alician Blue Positive staining for Alician Blue positive was found in ASCs and BM-MSCs at day 14 and the intensity of the stain was increase at day 21 culture (Figure6 6A & C). Alician Blue staining positive signals were also found in DFs culture but signals were weaker as compared to ASCs and BM-MSCs (Figure 6B).

**4d. Analysis of adipocytes, osteocytes, and chondrocytes lineages specific genes.**

ASCs, BM-MSCs, or DFs, which were cultured in adipogenic, osteogenic, and chondrogenic medium respectively, were harvested at day 8, day 21, and day 28. Total RNA was prepared by treatment with Trizol Reagent (Sigma-Aldrich, St. Louis, MO). To make cDNA, contaminated genomic DNA during RNA preparation was removed using the Turbo DNA-free kit (Ambion, Austin, TX). cDNA was made from total RNA using superscript II (Invitrogen, Carlsbad, CA) with the use of random primers (100 ng) (Invitrogen). For quantitative analyses of the expression level of mRNAs, real-time PCR analyses using SYBR green I were performed using an ABI prism 7000 sequence detection system (Applied Biosystems, Foster City, CA). PCR primers were designed using the primer3 program (http://frodo.wi.mit.edu/). Expression of each gene was normalized to the level of glyceraldehyde-3-phosphate dehydrogenase (GAPDH) to get a $\Delta$Ct. The $2^{-\Delta\Delta Ct}$ method was used to calculate gene expression difference between differentiated and control samples. Expression of adiponectin, osteopontin, and Col10a1– which are specific markers of adipocytes, osteocytes, and chondrocytes, respectively – were analyzed. Expression of genes was detected by PCR with the following oligonucleotides – GAPDH (5' AGGTCATCCACGACCACTTC -3' and 5'-GTGAGTTTCCCGTTCAGCTC -3'), adiponectin (5'-CCTGGTGAGAAGGGTGAAAA -3' and 5'

GCTGAGCGGTAGACATAGGC -3'), osteopontin (5' AGGATGAGGACGATGACCAC -3' and 5'-CACGGCCGTCGTATATTTCT -3'), col10a1 (5'- GGAAAACAAGGGGAGAGAGG - 3' and 5' - CCAGGAGCACCATATCCTGT -3').

Expression of an adipocytes specific gene, adiponectin, was increased by 35-fold and 17-fold in ASCs and BM-MSCs when cultured in adipogenic medium for 8 days (Figure 7A). However, induction of adiponectin in DFs was not found in the same culture condition. Expression of an osteocytes specific gene, osteopontin, was increased by 3.2- fold and 2.7-fold in ASCs and BM-MSCs, respectively, when cultured in the osteogenic medium for 28 days (Figure 7B). In contrast, expression of osteopontin in DFs was decreased by 0.1-fold under the same culture conditions. Expression of a chondrocytes specific gene, Col10a1, was increased by 6-fold, 12-fold, and 1,515-fold in DFs, ASCs, and BM-MSCs, respectively, when cultured in the chondrogenic medium for 21 days (Figure 7C).

**III. Wound healing and hypertrophic scarring studies in the rabbit ear model**

**1. Animal model**

Young, adult New Zealand White rabbits (3-6 months, ~2-4 kg) were acclimated to standard housing and fed ad libitum under an experimental protocol approved by the Northwestern University Animal Care and Use Committee. Rabbits were anesthetized with an intramuscular injection of ketamine (45 mg/kg) and xylazine (7 mg/kg). Four to Six wounds were created per ear. Wounds were made with a 7 mm surgical punch biopsy (Acuderm, Ft. Lauderdale, FL) down to, but not through, the cartilage. Pressure was applied to create a small nick in the cartilage for histological identification, without causing a full thickness defect in the cartilage. Tissue was then elevated in an effort to remove epidermis and dermis, but left the perichondrium intact. Wounds were covered with semi-occlusive dressings (Tegaderm™, 3M Health Care, St. Paul, MN). Elizabethan collars were applied to prevent self-inflicted trauma to wounds.

**2. Wound harvesting and histological analysis**

For wound healing studies, on post-operative day 7, rabbits were anesthetized by intramuscular injection of ketamine (45 mg/kg) and xylazine (7 mg/kg). Rabbits were then euthanized with the administration of 200 mg/kg intracardiac Euthasol followed by a bilateral thoracotomy (Figure 8). Ears were transected and individual wounds were isolated with a 10 mm surgical punch biopsy tool (Acuderm). Wounds were then bisected, with one half immersed immediately in 10% zinc-formalin and the other half embedded in tissue-Tek OCT (Sakura, the Netherlands) and snap frozen for future immunohistochemical analysis. Formalin-fixed wounds were processed, embedded in paraffin blocks, and then sectioned on a microtome at a thickness of 5 μm. Sections were dried on glass slides and then stained with hematoxylin and eosin (H&E) according to standard protocols. Slide images were digitized from a Nikon Eclipse 50i light microscope and subsequently analyzed using NIS Elements BR software (Nikon, Melville, NY) for the PC (Figure 9). Epithelial gap was defined as the one-dimensional distance between the encroaching epithelial edges of the two sides on a cross section, while granulation tissue gap was defined as the distance between the new granulation tissue on either side. Values were normalized for a nick-to-nick distance of 7 mm ("adjusted gap"). Epithelial and granulation tissue areas were quantified two dimensionally by encircling the respective areas on the digitized fields. Slides were analyzed and scored in a blinded fashion. Any wounds with gross and/or histological evidence of desiccation, contamination, or physical trauma were excluded from the analysis. Results were tabulated using Microsoft Excel. In planning the experiments, an effort was also made to vary which ear received treatment (e.g., for saline vs. fibrin sealant, if saline were applied to the right ear and fibrin sealant to the left ear in the first rabbit, this pattern was reversed in the next rabbit and so on). Statistical comparisons were made with the Student's t test using a significance level of $p < 0.05$.

## 3. Determining optimum ASCs delivery vehicles in wound healing

Though stem cells themselves are multipotent, the interactions between stem cells and their environment are important for maintaining the proper function of stem cells, i.e., differentiation into various cell types and production of signaling molecules. Proper delivery of stem cells to the wound is critical for skin and tissue repair and regeneration. Cells in suspension have been delivered to target tissues by either direct injection or systemic circulation. Alternatively, cells have been delivered using biocompatible and biodegradable matrices which support the growth of cells.

In the first series of experiments, our objective was to determine the optimal delivery vehicles for ASCs. The delivery vehicle should not have beneficial nor adverse effects in both promoting wound healing and reducing scar formation in order to determine the true effect of ASCs in the healing process. We selected fibrin and hydrogel as delivery vehicles for our test. The rationale is that fibrin, which is a natural biopolymer of blood proteins fibrinogen and thrombin, has been used as a vehicle to deliver fibroblasts, keratinocytes, and MSCs [7-11]. Likewise, hyaluronic acid, a natural component of the extracellular matrix present in dermis and in wound environments, has also been used widely in the form of hydrogel to deliver cells such as chondrocytes, valvular interstitial cells, and MSCs [12-15].

### 3a. Comparison fibrin vs. saline as delivery vehicles

Aliquots of the fibrinogen and thrombin components of fibrin sealant (Haemacure Corp., Sarasota, FL or Sigma-Aldrich) were prepared at concentrations of 17.3 mg/mL and 167 U/mL, respectively. This was based on our previous work involving fibrin sealant as a delivery vehicle for use to deliver rabbit dermal fibroblasts to rabbit ear wounds [11]. For each ear (i.e., each set of 4-6 wounds), 20 µl of fibrin sealant or 15 µl of saline was delivered. Wounds were harvested at postoperative day 7 (Figure 8) and histological differences were quantified by digitization of microscope slide images and measurement of epithelial and granulation tissue distances and areas (Figure 9). Fibrin sealant treated wounds (n=8) showed similar results in the epithelial gap (Figure 10A,
3,341 ± 445 (fibrin) vs. 2,467 ± 492 µm (saline), p =0.35), percentage healed (Figure 10B, 0.52 ± 0.06 vs. 0.65 ± 0.07%, p =0.35), granulation tissue distance (Figure 10C, 1,099 ± 122 vs. 1,368 ± 124 µm, p =0.10), and granulation tissue area (Figure 10D, 707,149 ± 132,072 vs. 806,342 ± 109,803 µm**2**, p =0.41) when compared with saline treated wounds (n=7). In a separate experiment, we compared Haemacure fibrin versus Sigma-Aldrich fibrin for use as a vehicle in rabbit ear wounds. There were no significant differences in the epithelial gap, percentage healed, granulation distance, and granulation tissue areas in wounds treated with either fibrin at postoperative day 7 (data not shown).

### 3b. Comparison hydrogels vs. saline as delivery vehicles

Three hyaluronan based hydrogel matrices (Extracel™, Extracel-HP™, and Hystem™) were prepared according to the manufacturer's protocol (Glycogsan BioSystems, Salt Lake City, UT). The Extracel™ consists of hyaluronan (a major constituent of native ECM) and gelatin (denatured collagen). The Extracel-HP™ consists of Heprasil™ (a combination of hyaluronan and heparin) and Gelin-S™ (thiol-modified gelatin). The Hystem™ contains hyaluronan. Matrices were solidified by adding a crosslinker (polyethylene glycol diacrylate) at room temperature for 25 minutes. For each ear (i.e., each set of 4-6 wounds), 20 µl of hydrogel or 15 µl of saline was delivered to each wound. Wounds were harvested at postoperative day 7 for histological analyses. We compared between ears on the same animal to minimize the effects of rabbit-to-rabbit variation in wound healing (data not shown). For the comparison of all test vehicles at the same time, wound healing parameters of each vehicle treated sample were compared the
pooled saline treated samples using the SAS ANOVA with Tukey's test (Figure 11). Hydrogel treated wounds (n=8/10/10 for Extracel, Extracel-HP, and Hystem, respectively) showed significant decrease of wound healing in the mean epithelial gap (Figure 11A, 4,599 ± 219 with p=0.0004 (Extracel), 5,159±247 with p<0.0001 (Extracel-HP), 5,374±193 with p<0.0001 (Hystem) vs. 2,384 ± 277 µm

(Saline)) and percentage healed (Figure 11B, 0.34± 0.03 with p=0.0005, 0.26±0.04 with p<0.0001, 0.23±0.03 with p<0.0001 vs. 0.66 ± 0.04) when compared with saline treated wounds (n=35). There was no significant difference in saline vs. hyrodgel treated wounds for granulation tissue distance (Figure 11C, 797 ± 94 with p=0.10, 751 ± 63 with p=0.02, 828 ± 59 with p=0.10 μm vs. 1,155 ± 75 μm) and granulation tissue area (Figure 11D, 452,299±56,734 with p=0.30, 464,995 ± 74,792 with p=0.30, 693,786 ± 53,336 with p=1 vs. 723,417 ± 76,271 μm**2**). Furthermore, infiltration of polymorphonuclear leukocytes (PMN) was drastically increased in hydrogel-treated wounds (data not shown).

In summary, while fibrin sealant does not affect wound healing in rabbit ear wounds, the hydrogels we tested provoked significant inflammatory reactions in host tissues.

**4. Comparison of saline vs. fibrin as delivery vehicles for ASCs in wound healing**

ASCs can be delivered to wounds either in suspension or in matrices. Extracellular matrices, synthetic or naturally derived, have served effectively as scaffolds for cell delivery and formation of new tissue [16, 17]. Enhanced wound healing by stem cells seeded on matrices has been reported [18, 19]. In this experiment we compared whether there is any difference in healing response between ASCs delivered in fibrin versus saline. On the day of surgery, ASCs were trypsinized from 10 cm plates, resuspended in media, and counted with the use of a hemacytometer. A total of 7×105 cells were harvest at 500 × g for 5 minutes, washed in PBS to remove cell culture medium, and resuspended in 70 μL of the fibrinogen component. Then, 1×105 cells in 10
μL of the fibrinogen were evenly placed in a 7 mm wound and 10 μL of the thrombin was applied to solidify the fibrin and ASCs mixtures. In the contralateral ear, 1×105 ASCs in 15 μl PBS was delivered to each wound. In addition, preparation of fibrins from different vendors was also tested. Same amounts of fibrins from Haemacure Corporation versus Sigma-Aldrich were used in the comparison. Wounds were harvested at postoperative day 7 and histological analysis was performed. As illustrated in Figure 12, Haemacure fibrin-treated wounds (n=10) showed similar results in the epithelial gap [Figure 12A, 3,788 ± 580 (Haemacure fibrin) vs. 4,408 ± 345 μm (saline), p =0.55], percentage healed (Figure 12B, 0.46 ± 0.08 vs. 0.37 ± 0.05, p =0.55), and granulation tissue distance (Figure 12C, 1,952± 393 vs. 1,941 ± 435 μm, p =0.45) when compared with saline treated wounds (n=9). More granulation tissue area was found in Haemacure fibrin- treated wounds as compared to that of saline-treated wounds (Figure 12D,
1,220,840 ± 210,981 vs. 743,558 ± 175,440 μm**2**, p =0.03). In addition Sigma-Adrich fibrin-treated wounds (n=8) showed similar results as compared to Haemacure fibrin treated wounds with regard to the epithelial gap [Figure 13A, 4,128 ± 295 (Sigma-Aldrich fibrin) vs. 3,109 ± 523 μm (saline), p =0.43], percentage healed (Figure 13B, 40.41 ± 0.04 vs. 0.56 ± 0.07, p =0.43), granulation tissue distance (Figure 13C, 41928 ± 417 vs. 1512 ± 169 μm, p =0.06), and granulation tissue area (Figure 13D, 1,091,682 ± 189,786 vs. 842,229 ± 209,110 μm**2**, p =0.03).

**5. *In Vitro* Optimization of Cell Seeding Density in Fibrin Gel**

Rabbit ASCs (P6-P7) were harvested with trypsin-EDTA and counted. Fibrinogen-containing component of the fibrin sealant was reconstituted and diluted using Tris-buffered saline (TBS) to yield a working stock solution of 17.3mg/mL. Three concentrations of ASCs (10,000 cells/μL, 1,000 cells/μL, 100 cells/μL) were resuspended in fibrinogen and added to a flat bottom 96-well plate (TPP, dia=6.7mm). Equal volumes of thrombin (167 U/mL) were added to each well and the fibrin mixture was allowed to further solidify at 37°C for 30min before serum-containing plating media was added to each well. The MTT assay (Molecular Probes) was used to determine cell viability and cell proliferation of rabbit ASCs in the fibrin sealant. Briefly, a stock solution of 3-(4,5-Dimethylthiazol-2-y)-2,5-diphenyltetrazolium bromide (MTT) was prepared at a concentration of 5 mg/mL. Ten μL of this solution was added to each well containing 100 μL of phenol red free DMEM/F12 + 10% serum, and incubated at 37°C and 5% CO2 for

4 hr. After complete removal of the media/MTT solution, 200 µL of isopropanol-acetone (IPA) mixture (1:3) was added to each well and incubated for 1hr. The absorbance of each of the wells was measured at 570 nm using a spectrophotometer. Cell proliferation of rabbit ASCs over the course of 7 days is shown in Figure 14 with three different initial seeding densities. At 1,000 cells/µL or 100 cells/µL, ASCs proliferated well, whereas at 10,000 cells/µL, a reduction in cell proliferation was seen over time. The Live/Dead Viability/Cytotoxicity Assay (Molecular Probes) was also used to provide a visualization of live and dead cells within the fibrin gel at different time points. The assay is based on the detection of two fluorescent probes (calcein AM for live cells and EthD-1 for dead cells). Briefly, the dye reagents were prepared by adding 5 µL EthD- 1 (2mM stock) and 1.25 µL Calcein AM (40mM stock) to 10 mL of 1xPBS. Two hundred µL of the dye solution was added to each well, and incubated at RT for 30 min. The dye was removed promptly at the end of incubation and replaced with 200 µL of PBS/well. The wells were imaged immediately with a fluorescent/confocal microscope. Representative images are shown in Figure 15. The results indicated that there was a loss of viability for ASCs seeding in high density in fibrin gel over time.

**6. Survival of delivered ASCs in wounds**

ASCs can contribute to wound healing by either cytokine expression or differentiation and repopulation in wounds. It has been thought that conventional infusion of stem cells by injection has limitations such as poor delivery, retention of cells, and cell death because of loss of anchorage. Our data showed that both saline and fibrin delivered ASCs have similar results in keratinocytes migration determined by epithelial gap (Figure 12 & 13). However, higher granulation tissue area was found in wounds where ASCs were delivered in a fibrin vehicle as compared to that of ASCs delivered in saline vehicle. We wanted to determine the survivability of transplanted ASCs in wound using GFPlabeled ASCs (Figure 16). A total of 1×105 ASCs per wounds were delivered as described above with fibrin vehicle in one ear and saline vehicle in the contralateral ear. Wounds were harvested at postoperative day 7 and histological analysis was performed. Five µm thick sections of wounds were deparaffinized in xylene followed by graded alcohols to water and treated with antigen retrieval solution for 20 minutes in a steamer. Endogenous peroxidase activity was blocked with 3% H2O2 for 10 minutes. Mouse anti- GFP (1: 1,000 dilution, Sigma-Aldrich) was used as the primary antibody. Signals were detected using the Vectastain kit (Vector laboratories, Burlingame, CA) and visualized using 3,3'-diaminobenzidine (DAB). As illustrated in Figure 16, GFP signal was found in the transplanted wounds where ASCs were delivered either by saline (Figures 16 A, B, and C) or fibrin (Figures 16A', B', and C'). In order to draw a conclusion, more wound samples are needed for the statistical analysis of survival or proliferation ratio of ASCs delivered with vehicles, fibrin vs. saline, in wounds at postoperative day 7.

In summary, ASCs both in saline and in fibrin were survived in wounds 7 days after transplantation. Though more granulation areas were found in fibrin treated wounds, there were not significant differences in epithelialization, which is the most important parameter in wound healing, between fibrin vs. saline carried ASCs. Several potential problems might be found in fibrin as a ASCs delivery vehicle in rabbit wounds; 1) fibrinogen and thrombin are human origin, which may evoke inflammation, 2) purify and quality of fibrinogen and thrombin will not be same among vendors, 3) though we used conditions based on our previous publication [11], in which fibroblasts were used, optimum condition of fibrinogen and thrombin for ASCs can be different. Thus, we will use saline as a vehicle of ASCs in wound healing study.

**7. Determining the optimal delivery vehicle for ASCs and their survival in hypertrophic scar**

$1\times10^5$ ASCs was delivered in either the fibrin vehicle (Haemacure Corporation or Sigma-Aldrich) or saline to each ear wound. Wounds in one of the ear in the animal would receive ASCs in fibrin whereas a similar amount of cells in saline was given to each wound of the contralateral ear. A total of 2 rabbits were used in this preliminary study. In order to observe the effects of treatment to scar, wounds are observed over a 28-day period. The experiment was initiated in the middle of

June. Wounds from two animals will be harvested at postoperative day 28 when hypertrophic scar is matured. The scar elevation index (SEI) will be measured to quantify the formation of hypertrophic scar. The SEI is a ratio of total scar area [area of newly formed dermis (neodermis) to the estimated area of unwounded dermis (non-scarred dermis)]. An SEI of 1 indicates that the wound healed essentially flat, with no scar hypertrophy and an SEI greater than 1 represents a raised, hypertrophic scar. An increasing magnitude in the SEI correlates with increasing scar prominence over the level of unwounded tissue. Wounds from two animals will be harvested in the middle of July 2011. In addition, to examine the effect of fibrin vehicle alone in the formation of scarring, fibrin or saline was treated without ASCs in wounds of rabbit ears. Wounds from two rabbits will be harvested at postoperative day 28 (middle of July 2011) and analyzed. ASCs can contribute to reducing hypertrophic scarring formation by either cytokine expression or differentiation and repopulation in wounds. Therefore, it is important to determine the survivability of ASCs in wounds over the course of 28 days. A preliminary experiment was initiated in the middle of June. A total of $1\times10^5$ GFP expressing ASCs per wounds were delivered as described above with fibrin vehicle in one ear and with saline vehicle in the contralateral ear of one rabbit. Wounds will be harvested and expression of GFP will be analyzed.

## IV. Construction and optimization of materials for animal experiments

### 1. Construction of living color protein expressing rabbit cells

ASCs, DFs, or rabbit dermal fibroblast cell line (CRL1414, ATCC) were labeled with green fluorescence protein (GFP) or red fluorescent protein (DsRed2) to determine the survival rate and fate of cells which are delivered in wounds. To stably express GFP (or DsRed2), ASCs were transduced with a lentivirus (LV-GFP or LV-DsRed2) in which GFP (or DsRed2) expression is driven by a cytomegalovirus (CMV) promoter (Figure 16). Briefly, 2 multiplicity of infection (MOI) of lentivirus was infected to cells in the presence of 6 g/ml of polybrene. Transduced cells were selected by treating 10 g/ml of blasticidin. We observed some ASCs which do not express GFP, though they grew in the presence of blasticidin (Figure 17). Thus, living color expressing cells were further selected by flow cytometry.

#### A. Construction of firefly luciferase (Fluc) expressing rabbit ASCs

To study topological distribution and quantitative analysis of delivered ASCs survival, Fluc was stably expressed in ASCs using lentivirus as described above (LV-Fluc, Figure 16). We used a bicistronic lentiviral vector (pLVX-IRES-ZsGreen1, Clontech, Mountain View, CA) in which Fluc and ZsGreen1 is expressed by CMV promoter and internal ribosome entry site (IRES), respectively (Figure 18). ASCs were infected with the lentivirus and ZsGreen1 expressing cells were selected by flow cytometry.

#### B. Optimization of immunohistochemical conditions for the study of molecular mechanism of wound healing and hypertrophic scar by MSCs treatment

The rabbit ear hypertrophic scar model has a number of parameters which behave in a similar fashion to that of human hypertrophic scar [20-24]. The model has the advantage of easy quantification of epithelialization and granulation tissue formation. In addition, the ability to create large numbers of wounds and relatively short time points for evaluation of hypertrophic scar (28-35 days) is a unique advantage of the rabbit ear model. This facilitates the determination of the role of stem cell therapy in acute and scarring wounds using the same animal model but by evaluating the wounds at different time points.

The disadvantages of working with rabbits are the lack of available published gene sequences, antibodies, and other probes as compared to rats and mice. However, the Broad Institute has completed a deep coverage (7x) draft of the rabbit genome (*Oryctolagus cuniculus*, OryCun2.0, released August, 2009). Annotation of OryCun2.0 by the National Center for

Biotechnology Information (NCBI) is available in Map Viewer. It has been suggested that MSCs suppress immune reactions and have reduced histocompatability antigens. In addition, allogeneic and xenogeneic therapeutics have been considered because they have reduced expression of histocompatibility antigens and secrete immunoregulatory molecules [25-29]. At present, inflammatory reactions induced by exogenous MSCs in transplanted host has not been well characterized yet. We have optimized the immunohistochemistry conditions to detect for the presence of neutrophils (Figure 19A) and macrophages (Figure 19D) in rabbits in order to study the potential immune reactions to transplanted MSCs in rabbit ear wounds. MSCs can contribute to wound healing and hypertrophic scarring by either cytokine expression or differentiation to specific cells in wounds. We detected GFP signals after 7 days transplantation of ASCs in wounds. However, non-proliferating ASCs might still have GFP positive signal because GFP is stable and exhibits a long half-life. To address proliferation of transplanted MSCs in wound, we have optimized the immunohistochemistry conditions for the detection of Ki67 (Figure 19B) in rabbits. In addition, detection of an endothelial
marker, CD31, has also been optimized (Figure 19C).

## V. Cytokine Expression Profile of Rabbit and Human MSCs

The cytokine secretion profile of rabbit and human MSCs was examined by analyzing conditioned media (CM) samples collected from each cell type via enzymelinked immunosorbent assay (ELISA). CM was prepared by incubating cells for up to 72hr in culture. Since there is a shortage of rabbit specific reagents, we resorted to commercially available human ELISA kits (R&D Systems, RayBiotech, Millipore) to measure the secretion of factors that have high percentage of homology between human and rabbit.

Under basal conditions, the expression of Transforming Growth Factor (TGF)-β1 was similar among rabbit ASCs and BMSCs, whereas the expression was significantly lower in DFs. No significant differences in the expression of TGF-β2 were found. Furthermore, TGF-β3 was not detected in both rabbit and human MSCs. Vascular Endothelial Growth Factor (VEGF) was detected in rabbit and human ASCs, BMSCs, and DFs cultured under normal conditions. The expression of VEGF was up-regulated in cells cultured in hypoxic conditions (1% O2) (data not shown).

Current and future efforts will include analysis of other angiogenic and proinflammatory factors such as HGF, bFGF, IL-6 and TNF-α. Table 1 is a summary of our current findings and future efforts.

**Table 1 Cytokine Expression Profile of Rabbit and Human MSCs**

| Cytokines* | Rb ASC[1] | Rb BMSC[2] | Rb DF[3] | hASC[4] | hBMSC[5] | hDF[6] |
|---|---|---|---|---|---|---|
| **TGF-$\beta_1$** | ++ | ++ | +[§] | ++ | ++ | + |
| **TGF-$\beta_2$** | + | + | + | + | + | + |
| **TGF-$\beta_3$** | - | - | - | - | - | - |
| **VEGF** | + | + | + | + | + | + |
| **bFGF[¥]** | TBD[€] | TBD | TBD | TBD | TBD | TBD |
| **HGF[¥]** | TBD | TBD | TBD | TBD | TBD | TBD |
| **EGF[¥]** | TBD | TBD | TBD | TBD | TBD | TBD |
| **IL-6[¥]** | TBD | TBD | TBD | TBD | TBD | TBD |
| **TNF-α[¥]** | TBD | TBD | TBD | TBD | TBD | TBD |

* Conditioned media were collected from cultured cells after 72 hour of incubation at 37$^{O}$C in 5% $CO_2$.
1: Rabbit adipose-derived mesenchymal stem cell; 2: Rabbit bone marrow-derived mesenchymal stem cell; 3: Rabbit dermal fibroblast; 4: Human adipose-derived mesenchymal stem cell; 5: Human bone marrow- derived mesenchymal stem cell; 6: Human dermal fibroblast.
§ +: presence of test cytokines.
¥ Growth Factor; HGF:Hepatocyte Growth Factor; EGF: Epidermal Growth Factor; IL 6; Interleukin-6; TNF-α:Tumor Necrosis Factor - α.
€ TBD:To Be Determined.

## Figures and Tables

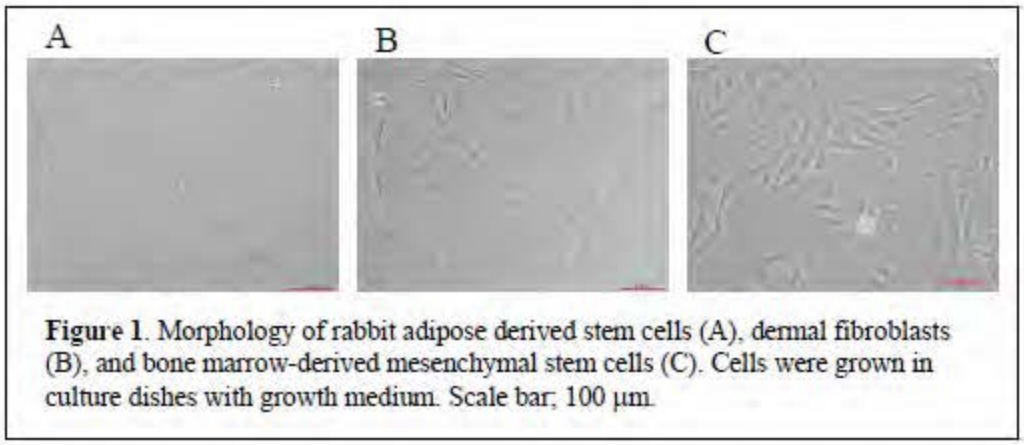


**Figure 1**. Morphology of rabbit adipose derived stem cells (A), dermal fibroblasts (B), and bone marrow-derived mesenchymal stem cells (C). Cells were grown in culture dishes with growth medium. Scale bar; 100 µm.

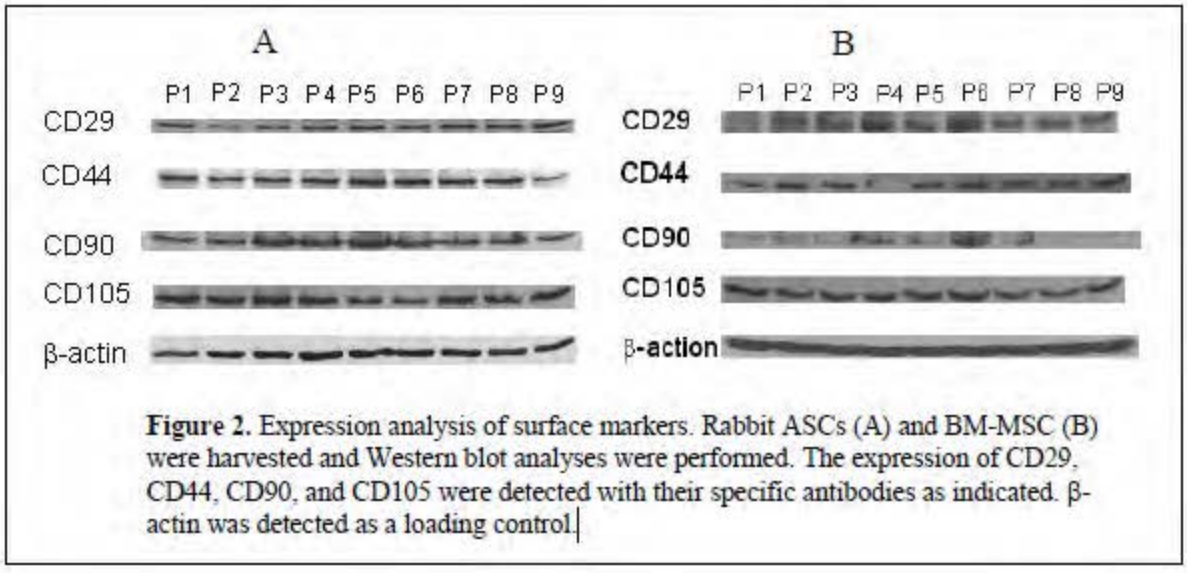


**Figure 2.** Expression analysis of surface markers. Rabbit ASCs (A) and BM-MSC (B) were harvested and Western blot analyses were performed. The expression of CD29, CD44, CD90, and CD105 were detected with their specific antibodies as indicated. β-actin was detected as a loading control.

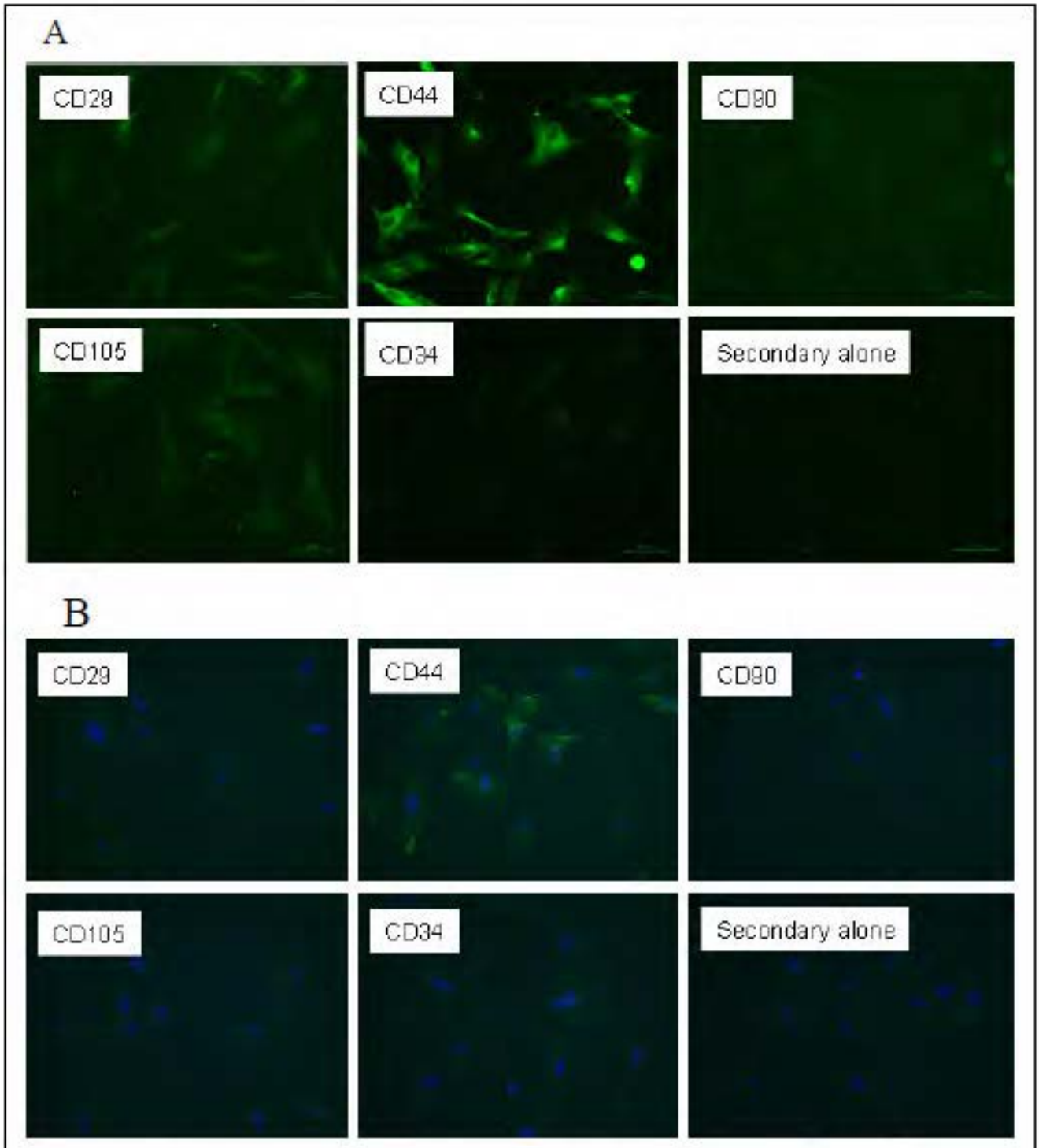


**Figure 3.** Expression analysis of surface markers. Rabbit ASCs at passage 1 (A) and BM-MSC at passage 2 (B) were cultured *in vitro* and immunostaining was performed. The expression of CD29, CD44, CD90, CD105, and CD44 were detected with their specific antibodies as indicated and Alexa Fluor 488 conjugated secondary antibodies were used to visualized the signal. Nuclei were stained with DAPI in B. Signals were captured with the same exposure time in each panel.


**Figure 4.** Adipogenic differentiation of MSCs. Rabbit ASCs (A), DFs (B), and BM-MSC (C) were cultured in adipogenesis differentiation medium for 8 days. Oil Red O staining was performed to detect lipid accumulation. Nuclei were stained with Hematoxylin.

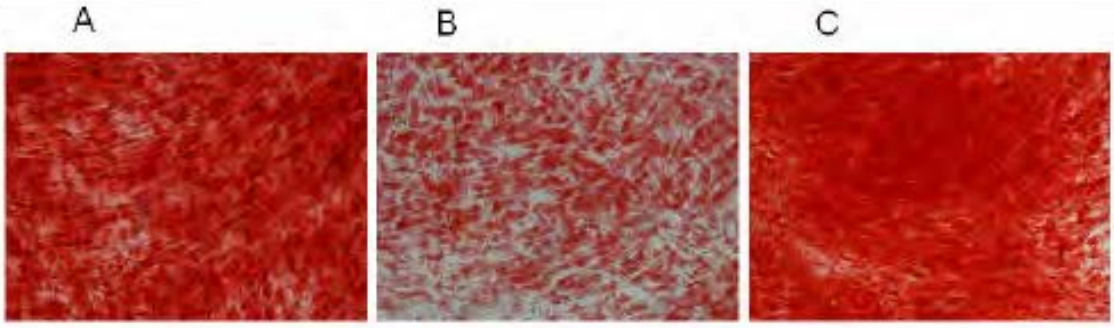


**Figure 5.** Osteogenic differentiation of MSCs. Rabbit ASCs (A), DFs (B), and BM-MSC (C) were cultured in osteogenesis differentiation medium for 35 days. Alizarin Red S staining was performed to detect calcium accumulation.

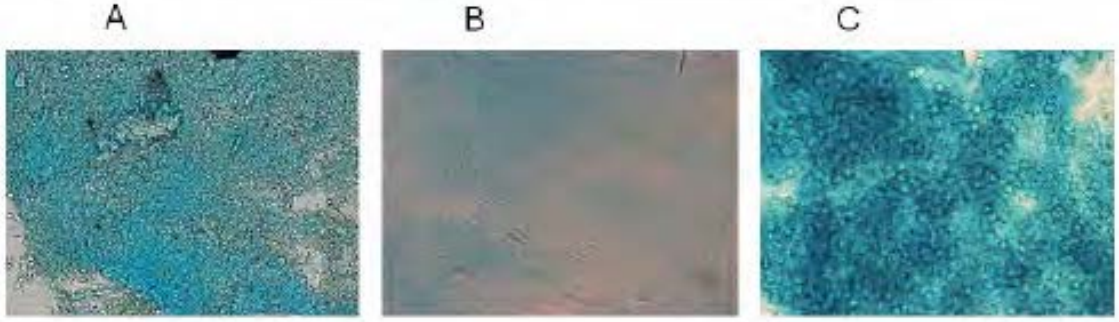


**Figure 6.** Chondrogenic differentiation of MSCs. Rabbit ASCs (A), DFs (B), and BM-MSC (C) were cultured in chondrogenesis differentiation medium for 21 days. Alician Blue staining was performed.

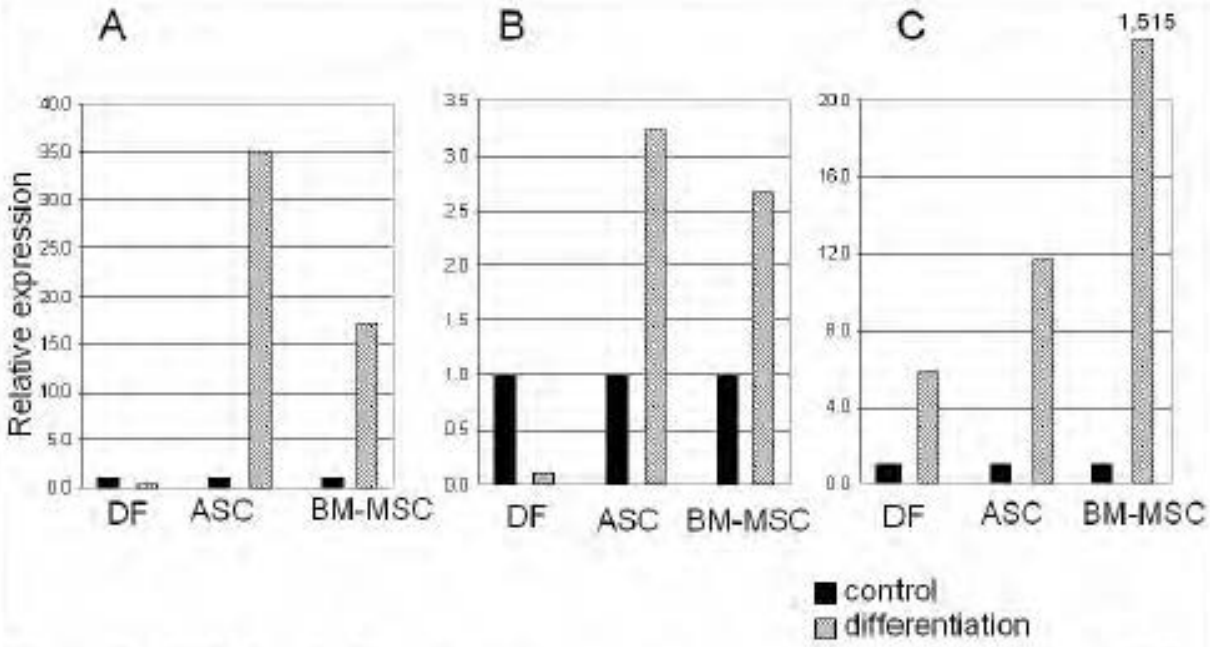


**Figure 7.** mRNA level of lineage specific genes was increased by differentiation. DFs, ASCs, and BM-MSCs were grown in adipogenic (A), osteogenic (B), or chondrogenic (C) medium for 8, 28, or 21 days. Total RNAs were isolated and quantitative real-time PCR was performed. Expression of adiponectin (A), osteopontin (B), and Col10a1 (C) was analyzed. Each gene expression was normalized according to the expression level of GAPDH. The level of gene expression in cells cultured in differentiation medium was compared to cells in cultured non-differentiated medium, which was set at 1.

**Figure 8.** A photograph of rabbit ear wounds at harvest. Fibrin sealant or saline was applied to 7 mm wounds in ear on the day of surgery (postoperative day 0). Wounds were harvested at postoperative day 7.

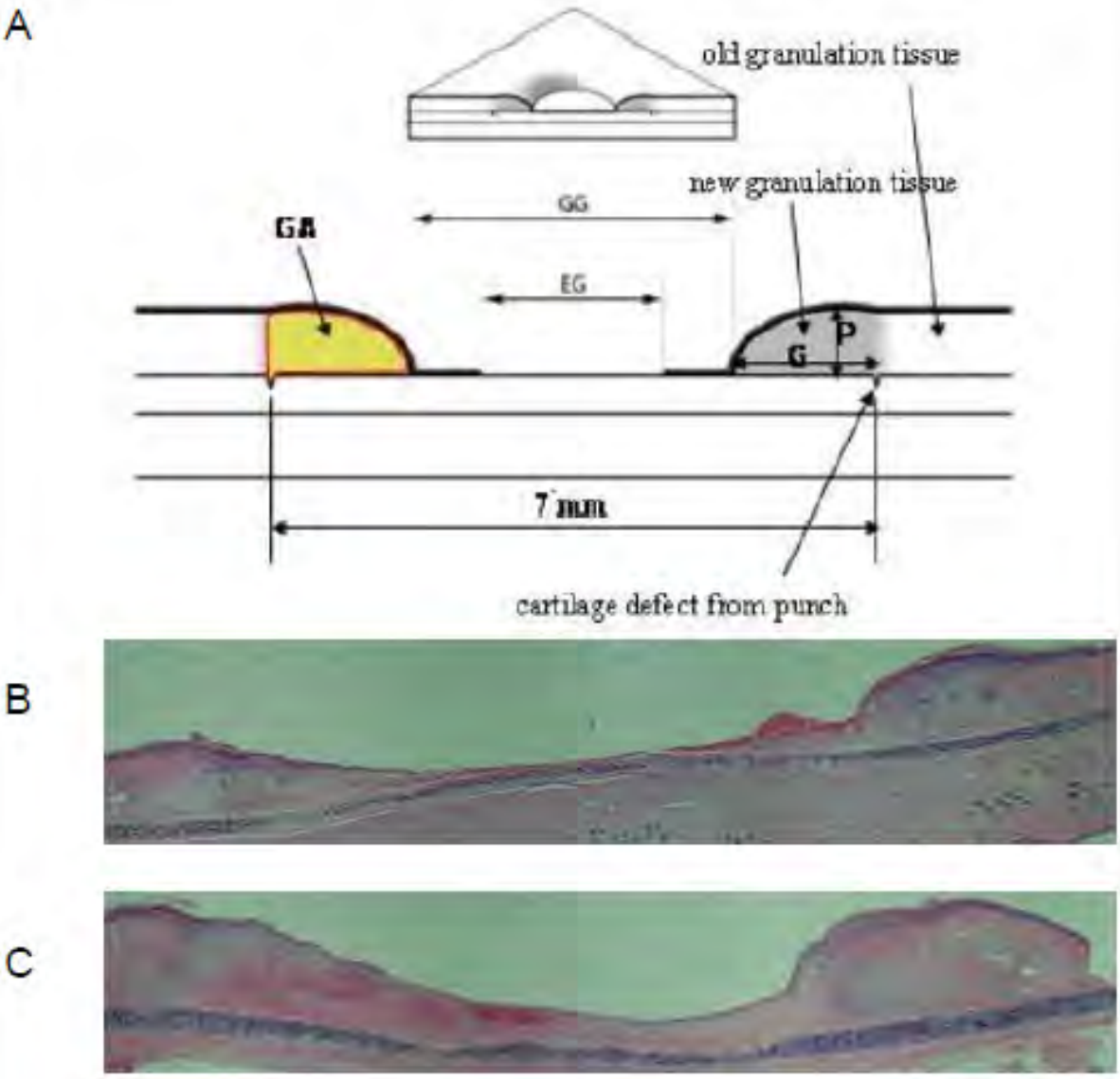


**Figure 9.** Schematic drawing of histological analysis. (A) EG, epithelial gap; GG, granulation gap; G, new granulation tissue distance; P, height of granulation tissue; GA, granulation area. (B, C) H&E staining of rabbit wounds 7 days after ASCs treatment either in saline (B) or in fibrin (C).

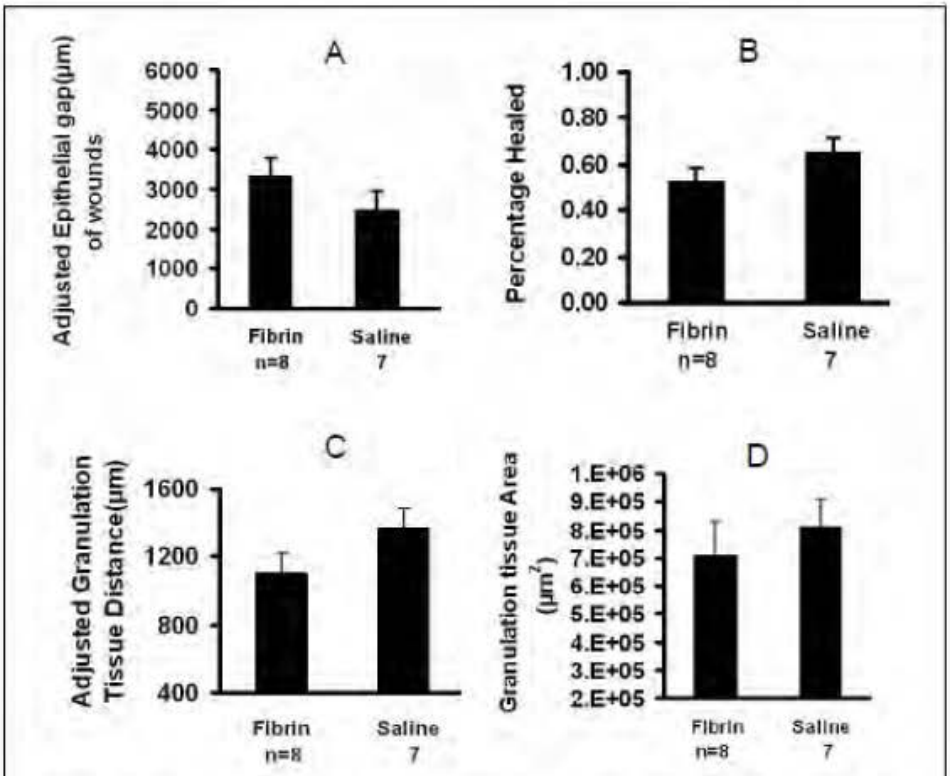


**Figure 10.** Histological quantification of fibrin vs. saline treated wounds. Wounds (7 mm) were analyzed for adjusted epithelial gap (A), percentage healed (B), adjusted granulation tissue distance (C), and granulation tissue area (D) at the postoperative day 7 harvest date. Data shown as mean ± SEM.

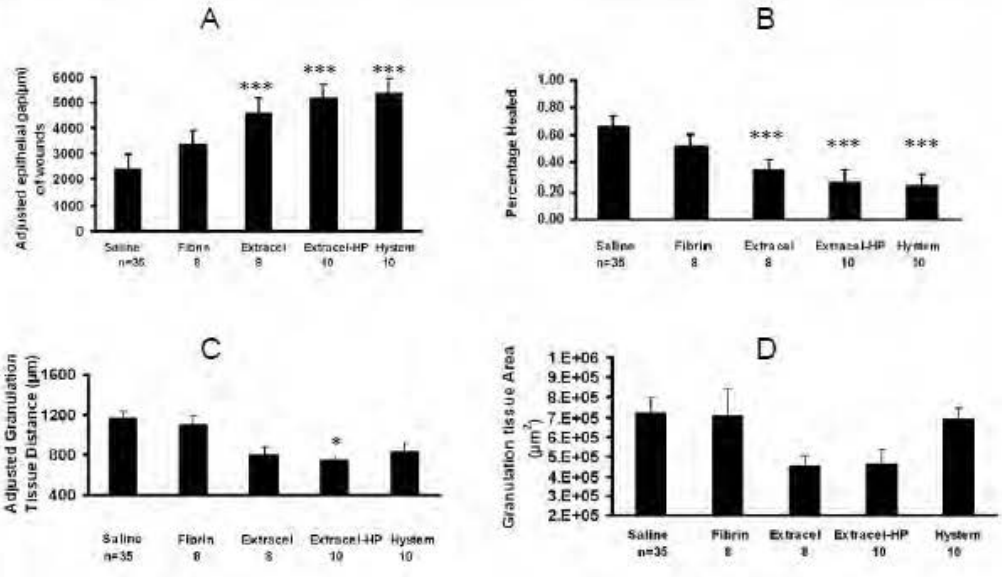


**Figure 11.** Histological quantification of vehicles treated wounds. Fibrin, Extracel, Extracel-HP, and Hystem treated wounds (7 mm) were compared to saline treated wounds at the postoperative day 7 harvest date. Adjusted epithelial gap (A), percentage healed (B), adjusted granulation tissue distance (C), and granulation tissue area (D) are shown. Data shown as mean ± SEM. ***$p<0.001$, *$p<0.05$

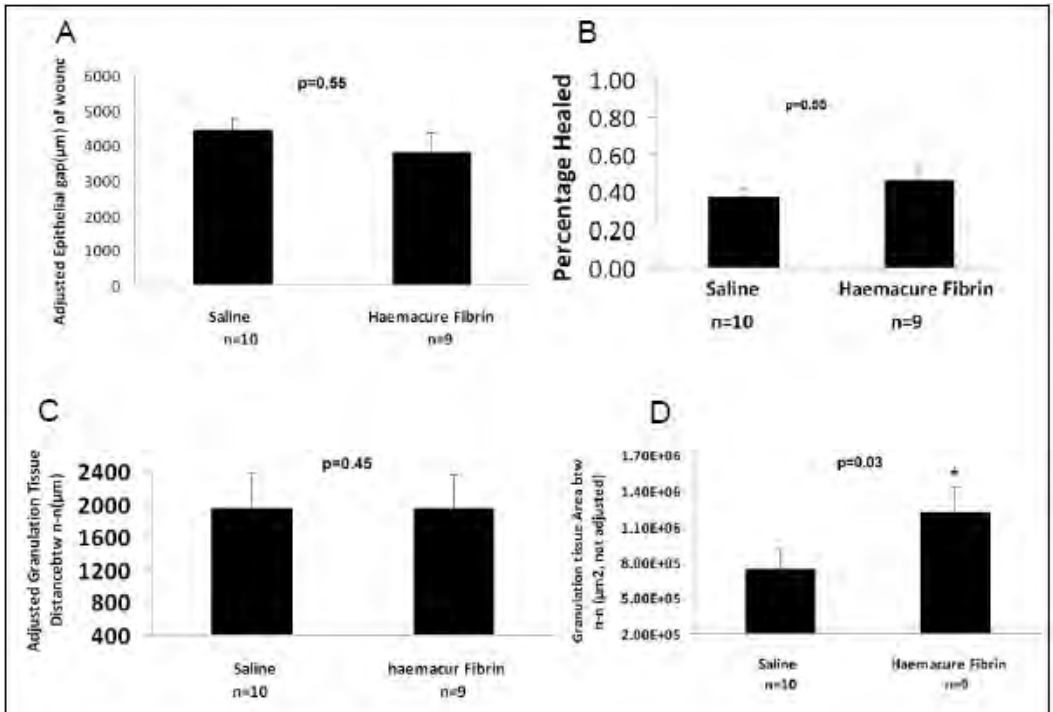


**Figure 12.** Histological quantification of ASCs treated wounds. ASCs at a concentration of 1 X $10^5$ were delivered to 7 mm wounds with Haemacure fibrin or saline. Wounds were harvested at the postoperative day 7 harvest and adjusted epithelial gap (A), percentage healed (B), adjusted granulation tissue distance (C), and granulation tissue area (D) were measure. Data shown as mean ± SEM. *p<0.05

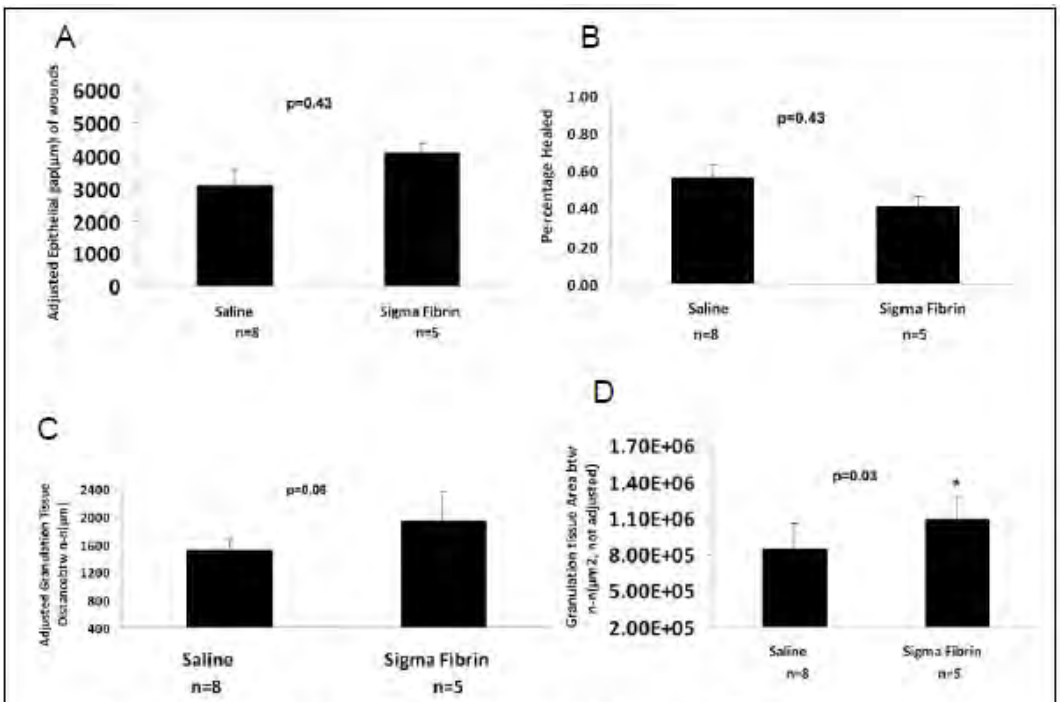


**Figure 13.** Histological quantification of ASCs treated wounds. ASCs at a concentration of 1 X $10^5$ were delivered to 7 mm wounds with Sigma-Aldrich fibrin or saline. Wounds were harvested at the postoperative day 7 harvest and adjusted epithelial gap (A), percentage healed (B), adjusted granulation tissue distance (C), and granulation tissue area (D) were measure. Data shown as mean ± SEM. *p<0.05

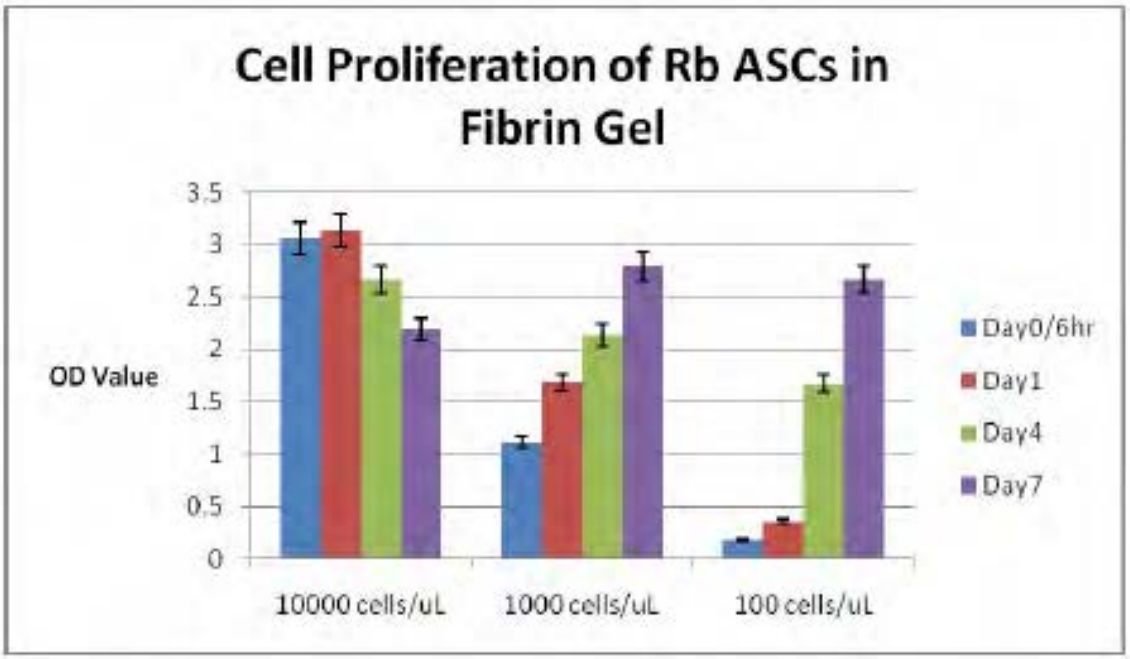


**Figure 14.** Cell proliferation of rabbit ASCs in fibrin gel over the course of 7 days with three different initial seeding densities (10,000 cells/μL, 1,000 cells/μL, and 100 cells/μL).


**Figure 15.** Representative images of live cells (green) and dead cells (red) in fibrin sealant at Day 7 (Zeiss LSM 710; magnification = ×100).

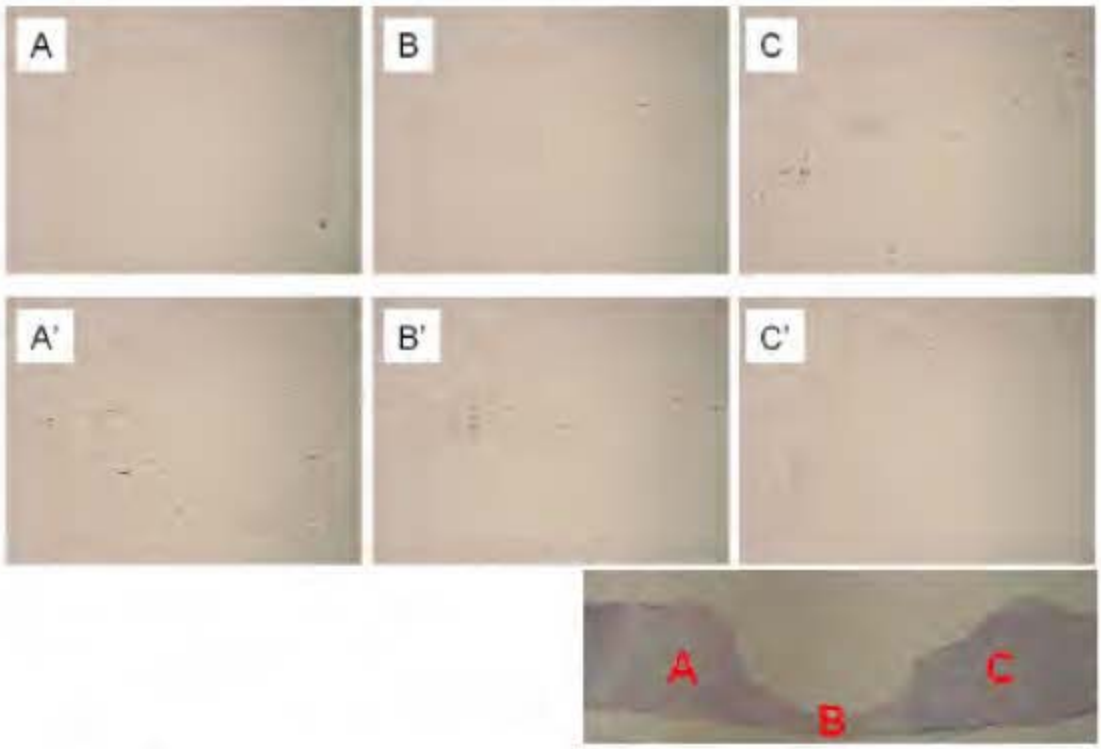


**Figure 16.** Detection of transplanted ASCs in rabbit ear wounds. GFP expressing ASCs at a concentration of 1 X $10^5$ were delivered to 7 mm wounds with saline (A, B, C) or fibrin (A', B', C'). At postoperative day 7 wounds were harvested, expression of GFP was visualized by immunohistochemistry. The analyzed areas were shown in a picture on the bottom which is stained with hematoxylin.

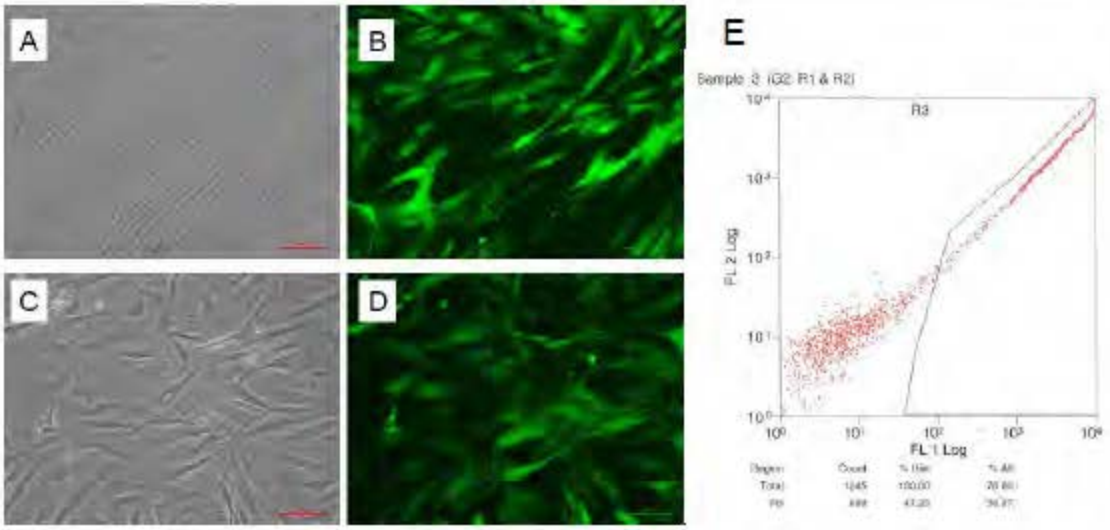


**Figure 17.** GFP-expressing rabbit ASCs. (A, B) ASCs were transduced with GFP-expressing lentivirus and cultured in the presence of selection marker, blasticidin. GFP negative cells were detected though they are resistant to blasticidin [compare bright image (A) and fluorescence image (B)]. (C, D) Most of the ASCs in bright field (C) showed GFP fluorescence (D) after flow cytometry. (E) An example of flow cytometry is shown. Approximately, 47% of ASCs express GFP before in the population before isolation by flow cytometry

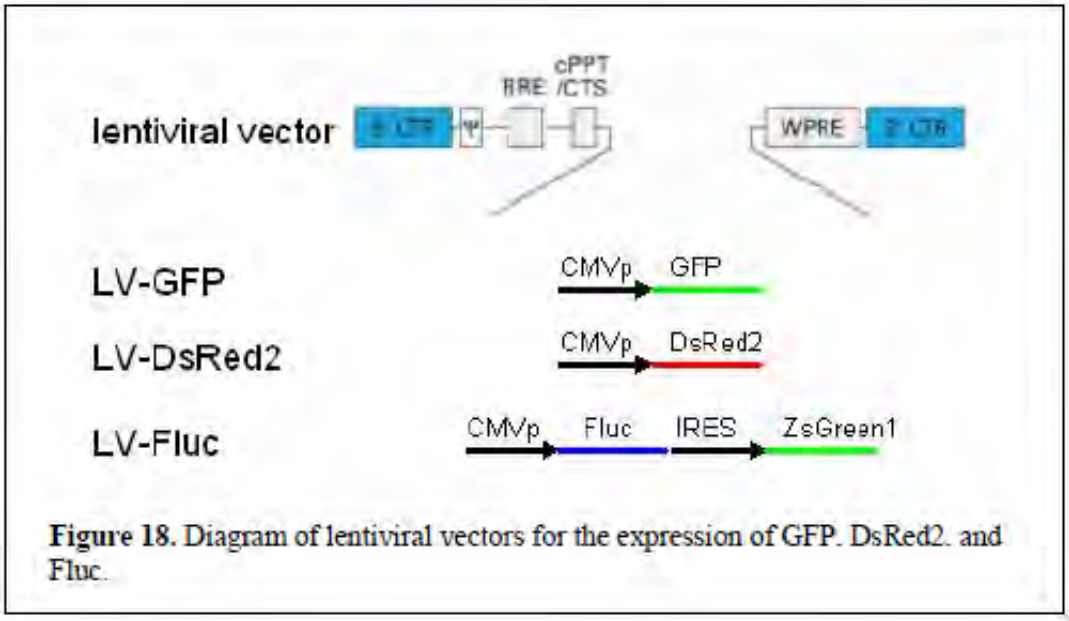


**Figure 18.** Diagram of lentiviral vectors for the expression of GFP. DsRed2. and Fluc.

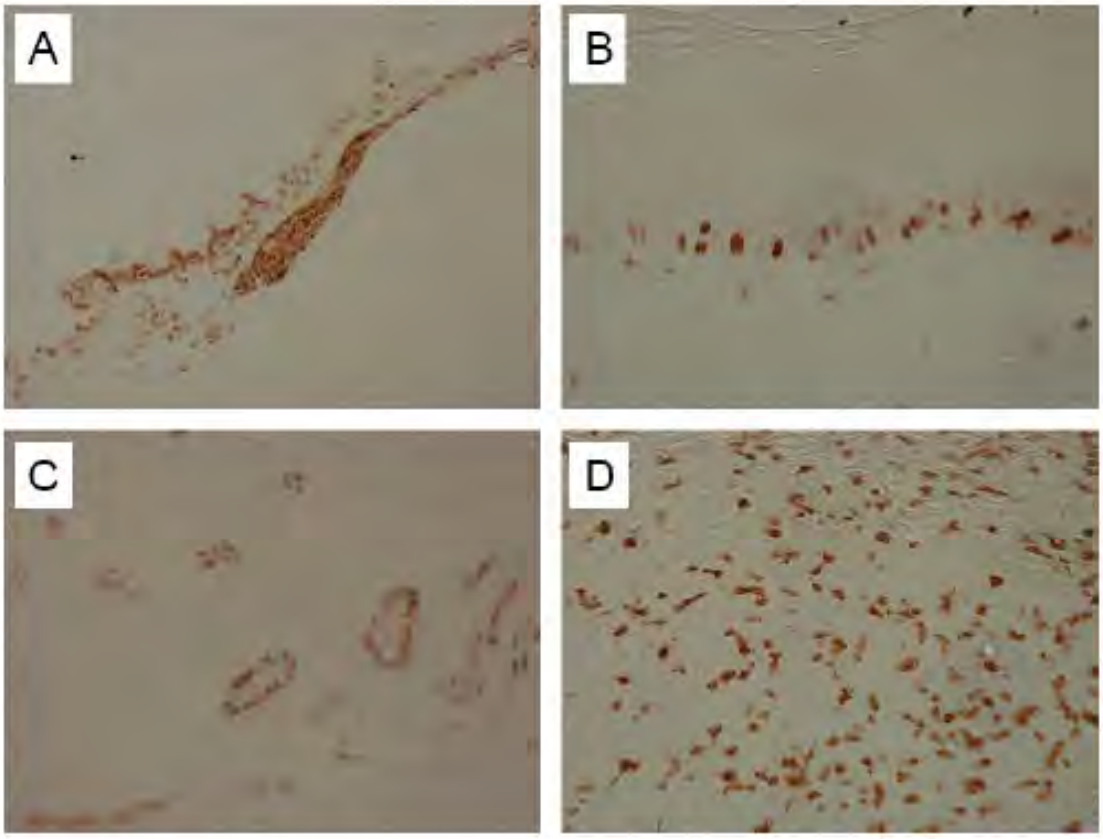


**Figure 19.** Optimization of immunohistochemitry condition to detect target proteins in rabbit ears. Paraffin embedded tissues were sectioned with 5 μm thickness and processed to incubated antibodies. Anti-neutrophil (A, 1: 1,000 dilution, Santa Cruz Biotechnology), anti-Ki67 (B, 1: 1,000 dilution, BD Biosciences), anti-CD31 (C, 1: 100 dilution, Abcam), and anti-macrophage (D, 1: 1,000 dilution, Abcam) were used as primary antibodies. Signal was visualized by DAB. Magnification A; ×200, B-D; ×400.

Year 2

## I. Effect of rabbit MSCs on wound healing.

### 1. Determination of the optimal number of rabbit adipose-derived stem cells (ASCs) to promote wound healing

We treated wounds with different amounts of ASCs to determine the optimal quantity to promote wound healing. Saline was used as the vehicle to deliver ASCs. Previous work in the laboratories has shown that the use of fibrin sealant and hydrogels as vehicles do not have added any beneficial effects in promoting wound healing. An early passage (P3) ASCs was used in these experiments. This is to avoid changes of ASC surface markers due to repetitive *in vitro* sub-culturing. ASCs were harvested, washed in PBS to remove cell culture medium, and re-suspended in PBS. Three different amounts of ASCs -3 x $10^5$, 1 x $10^5$, and 3 x $10^4$ - in 7 µl of PBS- were delivered to each 7 mm wound of one of the ears. In the contralateral ear, 7 µl of PBS was delivered to each wound as a control. Wounds were harvested at Post-operative Day (POD) 7 and wound healing parameters such as epithelial and granulation tissue distances and areas were digitally quantified from histological sections of the control wounds and wounds that were treated with ASCs.

ASC treated wounds showed increased granulation tissue distance and granulation tissue area when compared to saline treated wounds (Figure 1B, C). Statistical significance of granulation tissue formation was found in wounds treated with the lowest number of ASCs (3 x $10^4$ ASCs). A minor inhibition of keratinocyte migration was observed in wounds that were treated with larger quantities of ASCs (Figure 1A).
However, this minor inhibition of keratinocytes migration was not statistically significant.

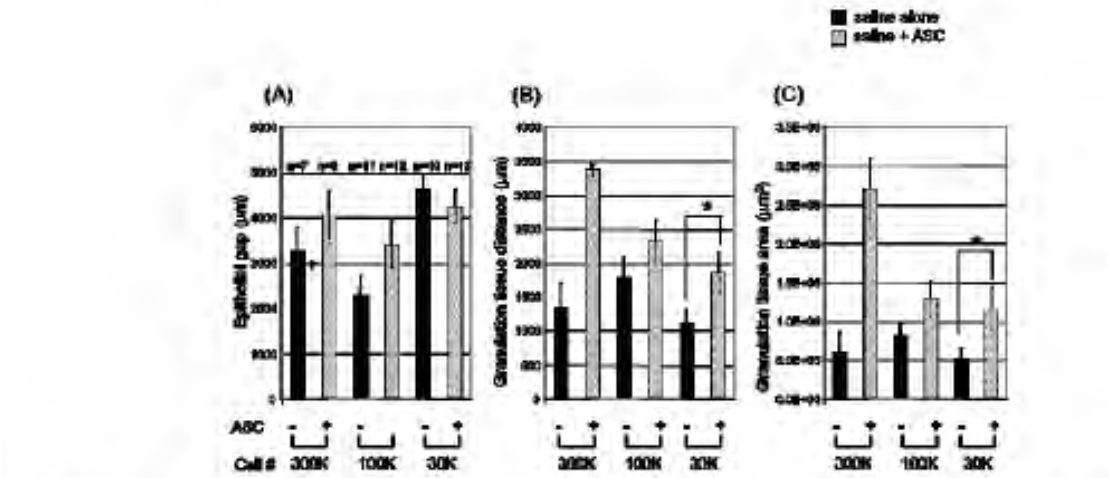


**Figure 1. Histological quantification of ASCs treated wounds.** Three different quantities of ASCs (3 x $10^5$, 1 x $10^5$, or 3 x $10^4$) in PBS were delivered to each 7 mm wound of one ear in each test animal. In the contra lateral ear, PBS alone was delivered as a control. Wounds were harvested at POD 7 and epithelial gap (A), granulation tissue distance (B), and granulation tissue area (C) were measured. Data were shown as mean ± SEM. *p<0.05.

To determine the dose of ASCs which does not inhibit epithelialization yet able to increase granulation tissue formation, wounds on each one of the ear in the test animals were treated with either 1 x $10^5$ ASCs or 3 x $10^4$ ASCs. Wounds transplanted with 1 x $10^5$ ASCs (n=11) had similar epithelial gaps (Figure 2A, 4,351 ± 423 µm) as compared to wounds with 3 x $10^4$ ASCs (n=12, 4,085 ± 322 µm). However, wounds treated with 1 x $10^5$ ASCs showed a greater granulation tissue distance (Figure 2B, 1,944 ± 315 vs. 1,454 ± 221 µm, p = 0.054) and the granulation tissue area (Figure 2C, 1,482,334 ± 214,419 vs. 950,926 ± 128,948 µm$^2$,9).

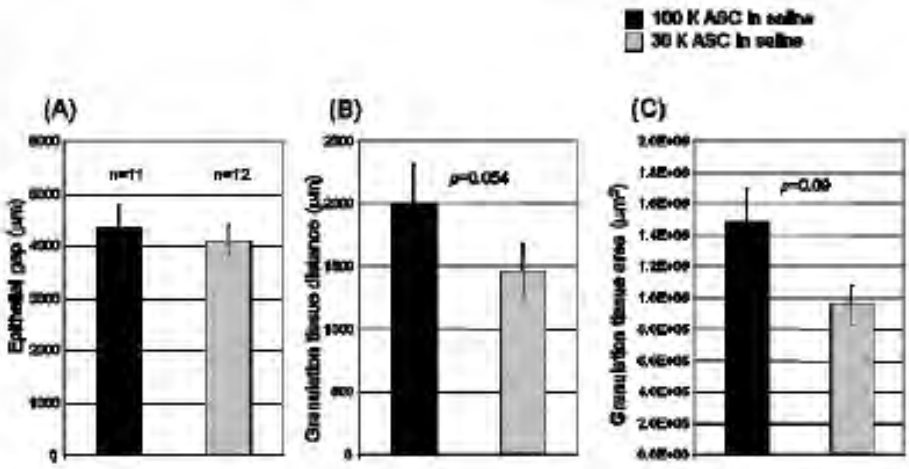


**Figure 2. Histological quantification of ASC-treated wounds.** 1 x $10^5$ ASCs were delivered to 7 mm wounds on one of the ears and 3 x $10^4$ ASCs were delivered to wounds on the contralateral ear of the test animals. Wounds were harvested at POD7 and epithelial gap (A), granulation tissue distance (B), and granulation tissue area (C) were measured. Data were shown as mean ± SEM.

It has been shown that ASCs secrete many cytokines and growth factors which are known to promote wound healing. We investigated whether ASCs can promote wound healing by the expression of these factors without proliferation or transdifferentiation to other cells. ASCs were treated with 10 µg/ml of Mitocmycin C (MitC) for 3 hours *in vitro* before harvest for application to wounds. Because MitC- treated ASCs are viable but unable to proliferate, higher concentration of ASCs was delivered to wounds to ensure an adequate secretion of growth factors. Histological analysis showed that wounds with MitC-treated ASCs had decreased granulation tissue distance (data not shown) and granulation tissue area (Figure 3B). Interestingly, increased epithelialization was found in wounds containing 1 x $10^5$ MitC-treated ASCs versus wounds containing 1 x $10^5$ of ASCs without MitC (Figure 3A; 4,258 ± 335 µm vs. 3,060 ± 489 µm, respectively; p =0.07).

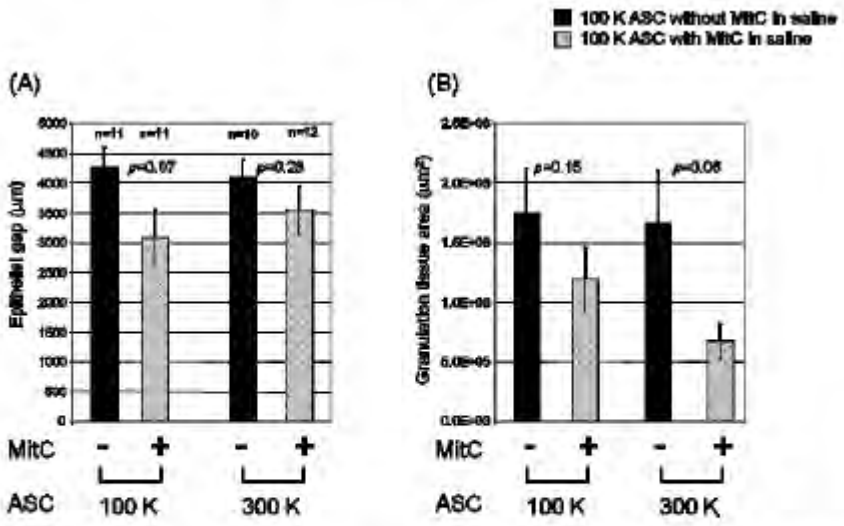


**Figure 3. Histological quantification of wounds treated with growth-arrested ASCs.** ASCs (1 x $10^5$ or 3 x $10^5$ per 7 mm wound) were treated with MitC (10 µg/ml) for 3 hours *in vitro* before delivery to wounds. ASCs without MitC treatment were delivered to wounds on the contralateral ear of each teat rabbit for comparison. Wounds were harvested at POD7 and epithelial gap (A) and granulation tissue area (B) were measured. Data were shown as mean ± SEM.

A. **Effects of rabbit mesenchymal stem cells (MSCs) on wound healing**

We determined that saline was the optimal MSC delivery vehicle and 1 x $10^5$ ASCs was the optimum number of ASCs to promote wound healing. To increase the power of statistical analyses, we increased the number of animals (and wounds) and compared the treated versus control wounds on the same animal to minimize the effects of rabbit-to-rabbit variation in wound healing.

**2.1 Effects of ASCs on wound healing**

P3 ASCs were harvested, washed in PBS, and resuspended in PBS. 1 x $10^5$ ASCs in 7 µl of PBS were delivered to each 7mm wound on one of the ears in rabbits. PBS (7µl; control) was applied to wounds on the contralateral ear. Wounds were harvested at POD7. Treatment with ASCs (n=36) did not affect epithelialization when compared to saline treated wounds (n=35) (Figure 4A; 3,913 ± 259 µm vs. 4,026 ± 306 µm, respectively; p =0.8). However, granulation tissue distance (1,748 ± 165 µm vs. 1,170 ± 147 µm, respectively, p <0.01) and granulation tissue area (1,133,933 ± 135,864 µm$^2$ vs. 503,530 ± 71,984 µm$^2$ ; p <0.001) were significantly increased by ASCs treatment (Figure 4B, C).

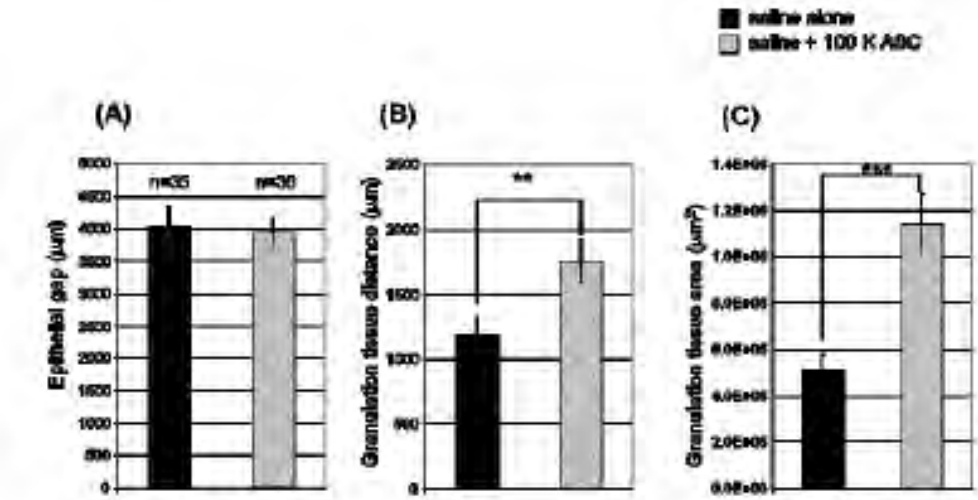


**Figure 4. Histological quantification of ASCs treated wounds.** 1 x $10^5$ ASCs in PBS was delivered to the 7 mm wounds. PBS alone was used as the vehicle control. Wounds were harvested at POD7 and epithelial gap (A), granulation tissue distance (B), and granulation tissue area (C) were measured. Data were shown as mean ± SEM. **p<0.01, ***p<0.001.

**2.2. Effects of bone marrow (BM) derived-MSCs on wound healing**

P3 BM-MSCs were harvested, washed in PBS, and resuspended in PBS. Each 7 mm wound of one of the ears of animals was treated with 1 x $10^5$ BM-MSCs in 7 µl of PBS. In the contralateral ear, 7 µl of PBS was delivered to each wound as a control.

Wounds were harvested at POD7. Treatment with BM-MSCs (n=20) inhibited epithelialization as compared to saline-treated wounds (n=17) (Figure 5A, 4,552 ± 243 µm vs. 2,765 ± 360 µm, respectively; p <0.01). Granulation tissue distance (2,283 ± 249 µm vs. 1,435 ± 212 µm, respectively; p <0.001) was increased in the treated wounds, although granulation tissue area (1,152,142 ± 133,463 µm$^2$ vs. 961,843 ± 322,652 µm$^2$ respectively; p = 0.72) was not significantly different from that of the control wounds (Figure 5B, C).

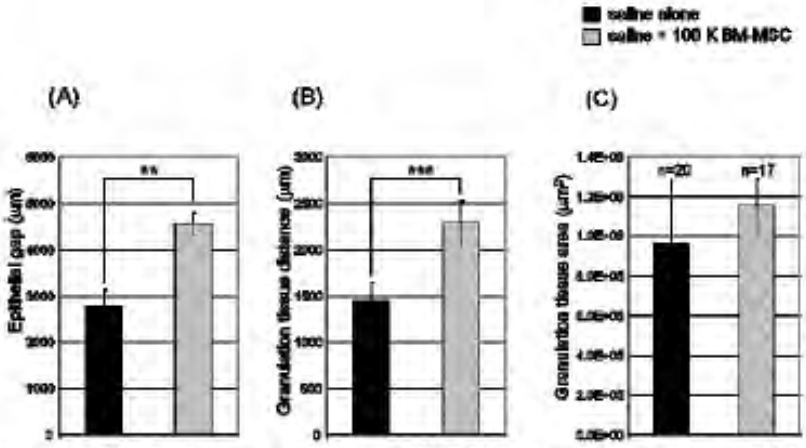


**Figure 5. Histological quantification of BM-MSCs treated wounds.** 1 x $10^5$ BM-MSCs in PBS was delivered to each 7 mm wound. PBS was used as the treatment control. Wounds were harvested at POD7 and epithelial gap (A), granulation tissue distance (B), and granulation tissue area (C) were measured. Data were shown as mean ± SEM. **p<0.01, ***p<0.001.

### 2.3. Effect of dermal fibroblasts (DFs) on wound healing

P3 DFs were harvested, washed in PBS, and re-suspended in PBS. Each 7 mm wound of one the ears was treated with 1 x $10^5$ DFs in 7 µl of PBS. In the contralateral ear, 7 µl of PBS per wound were delivered as a control. Wounds were harvested at POD7. Treatment with DFs (n=24) inhibited epithelialization as compared to saline-treated wounds (n=17) (Figure 6A, 4,279 ± 317 µm vs. 2,304 ± 347 µm, respectively; p <0.01). Neither granulation tissue distance (1,719 ± 244 µm vs. 1,262 ± 153 µm; p = 0.13) nor granulation tissue area (703,357 ± 97,286 vs. 623,852 ± 96,976 $\mu m^2$; p = 0.45) was significantly changed in treated versus control wounds (Figure 6B, C).

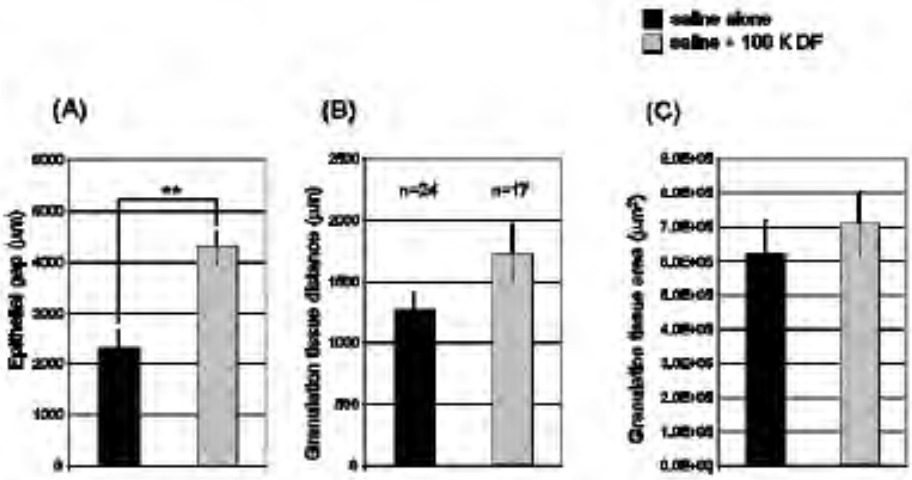


**Figure 6. Histological quantification of DFs treated wounds.** 1 x $10^5$ DFs in PBS was delivered to 7 mm wounds on one ear. In the contralateral ear, PBS alone was delivered as a control. Wounds were harvested at POD7 and epithelial gap (A), granulation tissue distance (B), and granulation tissue area (C) were measured. Data were shown as mean ± SEM. **p<0.01.

### 2.4. Effect of growth-arrested rabbit ASCs (MitC-ASCs) on wound healing

P3 ASCs were treated with 10 µg/ml of MitC for 3 hours, harvested, washed in PBS, and re-suspended in PBS. Each 7 mm wound of one ear was treated with 1 x $10^5$ MitC-treated ASCs in 7 µl of PBS. In the contralateral ear, 7 µl of PBS were delivered to each wound as a control. Wounds were harvested at POD7. Treatment with MitC-treated ASC (n=23) did not affect epithelialization of epidermis when compared to saline treated wounds (n=24) (Figure 7A, 3,426 ± 240 µm vs. 2,873 ± 279 µm, respectively; p =0.17). Neither granulation tissue distance (1,346 ± 155 µm vs. 1,670 ± 194 µm, respectively; p = 0.17) nor granulation tissue area (983,928 ± 248,884 $\mu m^2$ vs. 990,601 ±171,666 $\mu m^2$, respectively; p = 0.93) was significantly changed (Figure 7, C).

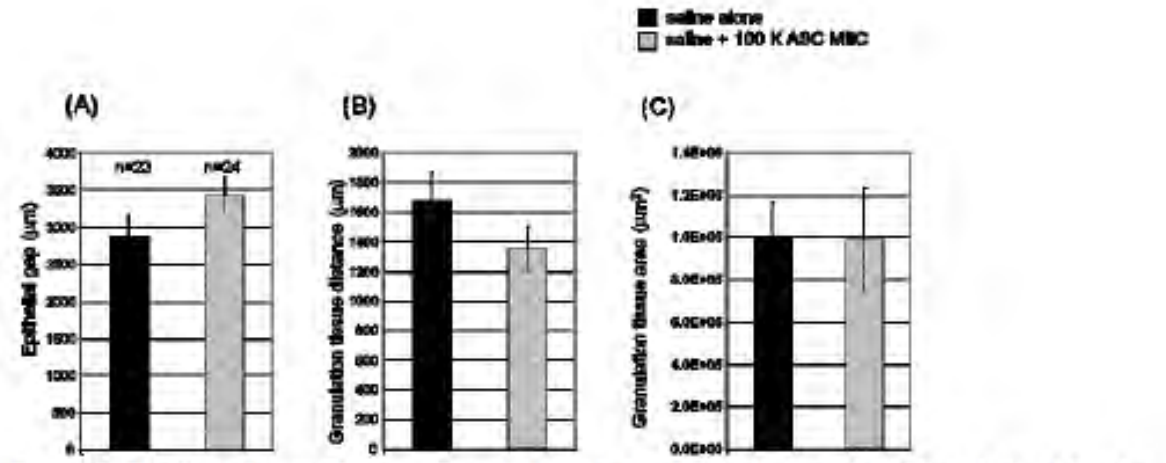


**Figure 7. Histological quantification of wounds treated with growth arrested ASCs (MitC-ASCs).** 1 x $10^5$ MitC-ASCs in PBS was delivered to each of the 7 mm wounds on one ear. In the contralateral ear, PBS alone was delivered as the control. Wounds were harvested at POD7 and epithelial gap (A), granulation tissue distance (B), and granulation tissue area (C) were measured. Data were shown as mean ± SEM.

## 3. Analysis of transplanted rabbit ASCs

### 3.1. Transplanted ASCs exhibit activated fibroblast phenotype

ASCs can contribute to wound healing either by the expression and secretion of cytokines/growth factors or differentiation and repopulation of the wound bed. The fate (or characteristics) of transplanted ASCs was addressed using the green fluorescent protein (GFP)-expressing ASCs (GFP-ASC). A total of 1×$10^5$ GFP-ASCs in saline was delivered as described above. Wounds were harvested at POD 7 and histological analyses were performed. Immunofluorescence staining with chicken anti-GFP antibody showed that transplanted ASCs were evenly distributed in the wound bed and granulation area (Figure 8A & 9A). During the wound repair process, fibroblasts migrate to the wound site and build up granulation tissue by depositing collagen and other extracellular matrices. These activated myofibroblasts are α-SMA (smooth muscle actin) positive. Immunofluorescence staining with mouse anti-α-SMA antibody detected endogenously activated fibroblasts (Figure 8B, B'). Interestingly, the majority of transplanted ASCs showed α-SMA signals (Figure 8C, C', D, D'). We also observed ASCs which do not express α-SMA (arrowhead in Figure 8D').

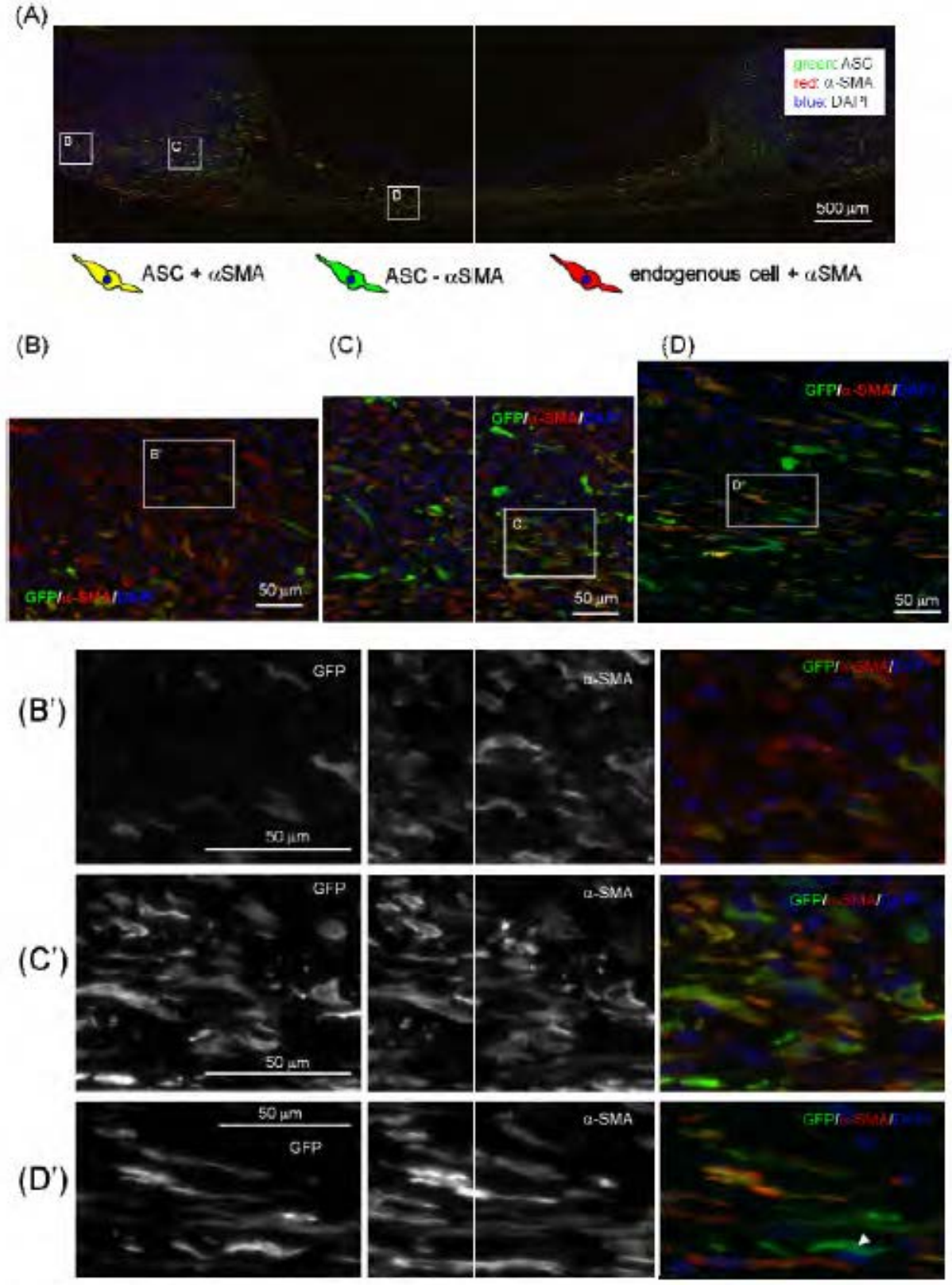


**Figure 8. Transplanted GFP-ASCs express α-SMA in wounds.** Rabbit ear wounds at POD7 were stained with chicken anti-GFP and mouse anti-α-SMA antibodies. Nuclei were stained with DAPI. Merged image of α-SMA (red) and GFP (green) indicates that α-SMA is expressed in ASCs. (A) A lower magnification of the wound. (B-D) Higher magnifications of the indicated regions (white squares) in A.

(B'-D') Higher magnifications of the indicated regions in B-D. Scale bars: 500 μm (A), 50 μm (B, C, D, B', C', D').

We next analyzed the expression of collagen III (Col III), which is produced by myofibroblasts prior to the synthesis of the mechanically stronger collagen I. It has been shown that fetal dermis, which forms less scar upon injury, has elevated level of Col III. Expression of Col III was detected outside of the wounding area (Figure 9B). Expression of Col III was also detected in the wound bed (Figure 9C, C') and granulation tissue (Figure 9D, D'), though the signal was weak.

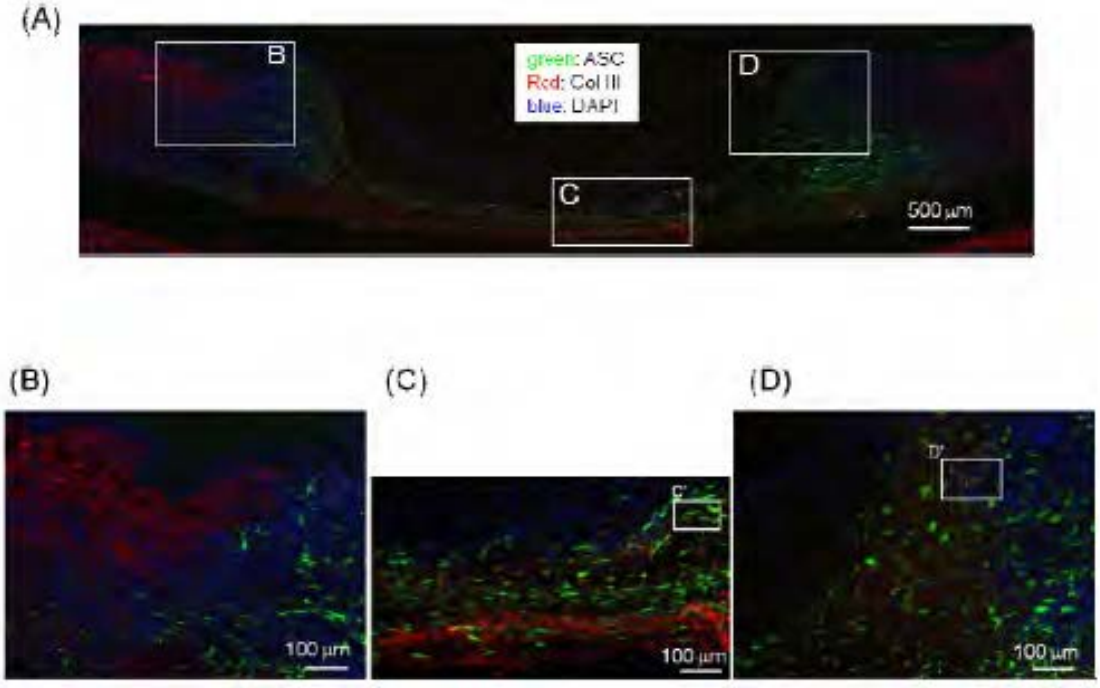

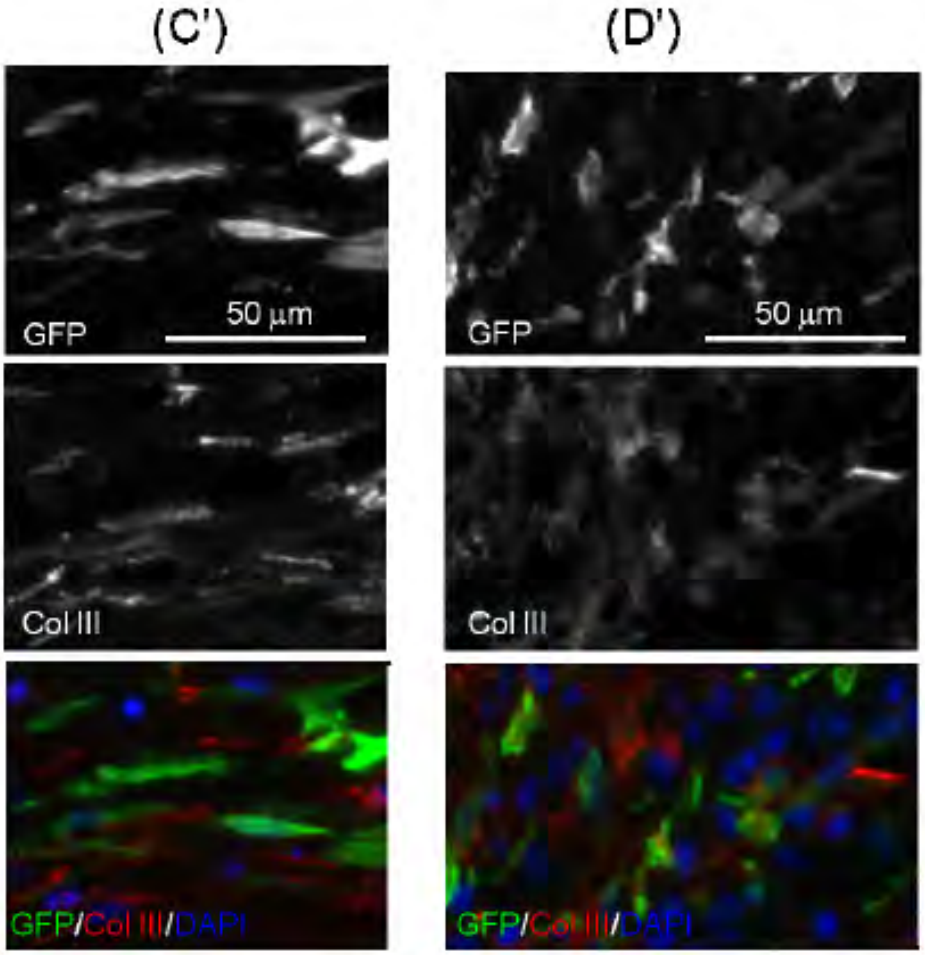


**Figure 9. Expression of collagen III (Col III) in wounds.** Rabbit ear wounds at POD7 were stained with chicken anti-GFP (green) and mouse anti-Col III (red) antibodies. Nuclei were stained with DAPI. (A) Low magnification of wounds. (B-D) Higher magnifications of the indicated regions (white squares) in A. (C'-D') Higher magnifications of the indicated regions in C, D. Scale bars: 500 μm (A), 100 μm (B, C, D), 50 μm (C', D').

Transdifferentiation of ASCs to endothelial cell was addressed using a platelet endothelial cell adhesion molecule (PECAM-1, CD31) - specific antibody. CD31 in blood vessels of non-wounded skin was prominently detected (data not shown). Expression of CD31 in wounds was also detected (Figure 10). However, co-expression of CD31 in transplanted ASC was not detected at POD7. Proliferation of transplanted ASCs was detected with Ki-67 or PCNA specific antibodies (Figure 11 & 12).


**Figure 10. Expression of CD31 (PECAM-1) in transplanted ASCs.** Rabbit ear wounds at POD7 were stained with chicken anti-GFP (A) and mouse anti-CD31 (B) antibodies. Nuclei were stained with DAPI. Merged image was shown in C. Scale bar; 50 μm.

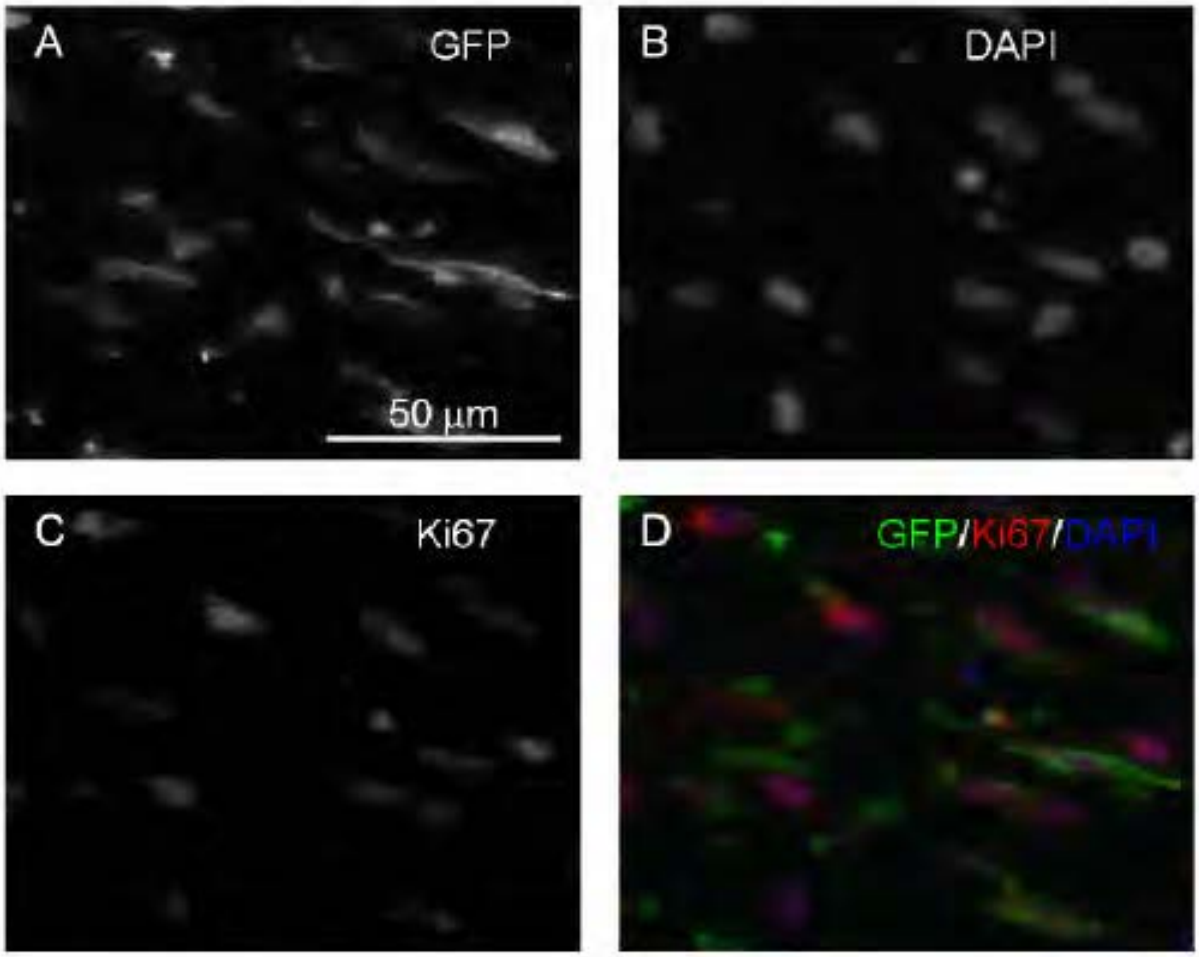


**Figure 11. Proliferation of transplanted ASCs in wounds.** Rabbit ear wounds at POD7 were stained with chicken anti-GFP (A) and mouse anti-Ki67 (C) antibodies. Nuclei were stained with DAPI (B). Merged image was shown in D. Scale bars: 50 μm.

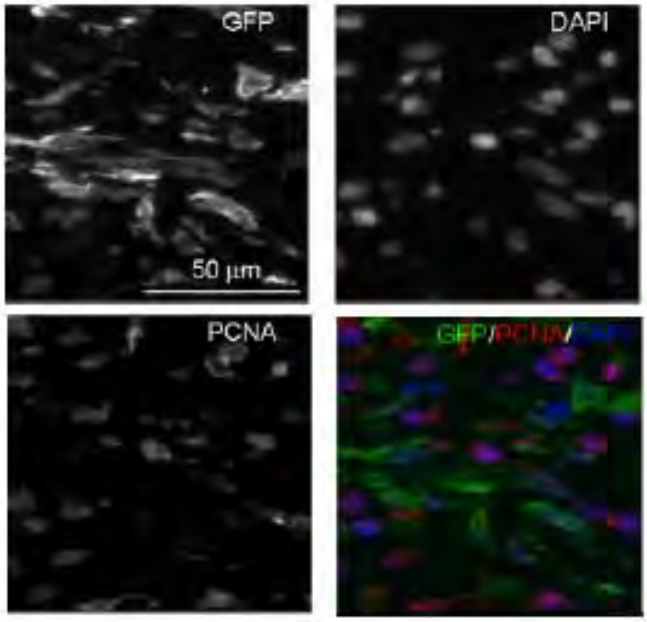


**Figure 12. Transplanted ASCs proliferate in wounds.** GFP-expressing ASCs were analyzed 7 days after transplanting in wounds. Chicken anti-GFP (A) and mouse anti-PCNA (C) antibodies were used. Nuclei were stained with DAPI (B). Merged image was shown in D. Scale bars: 50 μm.

### 3.2. ASCs enhance wound healing by increased recruitment of macrophages

We further analyzed ASCs treated- and vehicle- (saline treated-) wounds immunohistochemically. Expression of $\alpha$-SMA was found in the granulation tissue of ASCs treated-wounds and saline-treated control wounds (Figure 13A & 13C). -SMA signals in Figure 13C are from endogenous activated fibroblasts and transplanted ASCs in ASCs-treated wounds (Figure 8). $\alpha$-SMA signals in Figure 13A are from endogenous activated fibroblast cells. Cells used in the transplantation are allogeneic ASCs. We investigated whether allogeneic ASCs evoke immune reaction *in vivo*, though ASCs in general possess immune modulatory properties and are not immunogenic. In this case, neither CD3 (T cell antigen) nor CD45 (common leukocyte antigen) positive signals were found in the wounds based on immunostaining using specific antibodies on treated- wounds at POD7 (Figure 13D and data not shown).

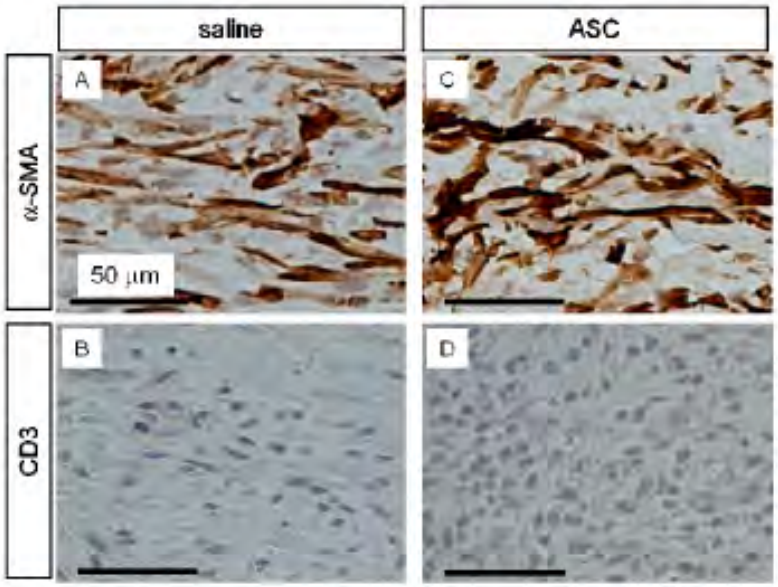


**Figure 13. Analysis of rabbit activated fibroblasts and T cells in ASC-treated wounds.** Saline (control; A, B) and ASCs (C, D) were delivered to wounds and harvested at POD7. α-SMA (A, C) and CD3 (B, D) were visualized by DAB after staining with their specific antibodies. Images were taken from the area labelled as 'D' in Figure 9A. Scale bars: 50 μm.

Angiogenesis is one of critical factors in wound healing process. Blood vessel formation in granulation tissue, which is determined by endothelial marker (CD31) staining, was detected in ASCs treated wounds and saline controls (Figure 14A & 14C). Interestingly, a few CD31 positive cells were found in the wound beds of ASCs-treated wounds, though blood vessel structures were not found (Figure 14D). In contrast, we were not able to detect CD31 positive cells in saline-treated wounds at POD7 (Figure 14B). Since transdifferentiation of ASCs to endothelial was not found at POD7 in our animal model (Figure 10), we speculate that these CD31+ cells were being recruited by the transplanted ASCs in wounds.

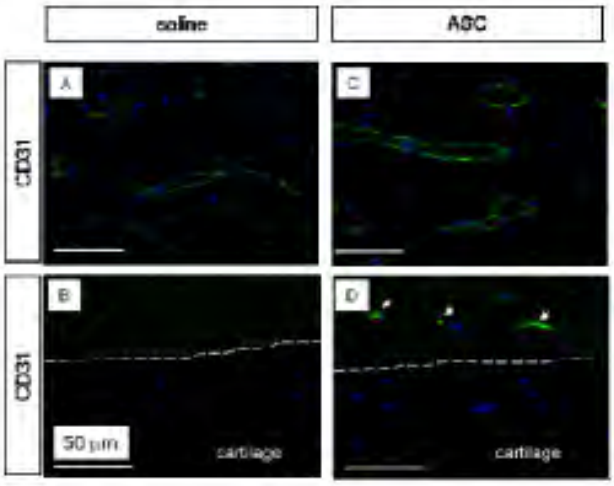


**Figure 14. Analysis of CD31 in rabbit ASC-treated wounds.** Saline (A, B) and ASCs (C, D) were delivered to wounds and harvested at POD7. CD31 was stained with its specific antibody and visualized using a fluorescence-conjugated secondary antibody. (A, C): images were taken from the area labelled as 'D' in Figure 9A. (B, D): images were taken from the area labelled as 'C' in Figure 9A. The junctional area between the cartilage and wound bed was demarcated by white dot lines. CD31 positive signals were indicated by arrows in D. Scale bars: 50 μm.

Upon tissue injury, neutrophils migrate to the wounded site and participate in the initial inflammatory phase of wound healing. Macrophages move to the site subsequently to clear the apoptotic neutrophils from the site and participate in the resolution phase of the inflammatory response and the beginning of the proliferation phase of wound healing by secreting cytokines and growth factors which attract cells such as fibroblasts that are involved in the process of wound repair, i.e., the remodeling of the extracellular matrix and the formation of granulation tissue to repair wounds. In our analysis of the treated wounds at POD7, we did not detect a significant number of neutrophils in the wounds treated with ASCs (Figure 15A & 15B). This is likely due to the fact that neutrophils are short-lived and it is likely to be cleared by the macrophages following the initial influx of neutrophils. By contrast, we detected an average of 16.4 macrophages in the granulation tissue near the migrating epidermis in high power microscopic fields (HPF, Figure 15C & Figure 16). The number of macrophages in the granulation tissue was markedly increased by ASCs treatment at POD7 (Figure 15D & Figure 16). Thus, our wound analysis suggested that transplanted ASCs exhibit an activated fibroblast phenotype and enhance wound repair by macrophage recruitment.

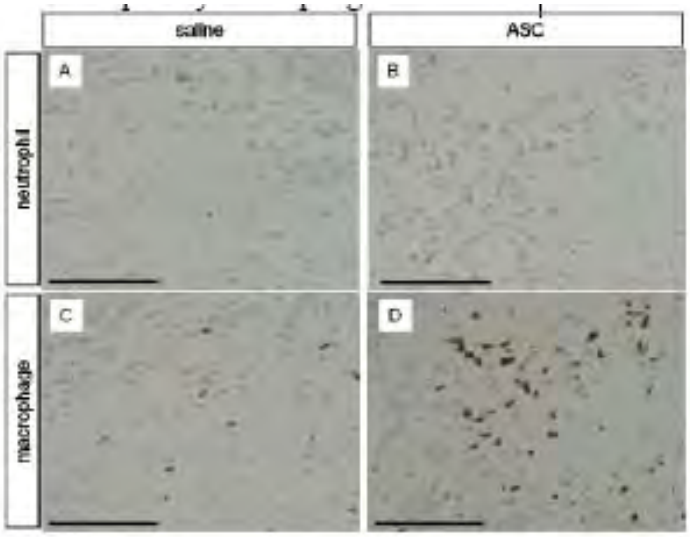


**Figure 15. Detection of rabbit neutrophils and macrophages in ASC treated wounds.** Saline (A, C) and ASCs (B, D) were delivered to wounds and harvested at POD7. Neutrophils (A, B) and macrophages (C, D) were visualized by DAB after staining with their specific antibodies. Scale bars: 100 μm.

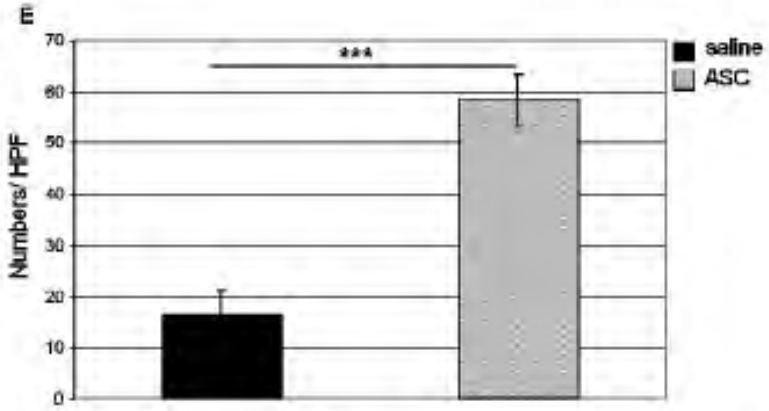


**Figure 16. A higher amount of infiltration of rabbit macrophages was found in ASC-treated wounds.** Macrophages per high-power microscopic field (HPF) (at 400 X magnification) were counted and averaged from four HPFs. Data are from four independent wounds and presented as mean ± SEM. ***$p<0.001$

## II. Effect of rabbit MSCs on hypertrophic scarring

### 1. Effect of rabbit ASCs on hypertrophic scarring

We have determined that saline is suitable as the vehicle to deliver MSC and 1 x $10^5$ of MSCs was found to be the optimum cell number for reducing hypertrophic scar**s** in our preliminary experiments. In order to increase the statistical power of analysis for determining the quantitative differences of measurement of SEI, we increased the number of wounds and animals. P3 ASCs were harvested, washed in PBS, and re-suspended in PBS. Each 7 mm wound on one of the ears of animals was treated with 1 x $10^5$ ASCs in 7µl of PBS. For wounds on the contralateral ear of the test animals, 7 µl of PBS was applied per wound to serve as the control. Wounds were harvested at POD28. There was no difference in SEI between samples treated with saline (SEI = 1.66 $\pm$ 0.07, n=33) or ASCs (SEI = 1.64 $\pm$ 0.07, n=34, p=0.82) (Figure 17A). No difference was found in scar area between the two groups (Figure 17B). Similar observations were found with the use of BM-MSCs and DFs.

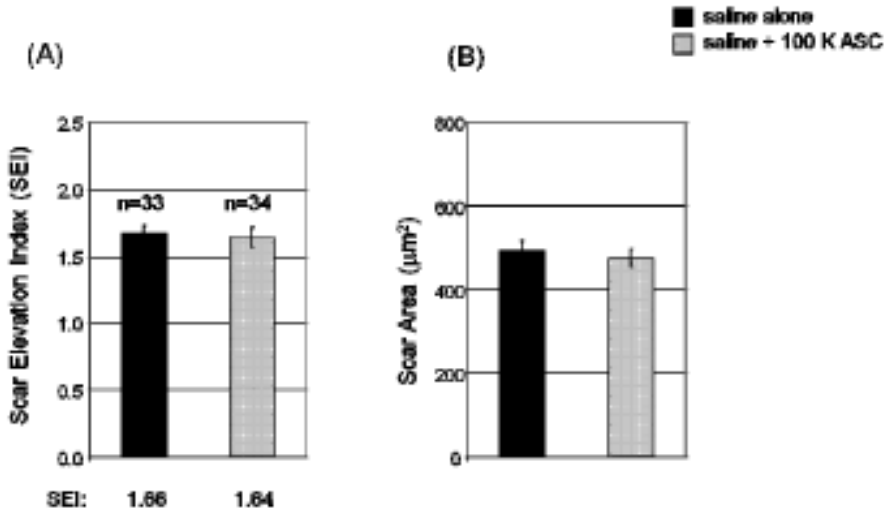


**Figure 17. Histological quantification of ASCs treated scars.** 1 x $10^5$ ASCs in PBS were delivered to 7 mm wounds on one ear. In the contralateral ear, PBS alone was delivered as a control. Wounds were harvested at POD28, and SEI and scar area were measured. Data were shown as mean $\pm$ SEM.

### 2. Analysis of the quality of scars

At present, the data indicated that rabbit ASCs, rabbit BM-ASCs, and rabbit DFs did not lessen the scarring of our rabbit ear wounds. The immediate plan is to analyze the quality of scar by immunostaining using col1 and col3 specific antibodies. In addition, immature and mature collagen will be quantified using the NIH ImageJ program after Picrosirius and Masson's Trichrome staining. To examine the functional recovery of wounds by ASCs, we will determine the stress strain curves and breaking points of scars using a tensometer. At the time of preparing this Progress Report, we have transplanted 1 x $10^5$ ASCs wounds to wounds on one ear and saline on the contralateral ear. These wounds will be harvested on POD28 and will be analyzed for scar quality as compared to PBS treated-wounds.

## III. Use of other matrices as MSCs delivery vehicles to reduce hypertrophic scarring

Though we observed survival of ASCs in wounds at POD7, long-term survival of ASCs in wound (such as at POD28) has not yet been addressed. Enhanced survival of ASCs may be necessary to reduce scar formation. As we discussed in the Y1 annual report, the purity and quality of fibrinogen and thrombin are not consistent among different vendors. Thus, we tested fibrins from

different vendors (e.g., Sigma-Aldrich) as a delivery vehicle. First, we treated 7 mm wounds with fibrin alone or saline alone (without ASCs), and analyzed scarring at POD28. There was no difference in SEI and scar area between samples treated with saline or fibrin (data not shown). Next, $1\times10^5$ P3 ASCs in a fibrin vehicle (Sigma-Aldrich) was delivered to each wound on one ear and the same quantity of ASCs in saline vehicle was delivered to wounds on the contralateral ear. Wounds which received ASCs in fibrin (n=9) showed reduction of SEI compared to wounds receiving ASCs in saline (n=7) (1.74 $\pm$ 0.08 vs. 2.13 $\pm$ 0.11, respectively; $p<0.05$) (Figure 18A). However, there was no statistical difference in scar area between the two groups (Figure 18B). These results suggest the need for optimization of MSCs delivery vehicles in order to determine the ability of ASCs to reduce scar formation. At present, we are optimizing the conditions for delivery of rabbit ASCs in fibrin.

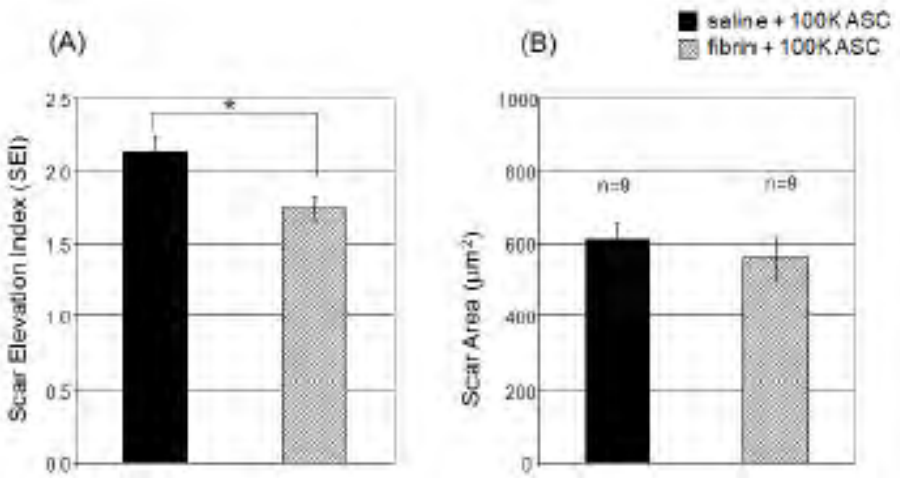


**Figure 18. Histological quantification of ASCs-treated scars. 1 X $10^5$ ASCs in Sigma-Aldrich fibrin or saline were delivered to the wounds. Wounds were harvested at POD28, and SEI and scar area were measured. Data are shown as mean $\pm$ SEM. *$p<0.05$.**

**IV. Comparison of allogeneic and autologous ASCs in stem cell therapy.**

Allogeneic ASCs have been used in our wound healing and scarring experiments as described above. We were interested in determining whether allogeneic ASCs have a similar ability, as compared to autologous ASCs, in promoting wound healing and reducing scarring. In this case, autologous ASCs were isolated from one of the inguinal fat pads and cultured *in vitro* prior to the application of the cells to the wounds of the animal (Figure 19).

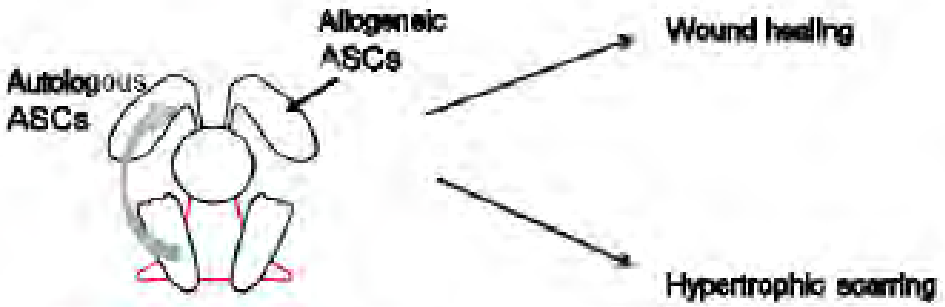


**Figure 19. Schematic drawing of autologous and allogeneic ASC treatments in rabbits.**

Once rabbits were fully recovered from surgery, P1 allogeneic or autologous ASCs ($1 \times 10^5$) in 7 µl of PBS were delivered to each 7 mm wound on one ear or the contralateral ear respectively. Wounds were harvested at POD7, 14, 28. Analysis of wounds at POD7 showed that there were no significant differences in wound healing parameters between the two test groups with regard to the epithelial gap (3,443 ± 524 µm vs. 2,702 ± 589 µm, autologous vs. allogeneic, respectively; p =0.6), granulation tissue distance (1,169 ± 67 µm vs. 1,135 ± 75 µm, respectively, p=0.37), and granulation tissue area (572,146 ± 68,226 $\mu m^2$ vs. 612,048 ± 46,521 $\mu m^2$ ; p =0.49) (Figure 20).

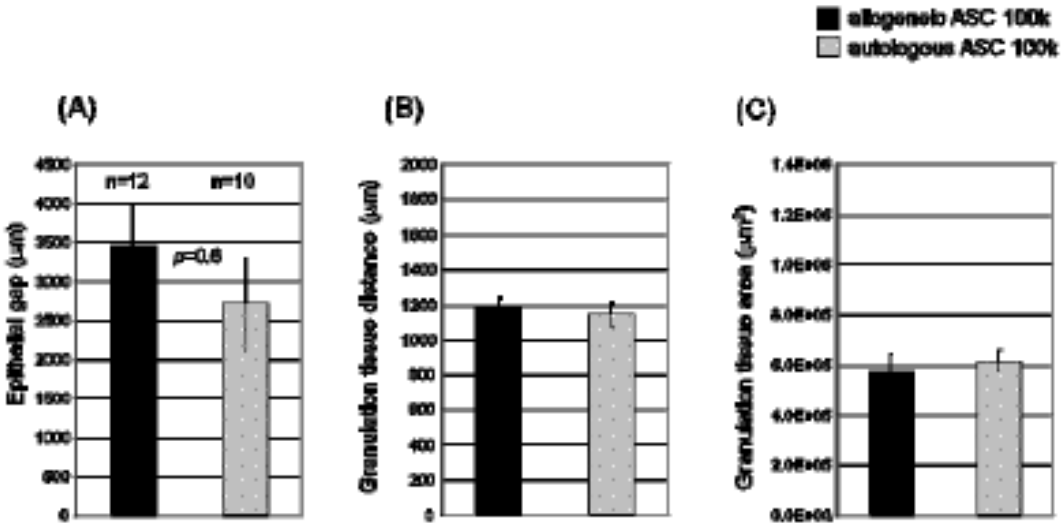


**Figure 20. Histological quantification of wounds treated with allogeneic and autologous ASCs.** P1 allogeneic or autologous ASCs ($1 \times 10^5$) in 7 µl of PBS were delivered to each 7 mm wound on one ear or the contralateral ear. Wounds were harvested at POD7 and epithelial gap (A), granulation tissue distance (B), and granulation tissue area (C) were measured. Data shown as mean ± SEM.

Scar analysis at POD28 showed no difference of SEI in wounds where allogeneic (SEI = 1.31 + 0.09, n=11) or autologous (SEI = 1.33 + 0.1, n=12, p=0.79) ASCs were transplanted (Figure 21A). No difference was found in scar area between the two groups (Figure 21B). We further analyzed for the presence of CD3 and CD45 marker cells in wounds treated with allogeneic or autologous ASCs to determine the occurrence of any immune reactions. Neither CD3 nor CD45 positive signals were found in these treated wounds at POD7, 14, and 28 using specific antibodies against these markers (data not shown). The results suggest that allogeneic ASCs do not have any excessive immune response and therefore could potentially be used in cell therapy.

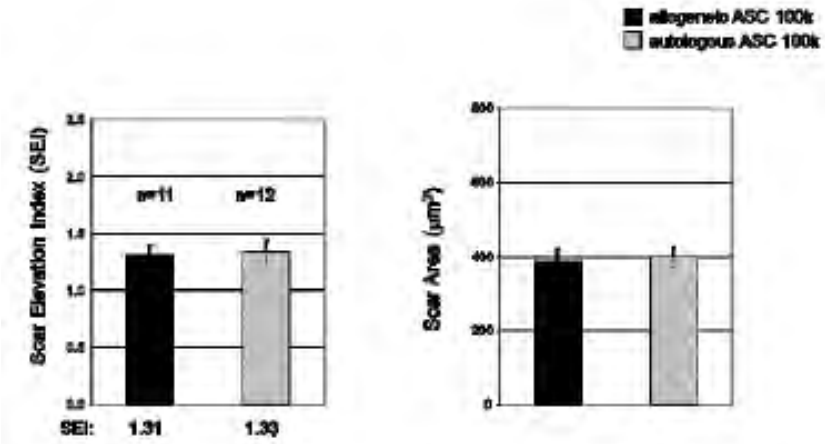


**Figure 21. Histological quantification of allogeneic and autologous ASCs treated scars.** P1 allogeneic or autologous ASCs ($1 \times 10^5$) in 7 µl of PBS were delivered to each 7 mm wound on one ear or the contralateral ear. Wounds were harvested at POD28, and SEI and scar area were measured. Data shown as mean ± SEM.

## V. *In Vitro* Characterization of Rabbit Mesenchymal Stem Cells (MSC) Aggregates

### 1. Synthesis and Culture of Rabbit MSC Aggregates

One of our objectives in the proposed study is to understand the paracrine profile of rabbit ASCs grown 2-dimensionally (2-D) versus 3-dimensionally (3-D). We have successfully generated scaffold-free, size-controlled cell aggregates via a forced aggregation technique using micropatterned wells (AggreWellTM, STEMCELL Technologies) originally developed for embryonic stem cells (ESC)/ induced pluripotent stem cells (iPS) research. We were capable of producing cell aggregates of different sizes ranging from 125 cells per aggregate to 16,000 cells per aggregate.

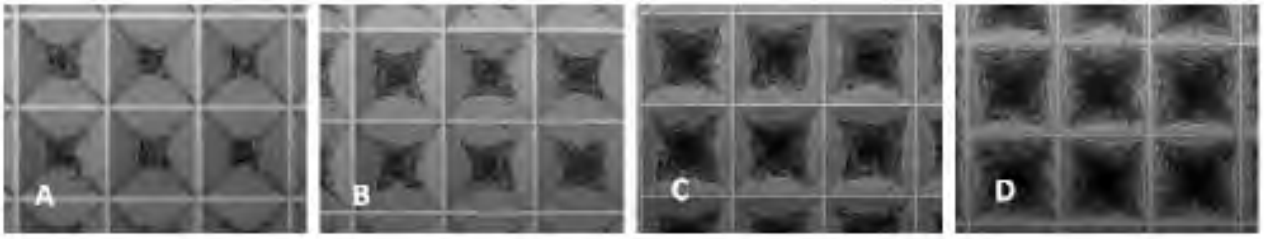


**Figure 22: Phase-contrast images of rabbit ASCs seeded in micropatterned wells at different cell densities.** 250 cells per aggregate (A), 500 cells per aggregate (B), 1000 cells per aggregate, and 2000 cells per aggregate. These images were taken right after plating and centrifugation. Magnification, ×50.

Figure 22 (a-d) are phase-contrast images of rabbit adipose-derived stem cells (ASCs) at four different seeding densities (250 cells/aggregate, 500 cells/aggregate, 1000 cells/aggregate, and 2000 cells/aggregate) right after plating and centrifugation. ASCs compacted to form self-assembling cell aggregates after overnight incubation (as shown in Figure 23). ASC aggregates can be cultured in micropatterned wells for extended periods of time without loss of cell viability. They can also be harvested from micopatterned wells and cultured in suspension.

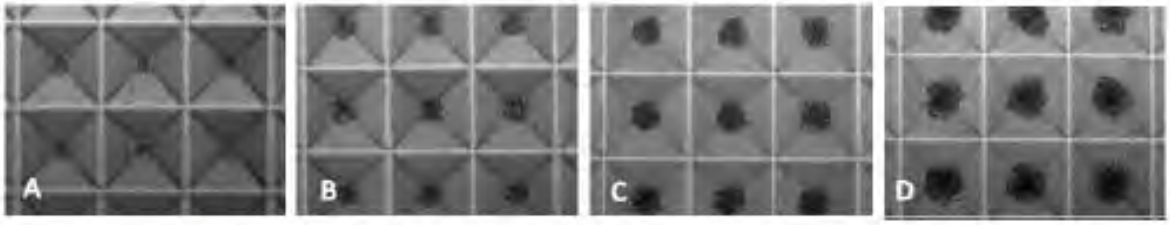


**Figure 23: Rabbit ASCs compacted to form cell aggregates overnight.**. (A) 250 cells per aggregate, (B) 500 cells per aggregate, (C) 1000 cells per aggregate, and (D) 2000 cells per aggregate. Magnification, ×50.

## 2. Gene Expression and Protein Expression of MSCs as 3D Aggregates vs. Adherent Monolayers

We have examined the expression of a selected panel of genes pertinent to wound healing in rabbit MSCs cultured under 3D vs. 2D conditions. An up-regulation of markers linked to angiogenesis such as vascular endothelial growth factor A (VEGFA), fibroblast growth factor 2 (FGF2), and hepatocyte growth factor (HGF) was observed in 3D aggregates of rabbit dermal fibroblasts (DFs), adipose-derived stem cells (ASCs), and bone marrow-derived stromal cells (BMSCs). An up-regulation of keratinocyte growth factor (KGF) and transforming growth factor β-1 (TGFβ-1) was also observed in all cell types cultured under 3D conditions, whereas a down-regulation of factors connective tissue growth factor (CTGF), epithelial growth factor (EGF), transforming growth factor β-2 (TGFβ-2) was observed. Most interestingly, transforming growth factor β-3 (TGFβ-3) was down-regulated in rabbit DFs and BMSCs, but was up-regulated in rabbit ASCs. TGFβ-3 has been implicated in reducing scarring in wounds. A summary of the gene expression data is depicted in Table 1.

**Table 1: Summary of the changes in gene expression in rabbit DFs, ASCs, and BMSCs cultured under3D vs. 2D conditions.**

| | VEGFA | FGF2 | HGF | KGF | EGF | CTGF | TGFβ$_1$ | TGFβ$_2$ | TGFβ$_3$ |
|---|---|---|---|---|---|---|---|---|---|
| Rb DF | ↑ | ↑ | ↑ | ↑ | ↓ | ↓ | ↑ | ↓ | ↓ |
| Rb ASC | ↑ | ↑ | ↑ | ↑ | ↓ | ↓ | ↑ | ↓ | ↑ |
| Rb BMSC | ↑ | ↑ | ↑ | ↑ | ↓ | ↓ | ↑ | ↓ | ↓ |

We have also confirmed the secreted protein expression of a few key factors. Due to the lack of commercially available rabbit reagents, we were constrained to human specific assays that have reported cross-reactivity with the rabbit. Some of these factors included VEGF, FGF2, TGFβ-1, and TGFβ-2. Our immunoassay data showed excellent correspondence with our gene expression findings.

Future work will focus on an extended list of genes from the wound healing, fibrosis, and inflammation panels via the use of a customized, high-throughput PCR Array technology (RT$^2$Profiler$^{TM}$ PCR Array, QIAGEN), where we can screen up to 84 genes per panel.

## *In Vitro* Characterization of Rabbit Mesenchymal Stem Cells (MSC) Aggregates

### 1. Synthesis and Culture of Rabbit MSC Aggregates

One of our objectives in the proposed study is to understand the paracrine profile of rabbit ASCs grown 2-dimensionally (2-D) versus 3-dimensionally (3-D). We have successfully generated scaffold-free, size-controlled cell aggregates via a forced aggregation technique using micropatterned wells (AggreWellTM, STEMCELL Technologies) originally developed for embryonic stem cells (ESC)/ induced pluripotent stem cells (iPS) research. We were capable of producing cell aggregates of different sizes ranging from 125 cells per aggregate to 16,000 cells per aggregate.

**Figure 1** shows rabbit ASCs seeded at several densities (**a, b, c, and d**) and compacted to form cell aggregates after overnight in culture (**e, f, g, and h**). As shown in **Figure 1i**, cell aggregates generated using the AggreWellTM product appear to be highly uniform in size, averaging 60.66±6.52 µm for aggregates composed of 125 cells/aggregate (AGG 125) the day after aggregate formation, 79.85±6.84 µm for AGG 250, 97.26±8.69 µm for AGG 500, 124.05±7.12 µm for AGG 1 000, 157.61±10.58 µm for AGG 2 000, 207.88±9.49 µm for AGG 4 000, 257.64±8.24 µm for AGG 8 000, and 382.12±18.43 µm for AGG 160 000. It is also important to note that further compaction of the cell aggregates was observed when they were maintained in micropatterned wells for extended periods of time in culture (up to 7 days). A gradual but continuous reduction in cell aggregate diameter over time is demonstrated in the aggregate size distribution graph in **Figure 1i.**

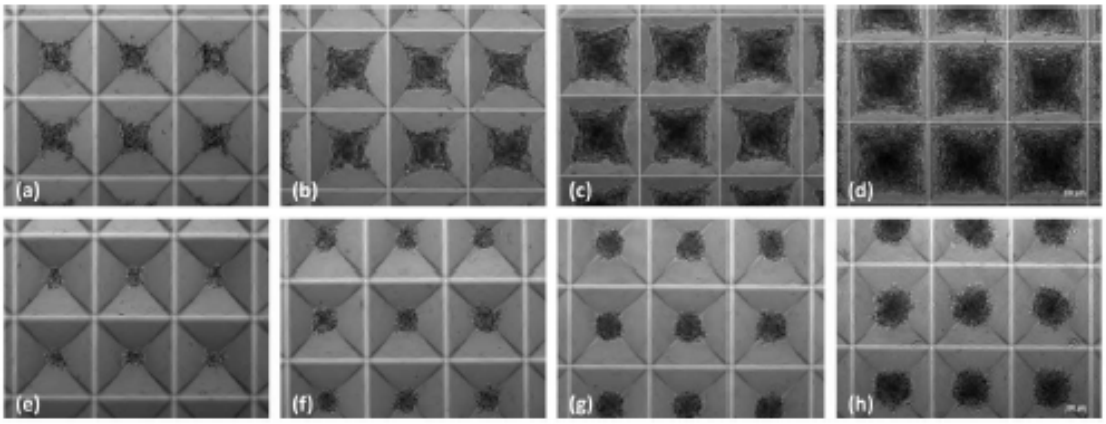

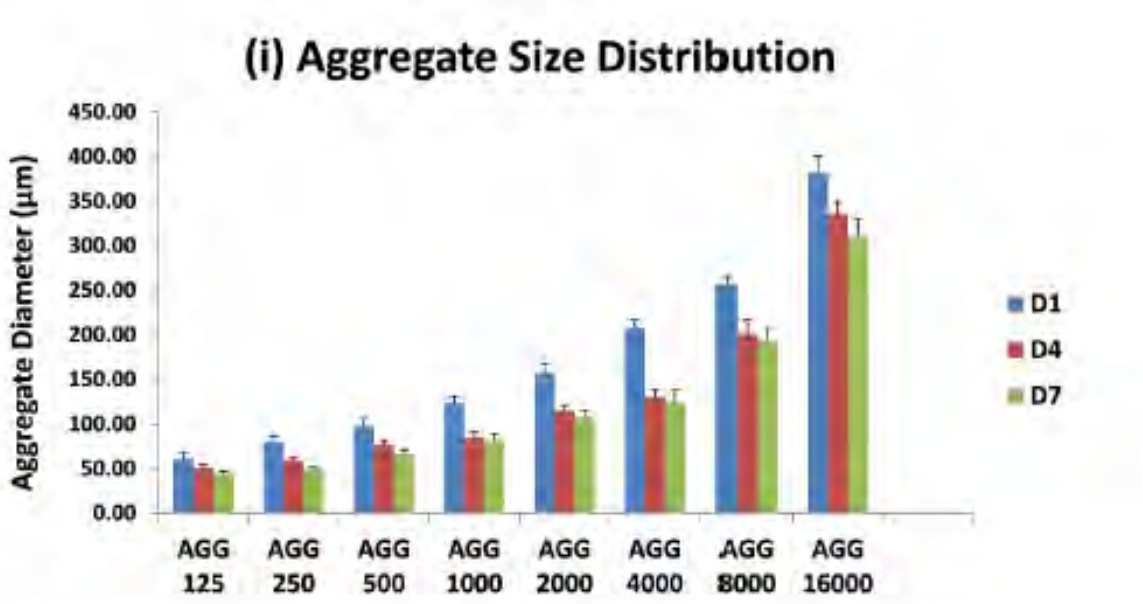


**Figure 1: Phase-contrast images of rabbit ASCs seeded in micropatterned wells at four representative cell densities.** (a) 250 cells per aggregate, (b) 500 cells per aggregate, (c) 1000 cells per aggregate, (d) and 2000 cells per aggregate. These images were taken after plating and centrifugation. Rabbit ASCs compacted to form cell aggregates overnight (e, f, g, h). Magnification of images is 50x. (j) Size distribution of ASC aggregates of different cell densities at different time points (Day 1, Day 4, and Day 7 in culture).

Cell viability and proliferation within ASC aggregates were examined qualitatively via Live/Dead staining and EdU incorporation. It was observed that smaller ASC aggregates maintained in micropatterned wells in regular growth media exhibited no evidence of cell necrosis up to 7 days in culture. However, non-viable cells were apparent after 24 hrs in culture with cell aggregates of larger sizes (especially greater or equal to 4 000 cells/aggregate). This is perhaps due to oxygen and nutrient diffusion limitations in larger cell aggregates. Interestingly, limited cell proliferation was observed in all cell aggregates, regardless of the size.

2. **Morphology and Ultrastructure of ASC Aggregates**

Scanning Electron Microscopy reveals the surface characteristics of the aggregates (500cells/aggregate)**,** showing that each cell aggregate is composed of many tightly compacted single cells, some of which lack clearly-defined cell-to-cell boundaries (**Figure 2b)**. The typical flattened and fairly featureless appearance of ASCs cultured on tissue culture plastic contrasted greatly with that of ASCs as 3D aggregates (**Figure 2a)**.

ASC aggregates were also processed and imaged for Transmission Electron Microscopy to analyze the internal organization of the cell aggregates. **Figure 2c** is a cross-section of a single cell aggregate, which is composed of mostly elliptical-shaped cell aggregates with large nuclei and high nuclear: cytoplasmic ratios without any indication of cell necrosis. Histological sections of ASC aggregates confirmed a densely packed structure with cells present through the center of the aggregate with no evidence of a necrotic core (data not shown).

Figure 2: SEM images of ASCs as 2D monolayers (a) and as 3D cell aggregates at 500 cells/aggregate (b). Magnification of images is 1000x (a) and 2500x (b). TEM image showing cross-section of ASCs as 3D cell aggregates after 24hr in culture (c). Magnification of images is 4000x.

## 3. Gene Expression and Protein Expression of MSCs as 3D Aggregates vs. Adherent Monolayers

We have examined the expression of a selected panel of genes pertinent to wound healing in rabbit MSCs cultured under 3D vs. 2D conditions. RT-qPCR showed up-regulation of key angiogenic factors such as Vascular Endothelial Growth Factor A (VEGFA), Fibroblast Growth Factor 2 (FGF2), and Hepatocyte Growth Factor (HGF) in rabbit BM-MSC, ASC, and DF aggregates as compared to 2D monolayer culture (**Figure 3a**). Up-regulation of Transforming Growth Factor β-1 (TGFβ-1) gene expression was observed in DFs, ASCs, and BMSCs in 3D culture, whereas down regulation of TGFβ-2 was observed in all three cell types. TGFβ-3 (TGFβ3) was down regulated in DFs and BMSCs, whereas a 5-fold increase in TGFβ-3 gene expression was observed in rabbit ASCs (**Figure 3b**). Furthermore, Epidermal Growth Factor (EGF) gene expression was significantly down regulated in 3D cell aggregates. Connective Tissue Growth Factor (CTGF) gene expression was also significantly down regulated in Rb DFs (>40 fold decrease) and in rabbit ASCs and BM-MSCs (>20 or 30 fold decrease) (**Figure 3c**). ELISA analysis revealed up-regulated secretion of VEGF, TGFβ-1, TGFβ-2, and bFGF by rabbit DFs, ASCs, and BM-MSCs when cultured as 3D cell aggregates vs. 2D monolayer (**Figure 4**).


**Figure 3 (a):** Gene Expression of selected angiogenic factors (VEGFA, FGF2, HGF). Fold change in mRNA levels of angiogenic markers in rabbit DF, ASC and BMSC aggregates compared to conventional 2D monolayer culture. VEGFA, FGF2, and HGF gene expression were all up-regulated in 3D culture. **(b):** Gene Expression of TGFβ-1, TGFβ-2, TGFβ-3. Up-regulation of TGFβ-1 gene expression was observed in DFs, ASCs, and BMSCs in 3D culture, whereas down regulation of TGFβ-2 was observed in all three cell types. TGFβ-3 was down regulated in DFs and BMSCs, whereas a 5-fold increase in TGFβ-3 gene expression was observed in rabbit ASCs. **(c):** Gene Expression of factors related to epithelialization (KGF, EGF, CTGF). EGF gene expression was significantly down regulated in 3D cell aggregates. CTGF gene expression was dramatically down regulated in Rb DFs (>40 fold decrease) and in rabbit ASCs and BMSCs (>20 or 30 fold decrease).

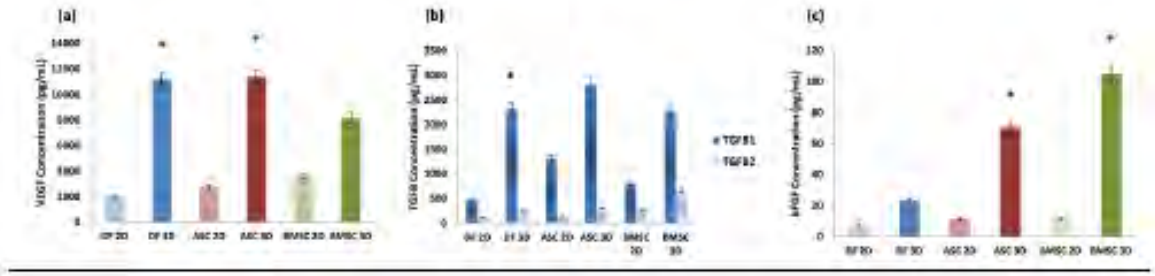


**Figure 4 (a):** VEGF Cytokine Expression. ELISA analysis of VEGF cytokine production by rabbit DFs, ASCs, and BMSCs when cultured as 3D cell aggregates vs. traditional 2D monolayer for 24hr. **(b):** TGFβ Cytokine Expression. ELISA analysis of TGFβ-1 and TGFβ-2 cytokine production by rabbit DFs, ASCs, and BMSCs when cultured as 3D cell aggregates vs. traditional 2D monolayer for 24hr. Rabbit TGFβ-3 could not be detected via this human specific multiplex immunoassay (no cross-reactivity was observed). **(c):** bFGF Cytokine Expression. ELISA analysis of bFGF cytokine production by rabbit DFs, ASCs, and BMSCs when cultured as 3D cell aggregates vs. traditional 2D monolayer for 24hr.

Mesenchymal stem cells secret a number of cytokines and growth factors that can promote wound healing and inhibit scarring (Caplan, 1991; Kilroy et al., 2007). Our findings may provide important mechanistic insights into the potential role MSCs have in modulating wound healing and scarring. It has been suggested that TGFβ-3 accelerates wound healing (Wu et al., 1997) and reduces scarring by decreasing type 1 collagen accumulation during repair (Hosokawa et al., 2003). CTGF, a downstream mediator of TGFβ activity, is thought to be associated with scar and fibrosis (Colwell et al., 2005; Sisco et al., 2008). Our results suggest that rabbit ASCs may have greater potential in ameliorating wound healing and reducing scarring than DFs or BM-MSCs, given the paracrine profiles exhibited by ASC aggregates (down regulation of CTGF, up-regulation of TGFβ-3 and other factors involved in wound repair and regeneration).

## 4. Tube Formation Assay

After 5-6 hrs of cultivation on Matrigel, HUVECs showed abundant networks of anastomosing cells that had a honeycomb appearance. These network structures were fully developed by 24 hr. The exogenous addition of proangiogenic growth factors in the HUVEC complete culture media or ASC or DF-conditioned media was able to augment *in vitro* capillary morphogenesis by HUVECs. In particular, the proangiogenic effect of 3D ASC-conditioned media was comparable to that of HUVEC complete media, and significantly greater than that of 2D ASC or DF-conditioned media (**Figure 5a-g**). **Figure 5h-j** shows quantification of typical tube formation parameters such as total loops formed, total branch points, and total length of tubular network of the four treatment groups including positive and negative controls.

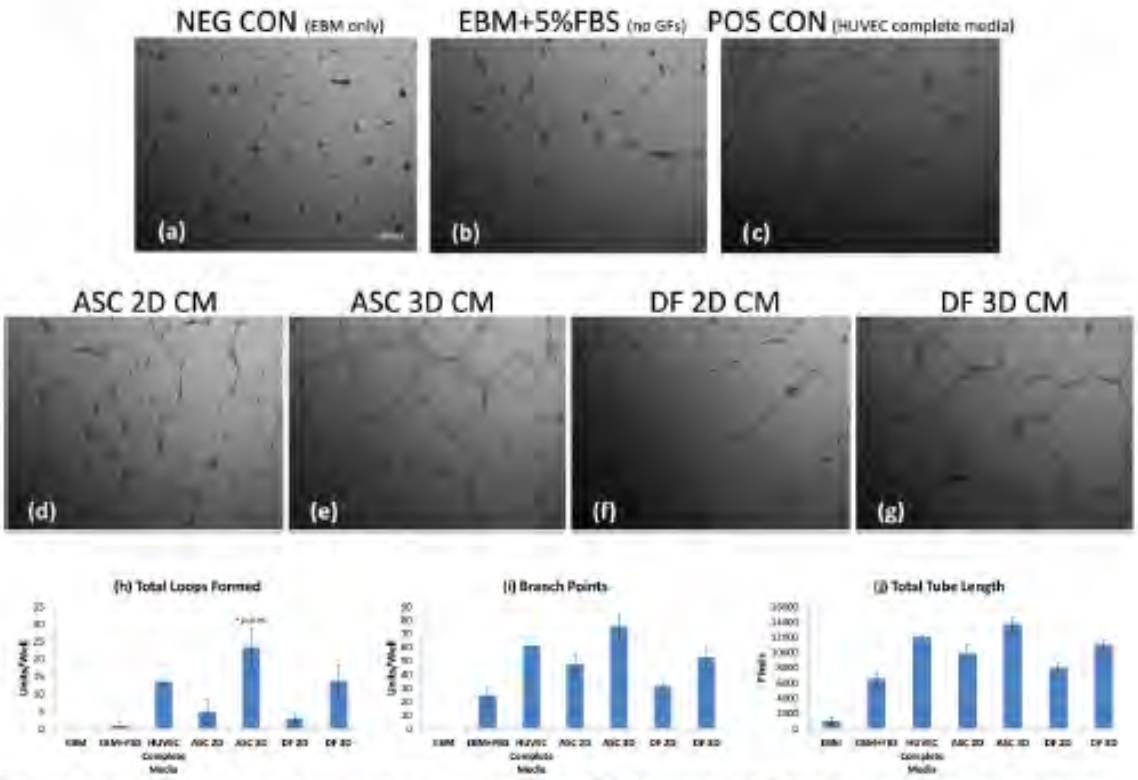


**Figure 5:** Tube Formation Assay. (a) Negative Control (EBM only), (b) EBM + 5% FBS without growth factor supplements, (c) Positive Control (HUVEC complete media), (d) ASC 2D CM, (e) ASC 3D CM, (f) DF 2D CM, (g) DF 3D CM. Images were taken 24hr after HUVECs were seeded on GFR Matrigel. Magnification of images is 50x. CM derived from ASC or DF populations (2D monolayers or 3D aggregates) was able to support the formation of tubular structures in HUVECs. Vessel networks were more pronounced in 3D CM-treated group. Quantification of tube formation parameters were shown in (h-j). ASC 3D CM and DF 3D CM exhibited comparable ability at supporting vascular network formation as the positive control (HUVEC complete media) in terms of the number of loops formed, total branch points and total length of tubular network. No loops or branch points were formed in the negative control (HUVECs treated with EBM).

**5. *In Vitro* Wound Healing/Scratch Assay**

CM from 2D culture induced a modest effect on repopulating the gap created in cultures, whereas 3D CM significantly enhanced the migration of HaCaT cells after wounding to fill the gaps (**Figure 6a-b**). At 24hr after wounding, the percentage of open area in HaCaT cultures maintained in 3D ASC CM was significantly smaller compared with 2D ASC CM. This observation was confirmed by HaCaT migration as measured by ECIS/electrical impedance (**Figure 6c)**.

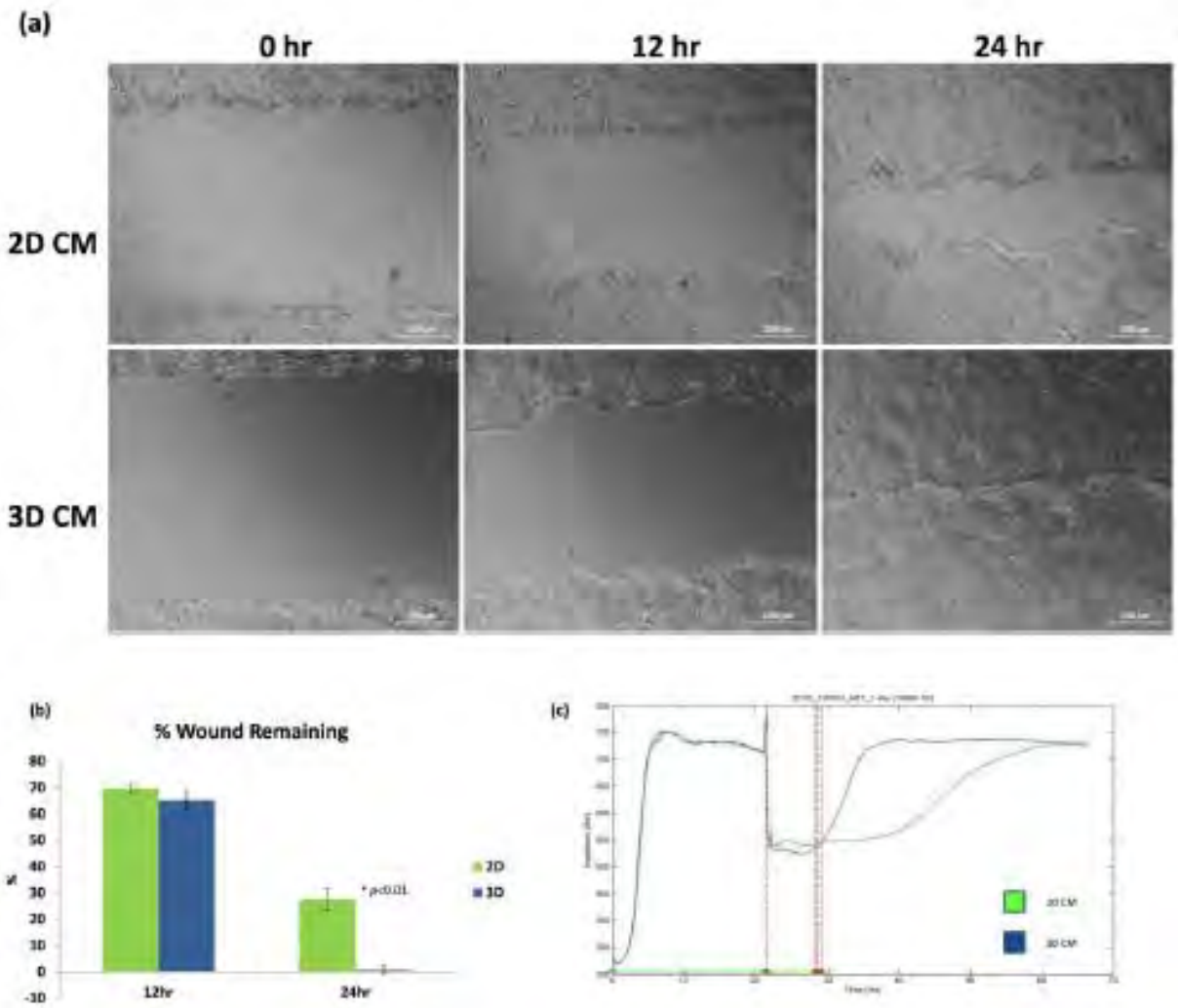


**Figure 6:** *In Vitro* Cell Migration Assay. Photographs show the effects of conditioned media on HaCaT cell migration (a). Wells were treated with 2D or 3D conditioned media. Note the lack of effect of the 2D conditioned media on the migration rates as compared to the 3D conditioned media. Photograph representative of multiple experiments. Zen 2011 software (Carl Zeiss Inc., Germany) was used to analyze the percentage of remaining wound area at 12 hr and 24 hr after wounding (b). HaCaT Wound Healing Measured by ECIS - representative graph of electrical impedance of HaCaT cells (c). HaCaT wound healing rate pattern was enhanced by 3D conditioned media.

Our *in vitro* functional assay data showed that CM from ASC aggregates exhibited: (a) comparable ability at supporting vascular network formation as the positive control (HUVEC complete media containing multiple growth factors) and (b) ability to accelerate wound closure as evidenced by an *in vitro* cell migration assay. Collectively, these observations suggest that ASC aggregates are good candidates for testing their effects on wound healing dynamics in an animal model.

No Cost Extension #2

**I. Gene Expression Profile Studies via PCR Arrays:**

Total RNA of rabbit ASC aggregates and adherent monolayers were extracted and purified using the RNeasy Mini Kit (Qiagen, Valencia, CA). Total RNA concentration was determined by optical density at 260 nm (OD 260) using a spectrophotometer (Nanodrop ND-1000, Thermo Scientific) and a denaturing agarose gel was run to ensure the quality and integrity of each sample. Complementary DNA (cDNA) for each sample was synthesized from 1μg of total RNA using the $RT^2$ First Strand Kit (Qiagen, Valencia, CA) and was mixed with the $RT^2$ SYBR Green Mastermix (Qiagen, Valencia, CA).

Custom Rabbit Wound Healing $RT^2$ Profiler PCR Arrays (Qiagen, Valencia, CA) were used to profile the expression of 84 genes central to the wound healing response. The Rabbit Wound Healing Array contains genes important for each of the three phases of wound healing, including ECM remodeling factors such as Collagen, type I, IV, Decorin (DCN), Vitronectin (VTN), and Tenascin C (TNC), inflammatory cytokines and chemokines (CCL2/MCP-1, CCL4, CXCL2, IL10, IL1A, IL1B, IL6, IL8), as well as growth factors and major signaling molecules (GMCSF, CTGF, FGF2, HGF, IGF1, TGFβ, WNT & etc). A comprehensive list of the genes examined is attached.

PCR Arrays were run in triplicates for each sample using a StepOne™ Plus Real- Time PCR system (Applied Biosystems, Foster City, CA). A dissociation/melting curve analysis was performed to verify PCR specificity. Gene expression data were analyzed using the ΔΔCt method normalized to a panel of 5 housekeeping gene controls with the aid of Qiagen's web-based PCR array data analysis software tool. Twenty-six out of 84 wound healing-related genes were up-regulated in ASCs cultured as 3D aggregates as compared to those cultured in monolayers, whereas 19 genes were found to be down regulated. **Table 1** contains the list of genes up-regulated in 3D ASC aggregates when compared with ASC monolayers ($p<0.05$). The table includes the gene symbol, description, as well as the average fold change across all three samples. **Table 2** shows the genes down regulated in ASC aggregates vs. monolayers ($p<0.05$).

**II. Quantitative Analysis of Engraftment and Survival of Transplanted Rabbit Adipose-derived Stem Cells (ASCs) with Real-Time Polymerase Chain Reaction:**

A variety of methods have been used to evaluate cell survival and engraftment after stem cell transplantation, including microscopic observation, assays for β- galactosidase activity, and terminal deoxynucleotidyl transferase-mediated dUTP nick end labeling (TUNEL) staining assay. Unfortunately, these methods are semi-quantitative, and cannot provide precise quantitative assessment of the implanted cells. In this study, we evaluated the accuracy and reproducibility of quantitative real-time PCR to measure the male-specific gene, SRY, in the rabbit. Using a well-established rabbit ear wound model, we delivered male rabbit ASCs to full-thickness wounds in a female rabbit recipient on POD3. The fraction of transplanted cells in each wound was determined by the copy numbers of the SRY gene via the RT-PCR technique.

C.**Isolation and Culture of ASCs from Male New Zealand White Rabbits:**

ASCs were isolated from inguinal fat pads of male New Zealand White rabbits (3- 4 months old, ~2.5-3.5 kg, Harlan Laboratories, Inc.). Briefly, the dissected fat pads were washed three times in pre-warmed phosphate-buffered saline (PBS), minced manually to the consistency of applesauce, and digested in 250 units/mL type I collagenase in Ham's DMEM/F12 for 1 hour at 37°C in a shaking water bath. After digestion and inactivation of the collagenase, the mixture was filtered through a 100 m sterile nylon mesh filter and spun at 1,200 *g* for 5 minutes. The resultant pellet was washed with Ham's DMEM/F12, resuspended in 10 mL of red blood cell (RBC) lysis buffer and allowed to sit at room temperature for 15 minutes. The RBC lysis buffer was prepared in Nanopure $H_2O$ with 10 mM $KHCO_3$, 150 mM $NH_4Cl$, and 0.1 mM EDTA. Following RBC lysis, the supernatant was removed and the pellet was washed twice with complete ASC media containing DMEM/F12 with 10% fetal bovine serum (FBS) and plated in T75 tissue culture flasks. Male ASCs passaged up to 4

times were used for sex-mismatched experiments. ASC aggregates were generated using the AggreWell™ 400 plates (STEMCELL Inc., Vancouver, BC).

D. **Sex-Mismatched Cell Transplantation Experiment:**

In one pilot experiment, four 10mm punch biopsy wounds were created on the ventral surface of each ear of a female New Zealand White rabbit in preparation for the sex-mismatched cell transplantation experiment. On POD3, $3x10^5$ male rabbit ASC aggregates resuspended in 15 µL of fibrinogen were delivered to each of the wounds, followed by an equal volume of thrombin. After gelling was confirmed, the wounds were dressed with Tegaderm. The animal started to display signs of distress (due to bowel obstruction) within 4 hours following the cell implantation procedure and was euthanized on the same day. Following euthanasia, 4 wounds from each ear containing male ASCs were harvested, two of which were fixed in 10% paraformaldehyde for histological analysis. Hematoxylin and eosin-stained section of a 10mm wound showing presence of implanted ASC aggregates 4hrs after transplantation is shown in **Figure 1**. The remaining wounds were snap frozen in liquid nitrogen and stored in -80°C until subsequent DNA extraction. Additional sex-mismatched cell transplantation experiments were planned to evaluate different cell concentrations and time points (0hr, immediate after transplantation; 24hr and 7 days after transplantation) but were not performed due to time constraints and budget issues.

E. **Extraction, Purification of Genomic DNA, and Quantification of Cell Engraftment via RT-PCR:**

Genomic DNA of each sample (rabbit tissue, rabbit ASCs, human tissue) was extracted and purified using Qiagen's DNeasy Blood & Tissue Kit (Qiagen, Valencia, CA) with minor modifications. In brief, each rabbit/human tissue sample was weighed, minced, and lysed in Buffer ATL with proteinase K at 56°C for 2-4hr or O/N, depending on tissue type (human vs. rabbit, presence of cartilage). A brief RNase A treatment was performed to remove contaminating RNA. Extraction of gDNA from rabbit ASCs followed a similar procedure, noticeable difference was in the amount of time required for tissue/cell lysis (30min for cells vs. minimum of 2-4hr for tissue). Isolated gDNA was resuspended in AE Buffer. DNA concentrations were determined by spectrophotometry. Forty milligrams of human/rabbit skin was determined to be the most optimal starting material.

For absolute quantification of gene copy number, a standard curve was constructed with samples derived from multiple log dilutions of genomic DNA isolated from male rabbit ear tissue. All samples were spiked with 50ng of female rabbit gDNA to control for any effects this may have on the reaction efficiency in the actual samples. The copy number of the SRY gene at each point of the standard curve was calculated based on the amount of DNA in each sample and the total mass of the rabbit genome per diploid cell (http://www.cbs.dtu.dk/databases/DOGS/index.html).

For each reaction, 50ng of template DNA was used in a Taqman polymerase chain reaction, using the SRY gene located on the Y chromosome as the target (forward primer sequence: CCAGGTGGCTCTGCAGAATC, reverse primer sequence: GGTGTCCCAGCTGCTTGCT, probe: CAAAATGCGAAACTCA). All samples were run in triplicates using the StepOne™ Plus Real-Time PCR system (Applied Biosystems, Foster City, CA).

The result from each reaction, copies of the SRY gene in 50ng of gDNA, was expressed as the number of engrafted cells/wound, first by calculating the copy number of SRY gene in the total amount of DNA corresponding to 40mg of tissue and then extrapolating to the total weight of each wound (since there is one copy of the SRY gene per cell). Negative control samples used were: NTC (PCR reagents without DNA template), female rabbit DNA, and male DNA of a different species (i.e. human).

The standard curve constructed showed excellent sensitivity of the assay, high efficiency of the reaction and linearity of the relationship between SRY gene copies and cell numbers (**Figure 2a**). **Figure 2b** is an amplification plot of the reactions corresponding to the points of the standard curve. **Figure 2c** shows the absolute number of cells per wound after transplantation (an average 28% or $8.4x10^4$ cells was retained 4hr post-transplantation).

## Figures and Tables

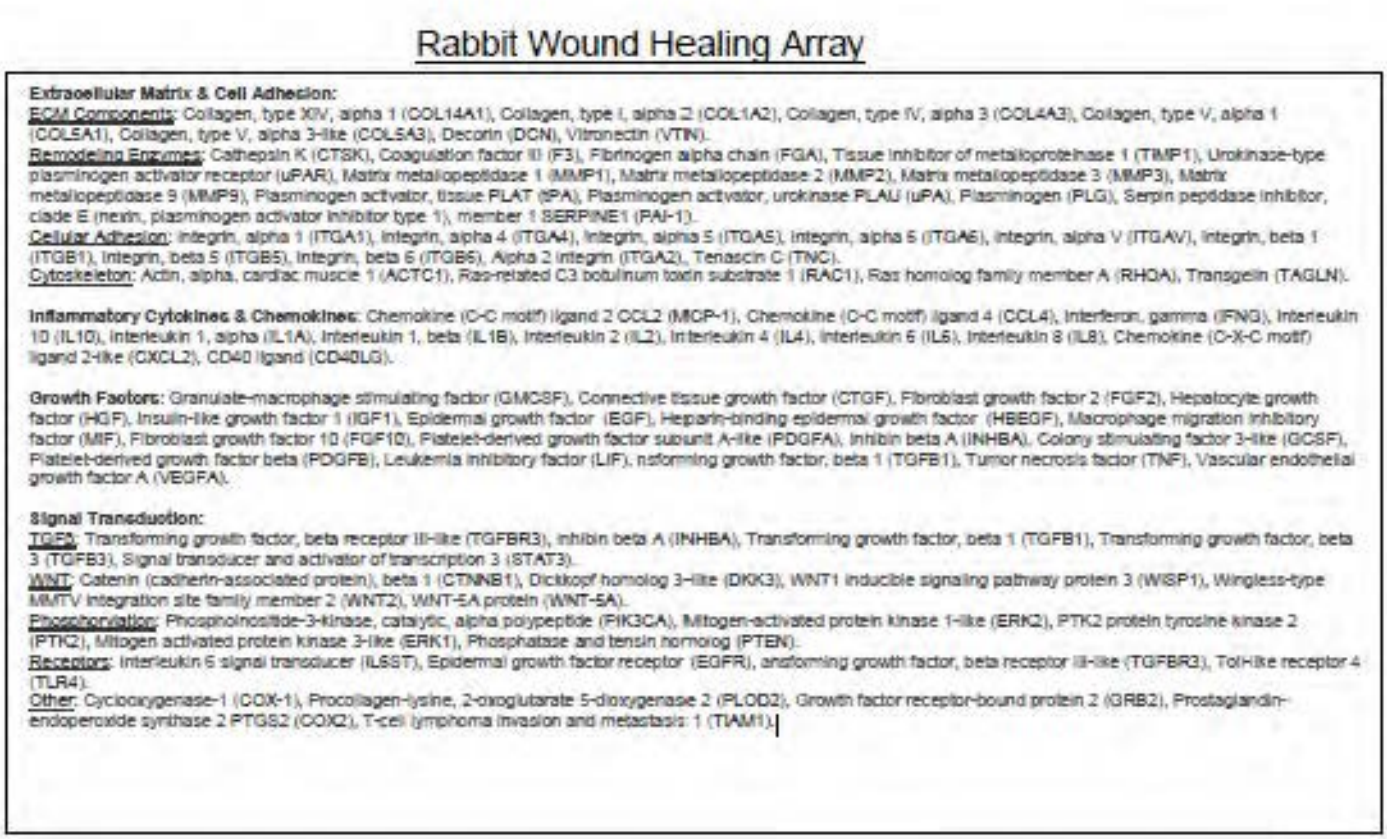

Rabbit Wound Healing Array

**Extracellular Matrix & Cell Adhesion:**
ECM Components: Collagen, type XIV, alpha 1 (COL14A1), Collagen, type I, alpha 2 (COL1A2), Collagen, type IV, alpha 3 (COL4A3), Collagen, type V, alpha 1 (COL5A1), Collagen, type V, alpha 3-like (COL5A3), Decorin (DCN), Vitronectin (VTN).
Remodeling Enzymes: Cathepsin K (CTSK), Coagulation factor III (F3), Fibrinogen alpha chain (FGA), Tissue inhibitor of metalloproteinase 1 (TIMP1), Urokinase-type plasminogen activator receptor (uPAR), Matrix metallopeptidase 1 (MMP1), Matrix metallopeptidase 2 (MMP2), Matrix metallopeptidase 3 (MMP3), Matrix metallopeptidase 9 (MMP9), Plasminogen activator, tissue PLAT (tPA), Plasminogen activator, urokinase PLAU (uPA), Plasminogen (PLG), Serpin peptidase inhibitor, clade E (nexin, plasminogen activator inhibitor type 1), member 1 SERPINE1 (PAI-1).
Cellular Adhesion: Integrin, alpha 1 (ITGA1), Integrin, alpha 4 (ITGA4), Integrin, alpha 5 (ITGA5), Integrin, alpha 6 (ITGA6), Integrin, alpha V (ITGAV), Integrin, beta 1 (ITGB1), Integrin, beta 5 (ITGB5), Integrin, beta 6 (ITGB6), Alpha 2 integrin (ITGA2), Tenascin C (TNC).
Cytoskeleton: Actin, alpha, cardiac muscle 1 (ACTC1), Ras-related C3 botulinum toxin substrate 1 (RAC1), Ras homolog family member A (RHOA), Transgelin (TAGLN).

**Inflammatory Cytokines & Chemokines:** Chemokine (C-C motif) ligand 2 CCL2 (MCP-1), Chemokine (C-C motif) ligand 4 (CCL4), Interferon, gamma (IFNG), Interleukin 10 (IL10), Interleukin 1, alpha (IL1A), Interleukin 1, beta (IL1B), Interleukin 2 (IL2), Interleukin 4 (IL4), Interleukin 6 (IL6), Interleukin 8 (IL8), Chemokine (C-X-C motif) ligand 2-like (CXCL2), CD40 ligand (CD40LG).

**Growth Factors:** Granulate-macrophage stimulating factor (GMCSF), Connective tissue growth factor (CTGF), Fibroblast growth factor 2 (FGF2), Hepatocyte growth factor (HGF), Insulin-like growth factor 1 (IGF1), Epidermal growth factor (EGF), Heparin-binding epidermal growth factor (HBEGF), Macrophage migration inhibitory factor (MIF), Fibroblast growth factor 10 (FGF10), Platelet-derived growth factor subunit A-like (PDGFA), Inhibin beta A (INHBA), Colony stimulating factor 3-like (GCSF), Platelet-derived growth factor beta (PDGFB), Leukemia inhibitory factor (LIF), nsforming growth factor, beta 1 (TGFB1), Tumor necrosis factor (TNF), Vascular endothelial growth factor A (VEGFA).

**Signal Transduction:**
TGFb: Transforming growth factor, beta receptor III-like (TGFBR3), Inhibin beta A (INHBA), Transforming growth factor, beta 1 (TGFB1), Transforming growth factor, beta 3 (TGFB3), Signal transducer and activator of transcription 3 (STAT3).
WNT: Catenin (cadherin-associated protein), beta 1 (CTNNB1), Dickkopf homolog 3-like (DKK3), WNT1 inducible signaling pathway protein 3 (WISP1), Wingless-type MMTV integration site family member 2 (WNT2), WNT-5A protein (WNT-5A).
Phosphorylation: Phosphoinositide-3-kinase, catalytic, alpha polypeptide (PIK3CA), Mitogen-activated protein kinase 1-like (ERK2), PTK2 protein tyrosine kinase 2 (PTK2), Mitogen activated protein kinase 3-like (ERK1), Phosphatase and tensin homolog (PTEN).
Receptors: Interleukin 6 signal transducer (IL6ST), Epidermal growth factor receptor (EGFR), ansforming growth factor, beta receptor III-like (TGFBR3), TolHike receptor 4 (TLR4).
Other: Cyclooxygenase-1 (COX-1), Procollagen-lysine, 2-oxoglutarate 5-dioxygenase 2 (PLOD2), Growth factor receptor-bound protein 2 (GRB2), Prostaglandin-endoperoxide synthase 2 PTGS2 (COX2), T-cell lymphoma invasion and metastasis 1 (TIAM1).

| Gene Symbol | Description | Fold Change (2D vs. 3D) |
|---|---|---|

| | | |
|---|---|---|
| GMCSF | Granulate-macrophage stimulating factor | 319.09 |
| ITGA2 | Alpha 2 integrin | 204.15 |
| IL1B | Interleukin 1, beta | 161.96 |
| MMP1 | Matrix metallopeptidase 1 | 128.65 |
| IL8 | Interleukin 8 | 127.88 |
| MMP3 | Matrix metallopeptidase 3 | 127.41 |
| MMP9 | Matrix metallopeptidase 9 | 50.57 |
| CXCL2 | Chemokine (C-X-C motif) ligand 2-like | 32.02 |
| IL1A | Interleukin 1, alpha | 32.00 |
| IL6 | Interleukin 6 | 20.17 |
| WNT2 | Wingless-type MMTV integration site family member 2 | 20.10 |
| VEGFA | Vascular endothelial growth factor A | 16.00 |
| PTGS2 | Prostaglandin-endoperoxide synthase 2 | 10.07 |
| TNC | Tenascin C | 8.00 |
| PLAU | Plasminogen activator, urokinase | 7.94 |
| HGF | Hepatocyte growth factor | 7.91 |
| WNT-5A | WNT-5A protein | 6.30 |
| LIF | Leukemia inhibitory factor | 5.07 |
| PDGFB | Platelet-derived growth factor beta | 4.03 |
| FGF10 | Fibroblast growth factor 10 | 4.01 |
| EGFR | Epidermal growth factor receptor | 4.01 |
| FGF2 | Fibroblast growth factor 2 | 3.99 |
| VTN | Vitronectin | 2.53 |
| ITGA5 | Integrin, alpha 5 | 2.03 |
| DCN | Decorin | 2.01 |
| HBEGF | Heparin-binding epidermal growth factor | 2.00 |
| RAC1 | Ras-related C3 botulinum toxin substrate 1 | 2.00 |

**Table1. PCR Array Analysis of Genes Upregulated in 3D ASC Aggregates.** This table shows the 26 most upregulated genes in 3D ASC aggregates when compared with monolayers ($p<0.05$).

| Gene Symbol | Description | Fold Change (2D vs. 3D) |
|---|---|---|
| ACTA2 | Actin, alpha 2, smooth muscle, aorta | -2035.93 |
| CTGF | Connective tissue growth factor | -128.15 |
| TAGLN | Transgelin | -127.88 |
| DKK3 | Dickkopf homolog 3-like | -31.95 |
| COL14A1 | Collagen, type XIV, alpha 1 | -16.04 |
| COL1A2 | Collagen, type I, alpha 2 | -16.01 |
| F3 | Coagulation factor III | -16.00 |
| SERPINE1 | Serpin peptidase inhibitor 1 | -15.99 |
| COL5A3 | Collagen, type V, alpha 3-like | -8.01 |
| ITGA4 | Integrin, alpha 4 | -7.97 |
| PLAT | Plasminogen activator, tissue | -7.96 |
| ITGA6 | Integrin, alpha 6 | -7.96 |
| TGFB3R | Transforming growth factor, beta receptor III-like | -7.90 |
| ACTB | Actin, beta | -6.33 |
| PDGFA | Platelet-derived growth factor subunit A-like | -5.06 |
| MIF | Macrophage migration inhibitory factor | -3.98 |
| MMP2 | Matrix metallopeptidase 2 | -2.51 |
| CTSK | Cathepsin K | -2.01 |
| PLOD2 | Procollagen-lysine, 2-oxoglutarate 5-dioxygenase 2 | -2.01 |
| TIMP-1 | Tissue inhibitor of metalloproteinase 1 | -2.00 |

**Table2. PCR Array Analysis of Genes Downregulated in 3D ASC Aggregates.** This table shows the 19 most downregulated genes in 3D ASC aggregates when compared SC monolayers ($p<0.05$).

**Figure 1.** Hematoxylin and eosin-stained section of a 10mm wound showing presence of implanted ASC aggregates (white arrows) 4hrs after transplantation. Magnification of image is 200x.

**Figure 2a:**

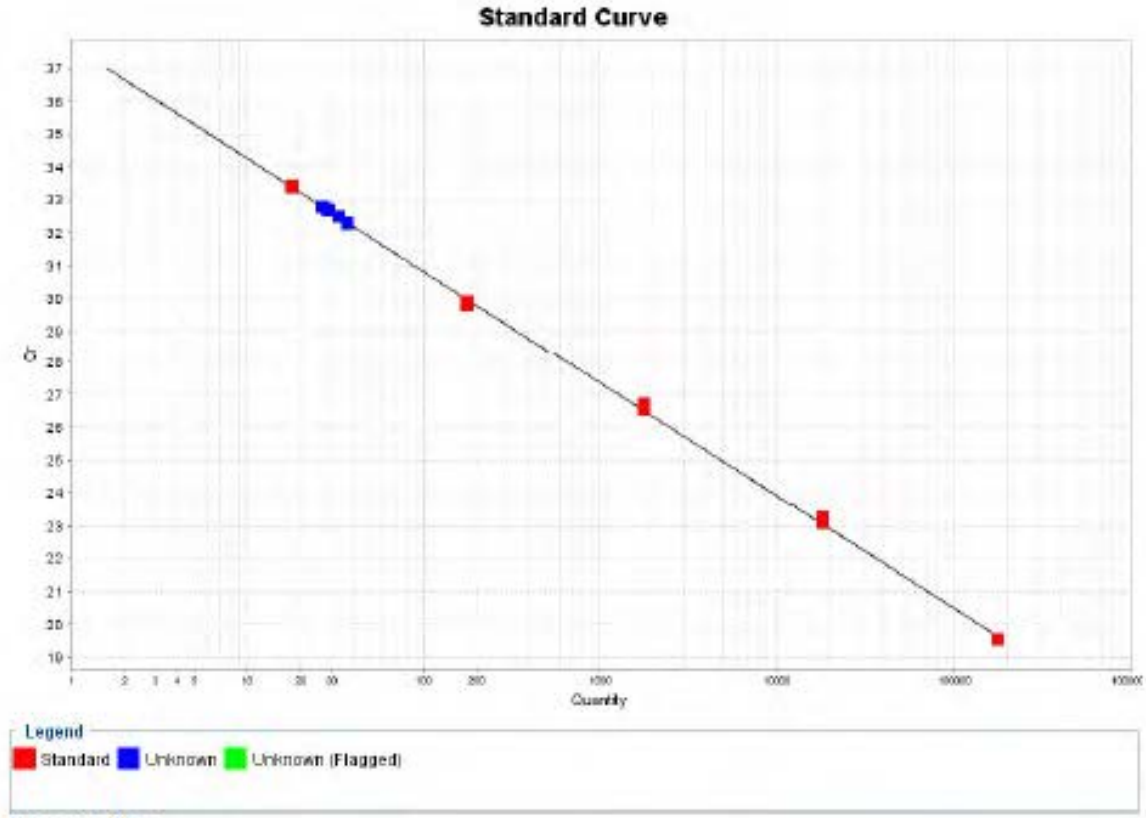


**Figure 2b:**

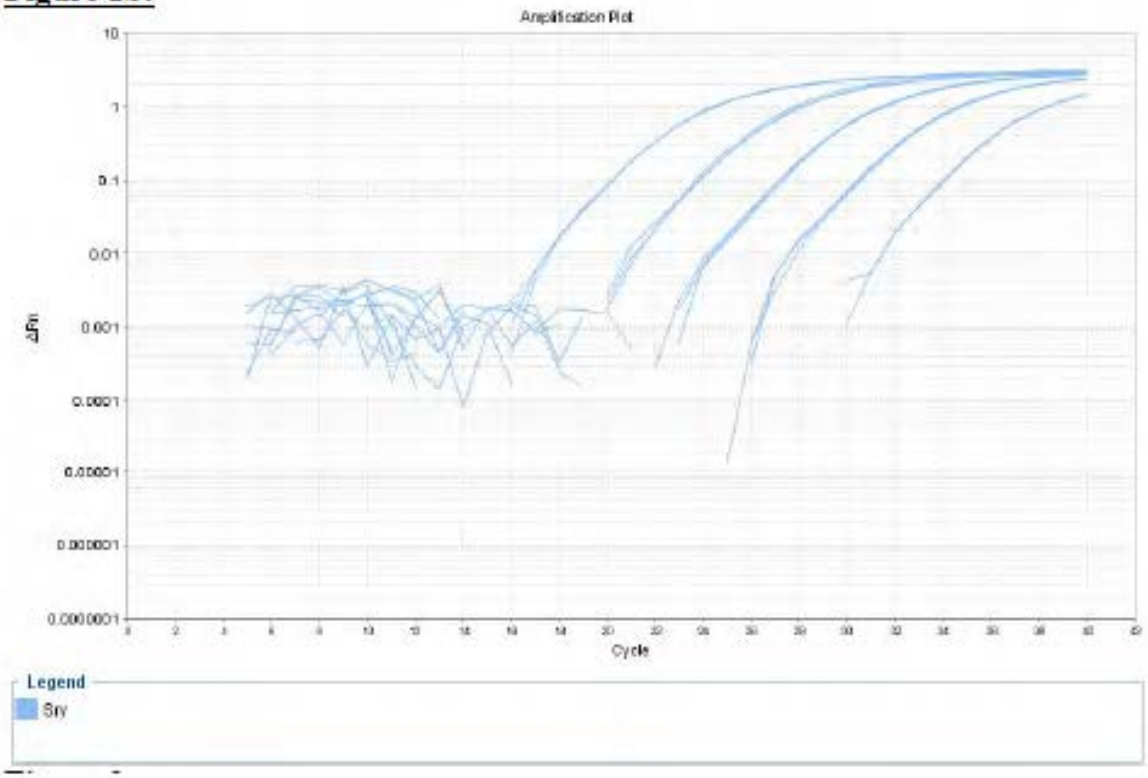

**Figure 2c:**

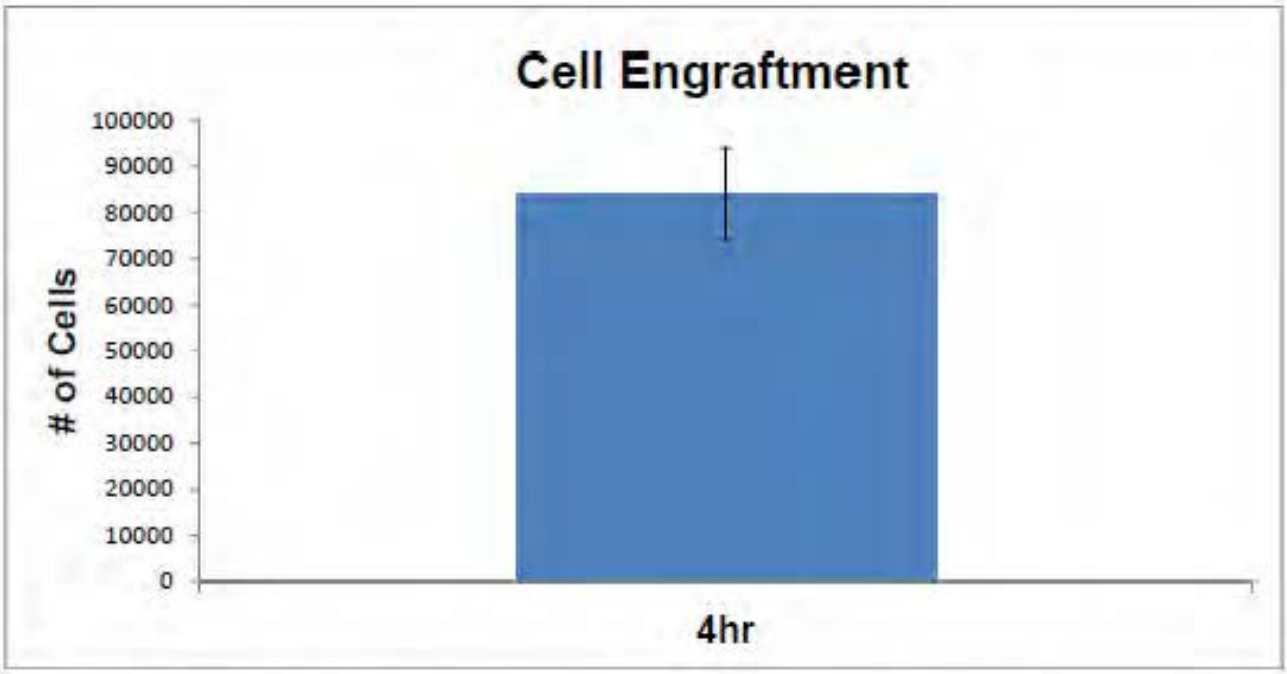


**Figure 2.** A quantitative RT-PCR standard curve was used for ex vivo quantification of male ASCs transplanted in female rabbit ear wounds. A genomic sequence of the male-specific SRY gene was used as the target. **(a)** The standard curve shows excellent sensitivity of the assay, high efficiency of the reaction and linearity of the relationship between SRY gene copies and cell numbers ($r^2$=0.999). **(b)** Amplification plot of the reactions corresponding to the points of the standard curve. **(c)** Absolute quantification of ASC engraftment at 4hr after cell transplantation. Data were analyzed with the StepOne™ Plus Software v2.0 (Applied Biosystems, Foster City, CA).

**KEY RESEARCH ACCOMPLISHMENTS:**

- Isolated and characterized four rabbit ASCs lines.
- Isolated and characterized eight rabbit BM-MSCs lines.
- Isolated and characterized three rabbit DFs lines.
- Established GFP (or DsRed2) expressing ASCs and DFs to study the fate of transplanted ASCs in wounds.
- Established firefly luciferase expressing ASCs.
- Optimized immunohistochemistry condition for rabbit neutrophils, macrophages, CD31, and Ki67.
- Determined saline as a MSCs delivery vehicle.
- Characterized survival of ASCs in wounds after 7 days transplantation.
- Started to perform hypertrophic scarring animal experiments.
- Rabbit and human MSC were able to secret higher levels of TGF-β1 as compared to that of fibroblasts.

B. Wound healing study

- Optimized the cell number of rabbit ASCs ($1 \times 10^6$ ASCs per 7 mm wound) for wound healing study.
- Completed histological analyses on the effects of ASCs, BM-MSCs, and DFs on wound healing.
- Demonstrated that rabbit ASCs promoted granulation tissue formation.
- Completed histological analysis of growth-arrested ASCs treated wounds and demonstrated that these MitC-treated cells did not any effect on wound healing.
- Determined that Transplanted ASCs exhibited the activated a phenotype.
- Determined that transplanted ASCs can proliferate in wounds.
- Demonstrated that ASCs enhanced wound healing by increased recruitment of macrophages.
- Preparation of a manuscript.

C. Hypertrophic scar study

- Optimized the cell number ($1 \times 10^6$ ASCs per 7mm wound) for hypertrophic scar study.
- Completed histological analyses on the effect of treatments by ASCs, BM-MSCs, and DF in reducing hypertrophic scarring.
- In the process of harvesting scars for the collagen analysis by immunostaining, Picrosirus staining, and Masson's Trichrome staining.
- In the process of determining the tensile strength of hypertrophic scars from wounds treated with rabbit ASCs as compared to that of controls.
- Determined that allogeneic ASCs could be used as cell therapy.

D. 3-D cell aggregate study

- As compared to 2-D cultures, 3-D ASCs showed an up-regulation of growth factors that include KGF, TGFβ-1, VEGF, FGF2, HGF, and TGFβ-3 at mRNA transcript levels and at protein levels with some of these factors (VEGF, TGFβ1 &2, and FGF2).
- Conditioned media obtained from ASCs grown under 3D conditions promoted tube formation and cell migration *in vitro* suggesting 3D grown ASCs possess potential in accelerating wound healing.
- Submitted a manuscript entitled "*In Vitro* Characterization of Scaffold-Free Three Dimensional Mesenchymal Stem Cell Aggregates" for consideration of publication.

**REPORTABLE OUTCOMES:**

Wound Healing Study

1. Demonstrated that rabbit ASCs promoted granulation tissue formation.
2. Determined that Transplanted ASCs exhibited the activated fibroblast phenotype.
3. Determined that transplanted ASCs can proliferate in wounds.
4. Demonstrated that ASCs enhanced wound healing by increased recruitment of macrophage.
5. Preparation of a manuscript

Hypertrophic Scar Study

1. Demonstrated that none of the cell treatments tested reduced scarring.
2. Determined that allogeneic ASCs could be used as cell therapy without inducing immunological responses.

3-D Cell Aggregate Study

1. As compared to 2-D cultures, 3-D ASCs showed an up-regulation of growth factors that include KGF, TGF β -1, VEGF, FGF2, HGF, and TGF β-1 at mRNA transcript levels and at protein levels with some of these factors (VEGF, TGF β1 &2, and FGF2).

Immediate Future Plan

1. In the process of harvesting scars for the collagen analysis by immunostaining, Picrosirus staining, and Masson's Trichrome staining.
2. In the process of determining the tensile strength of hypertrophic scars from wounds treated with rabbit ASCs as compared to that of controls.
3. Test the 3D grown rabbit ASC in reducing hypertrophic scarring in our rabbit ear hypertrophic scar model.

**CONCLUSION:**

The research evaluated the hypothesis that adipose-derived mesenchymal stem cells applied to wounds can reduce inflammation, increase angiogenesis, integrate into wounds, speed the restoration of barrier function, and/or improve scar quality. The completed activities and the findings made in evaluating this hypothesis are listed below.

A. Establishment of cell lines and reagents

- Isolated and characterized 4 rabbit ASCs lines, 8 rabbit BM-MSCs lines, and 3 rabbit dermal fibroblast lines.
- Established GFP (or DsRed2) expressing ASCs and DFs to study the fate of transplanted ASCs in wounds.
- Established firefly luciferase expressing ASCs.
- Optimized immunohistochemistry conditions for rabbit neutrophils, macrophages, CD31, and Ki67.
- Characterized survival of ASCs in wounds after 7 days transplantation.
- Determined the higher level of secreted TGF-β1 from rabbit and human MSC than from fibroblasts.

B. Wound healing study

- Optimized the number of rabbit ASCs (1 x 106 ASCs per 7 mm wound) for wound healing study.
- Completed histological analyses on the effects of ASCs, BM-MSCs, and DFs on wound healing.
- Demonstrated promotion of granulation tissue formation by rabbit ASCs.
- Completed histological analysis of wounds treated with growth-arrested ASCs and demonstrated that these MitC-treated cells did not affect wound healing.

- Determined the activated phenotype and proliferation of ASCs transplanted to wounds.
- Demonstrated that ASCs enhanced wound healing by increasing recruitment of macrophages.

C. Hypertrophic scar study

- Optimized cell number for hypertrophic scar study (1 x 106 ASCs per wound).
- Determined the effect of treatment of wounds with ASCs, BM-MSCs, and DF in reducing hypertrophic scarring.
- Demonstrated that none of the cell treatments tested reduced scarring.

D. 3-D cell aggregate study

- As compared to 2-dimensional cultures, 3-dimensional ASC cultures up-regulated growth factor production, including KGF, TGFβ-1, VEGF, FGF2, HGF, and TGFβ-3, some were up-regulated at both mRNA and protein levels (VEGF, TGFβ1 &2, and FGF2).
- Conditioned media from 3D-cultured ASCs promoted tube formation and cell migration *in vitro* suggesting 3D grown ASCs could have greater potential to accelerate wound healing.
- Submitted a manuscript entitled "*In Vitro* Characterization of Scaffold-FreeThree-Dimensional Mesenchymal Stem Cell Aggregates" for consideration of publication.

**REFERENCES:**


1. J.M. Gimble, A.J. Katz, B.A. Bunnell, Adipose-derived stem cells for regenerative medicine, Circulation Research 100 (2007) 1249-1260.
2. A. Schaffler, C. Buchler, Concise review: adipose tissue-derived stromal cells-- basic and clinical implications for novel cell-based therapies, Stem Cells 25 (2007) 818-827.
3. B. Lindroos, R. Suuronen, S. Miettinen, The potential of adipose stem cells in regenerative medicine, Stem Cell Rev 7 (2011) 269-291.
4. C.S. Lin, Z.C. Xin, C.H. Deng, H. Ning, G. Lin, T.F. Lue, Defining adipose tissue-derived stem cells in tissue and in culture, Histol Histopathol 25 (2010) 807-815.
5. B.A. Bunnell, B.T. Estes, F. Guilak, J.M. Gimble, Differentiation of adipose stem cells, Methods Mol Biol 456 (2008) 155-171.
6. C.T. Gomillion, K.J. Burg, Stem cells and adipose tissue engineering, Biomaterials 27 (2006) 6052-6063.
7. E. Mansilla, G.H. Marin, F. Sturla, H.E. Drago, M.A. Gil, E. Salas, M.C. Gardiner, G. Piccinelli, S. Bossi, E. Salas, L. Petrelli, G. Iorio, C.A. Ramos, C. Soratti, Human mesenchymal stem cells are tolerized by mice and improve skin and spinal cord injuries, Transplant Proc 37 (2005) 292-294.
8. L.J. Currie, J.R. Sharpe, R. Martin, The use of fibrin glue in skin grafts and tissue-engineered skin replacements: a review, Plast Reconstr Surg 108 (2001) 1713- 1726.
9. S.J. Gwak, S.S. Kim, K. Sung, J. Han, C.Y. Choi, B.S. Kim, Synergistic effect of keratinocyte transplantation and epidermal growth factor delivery on epidermal regeneration, Cell Transplant 14 (2005) 809-817.
10. W. Ho, B. Tawil, J.C. Dunn, B.M. Wu, The behavior of human mesenchymal stem cells in 3D fibrin clots: dependence on fibrinogen concentration and clot structure, Tissue Eng 12 (2006) 1587-1595.
11. J. Mogford, B. Tawill, X. Jia, T. Mustoe, Fibrin sealant combined with fibroblast and platelet-derived growth factor enhance wound haealing in excisional wounds, Wound Rep Reg 17 (2009) 405-410.
12. C.H. Jang, H. Park, Y.B. Cho, C.H. Song, Mastoid obliteration using a hyaluronic acid gel to deliver a mesenchymal stem cells-loaded demineralized bone matrix: an experimental study, Int J Pediatr Otorhinolaryngol 72 (2008) 1627-1632.
13. G.D. Prestwich, J.W. Kuo, Chemically-modified HA for therapy and regenerative medicine, Curr Pharm Biotechnol 9 (2008) 242-245.

14. D.N. Shah, S.M. Recktenwall-Work, K.S. Anseth, The effect of bioactive hydrogels on the secretion of extracellular matrix molecules by valvular interstitial cells, Biomaterials 29 (2008) 2060-2072.
15. D.M. Yoon, S. Curtis, A.H. Reddi, J.P. Fisher, Addition of Hyaluronic Acid to Alginate Embedded Chondrocytes Interferes with IGF-1 Signaling In Vitro and In Vivo, Tissue Eng Part A (2009).
16. G.C. Gurtner, S. Werner, Y. Barrandon, M.T. Longaker, Wound repair and regeneration, Nature 453 (2008) 314-321.
17. D.E. Discher, D.J. Mooney, P.W. Zandstra, Growth factors, matrices, and forces combine and control stem cells, Science 324 (2009) 1673-1677.
18. A.M. Altman, N. Matthias, Y. Yan, Y.H. Song, X. Bai, E.S. Chiu, D.P. Slakey, E.U. Alt, Dermal matrix as a carrier for in vivo delivery of human adipose- derived stem cells, Biomaterials 29 (2008) 1431-1442.
19. A.M. Altman, Y. Yan, N. Matthias, X. Bai, C. Rios, A.B. Mathur, Y.H. Song, E.U. Alt, IFATS collection: Human adipose-derived stem cells seeded on a silk fibroin- chitosan scaffold enhance wound repair in a murine soft tissue injury model, Stem Cells 27 (2009) 250-258.
20. D.E. Morris, L. Wu, L.L. Zhao, L. Bolton, S.I. Roth, D.A. Ladin, T.A. Mustoe, Acute and chronic animal models for excessive dermal scarring: quantitative studies, Plast Reconstr Surg 100 (1997) 674-681.
21. O. Kloeters, A. Tandara, T.A. Mustoe, Hypertrophic scar model in the rabbit ear: a reproducible model for studying scar tissue behavior with new observations on silicone gel sheeting for scar reduction, Wound Repair Regen 15 Suppl 1 (2007) S40-45.
22. J.R. Marcus, J.W. Tyrone, S. Bonomo, Y. Xia, T.A. Mustoe, Cellular mechanisms for diminished scarring with aging, Plast Reconstr Surg 105 (2000) 1591-1599.
23. A.S. Saulis, J.D. Chao, A. Telser, J.E. Mogford, T.A. Mustoe, Silicone occlusive treatment of hypertrophic scar in the rabbit model, Aesthet Surg J 22 (2002) 147- 153.
24. L. Lu, A.S. Saulis, W.R. Liu, N.K. Roy, J.D. Chao, S. Ledbetter, T.A. Mustoe, The temporal effects of anti-TGF-beta1, 2, and 3 monoclonal antibody on wound healing and hypertrophic scar formation, J Am Coll Surg 201 (2005) 391-397.
25. A. Uccelli, L. Moretta, V. Pistoia, Mesenchymal stem cells in health and disease, Nat Rev Immunol 8 (2008) 726-736.
26. A.I. Caplan, Why are MSCs therapeutic? New data: new insight, J Pathol 217 (2009) 318-324.
27. A. Bartholomew, C. Sturgeon, M. Siatskas, K. Ferrer, K. McIntosh, S. Patil, W. Hardy, S. Devine, D. Ucker, R. Deans, A. Moseley, R. Hoffman, Mesenchymal stem cells suppress lymphocyte proliferation in vitro and prolong skin graft survival in vivo, Exp Hematol 30 (2002) 42-48.
28. K. McIntosh, S. Zvonic, S. Garrett, J.B. Mitchell, Z.E. Floyd, L. Hammill, A. Kloster, Y. Di Halvorsen, J.P. Ting, R.W. Storms, B. Goh, G. Kilroy, X. Wu, J.M. Gimble, The immunogenicity of human adipose-derived cells: temporal changes in vitro, Stem Cells 24 (2006) 1246-1253.
29. B. Puissant, C. Barreau, P. Bourin, C. Clavel, J. Corre, C. Bousquet, C. Taureau, B. Cousin, M. Abbal, P. Laharrague, L. Penicaud, L. Casteilla, A. Blancher, Immunomodulatory effect of human adipose tissue-derived adult stem cells: comparison with bone marrow mesenchymal stem cells, Br J Haematol 129 (2005) 118-129.
30. Caplan, A.I. 1991. Mesenchymal stem cells. Journal of orthop edic research: official publication of the Orthopedic Research Society. 9:641-650.
31. Colwell, A.S., S.R. Beanes, C. Soo, C. Dang, K. Ting, M.T. Longaker, J.B. Atkinson, and H.P. Lorenz. 2005. Increased angiogenesis and expression of vascular endothelial growth factor during scarless repair. Plastic and reconstructive surgery. 115:204-212.

32. Hosokawa, R., K. Nonaka, M. Morifuji, L. Shum, and M. Ohishi. 2003. TGF-beta 3 decreases type I collagen and scarring after labioplasty. Journal of dental research. 82:558-564.
33. Kilroy, G.E., S.J. Foster, X. Wu, J. Ruiz, S. Sherwood, A. Heifetz, J.W. Ludlow, D.M.Stricker, S. Potiny, P. Green, Y.D. Halvorsen, B. Cheatham, R.W. Storms, and J.M. Gimble. 2007. Cytokine profile of human adipose-derived stem cells: expression of angiogenic, hematopoietic, and pro-inflammatory factors. Journal of cellular physiology. 33.212:702-709.
34. Sisco, M., Z.B. Kryger, K.D. O'Shaughnessy, P.S. Kim, G.S. Schultz, X.Z. Ding, N.K. Roy, N.M. Dean, and T.A. Mustoe. 2008. Antisense inhibition of connective tissue growth factor (CTGF/CCN2) mRNA limits hypertrophic scarring without affecting wound healing in vivo. Wound repair and regeneration: official publication of th e Wound Healing Society [and] the European Tissue Repair Society. 16:661-673.
35. Wu, L., A. Siddiqui, D.E. Morris, D.A. Cox, S.I. Roth, and T.A. Mustoe. 1997. Transforming growth factor beta 3 (TGF beta 3) accelerates wound healing without alteration of scar prominence. Histologic and competitive reverse-transcription polymerase chain reaction studies. Archives of surgery. 132:753-760.

**APPENDICES**

None